U.S. DEPARTMENT OF COMMERCE
Environmental Science Services Administration
Research Laboratories

ESSA Technical Memorandum ERLTM-NSSL 46

SEVERE THUNDERSTORM RADAR ECHO MOTION AND RELATED WEATHER EVENTS HAZARDOUS TO AVIATION OPERATIONS

Peter A. Barclay
Kenneth E. Wilk

NOTICE

Technical Memoranda are used to insure prompt dissemination of special studies which, though of interest to the scientific community, may not be ready for formal publication. These papers may later be published in a modified form to include more recent information or research results. Contact the author for additional information on the subject matter discussed in this Memoranda.

National Severe Storms Laboratory
Norman, Oklahoma
June 1970

2nd Printing, March 1972

TABLE OF CONTENTS

	Page
ABSTRACT	1
1. INTRODUCTION	1
2. COMPUTER PROCESSING TECHNIQUES FOR DIGITAL WEATHER RADAR DATA	4
2.1 Echo Isolation and Echo Centroid Calculations	4
2.2 Computer Matching of Radar Echoes	5
3. ECHO MOVEMENT OF STORMS ANALYZED	10
3.1 Minimum Temporal Resolution of Echoes for Extrapolation Purposes	11
3.2 Extrapolation of Echo Path	17
3.3 Application of Cell Track Extrapolation	21
4. DIURNAL VARIATION OF SEVERE WEATHER	22
5. SURFACE WIND GUSTS ASSOCIATED WITH SEVERE STORMS	25
5.1 Gust Characteristics	30
5.2 Wind Shear and Aircraft Operations	35
6. SEVERE TURBULENCE ADVISORIES FOR AVIATION OPERATIONS	42
6.1 V.O.R. Dissemination	44
7. CONCLUSIONS	45
8. ACKNOWLEDGMENTS	46
9. REFERENCES	47
APPENDIX A - Analysis of a Few T33 Aircraft Flights During Spring 1969	49
APPENDIX B - Objective Analyses of Surface Wind Speed during Gust Front Passage, 31 May 1969	59

SEVERE THUNDERSTORM RADAR ECHO MOTION AND RELATED WEATHER EVENTS HAZARDOUS TO AVIATION OPERATIONS

Peter A. Barclay and Kenneth E. Wilk
National Severe Storms Laboratory*

ABSTRACT

Objective techniques for identifying and tracking individual storms by radar are described, using digital weather radar data with space resolution of approximately 1 n mi. The minimum time interval between observations required for deriving storm centroid velocity is 2 to 3 minutes. The optimum signal threshold for defining storm "cores" for tracking is 10^3 to $10^4 mm^6 m^{-3}$ for isolated storms and 10^2 to $10^3 mm^6 m^{-3}$ for squall lines.

A technique is suggested for the extrapolation of arrival of a thunderstorm core into a control zone of an airport. The degree of confidence in the extrapolated path is measured in terms of timing and distance errors resulting from the variance in storm velocity.

Analyses of the wind fields associated with several severe squall lines show narrow zones of high winds that veer sharply with increased speed and contain strong gusts that also increase with mean wind speed. The application of the Power Law to the assessment of vertical wind shear is reviewed.

Operational implications for processing and disseminating severe weather advisories are discussed.

1. INTRODUCTION

This report summarizes research applications of radar for the identification of turbulence and weather echo analysis techniques appropriate to aviation operations.

Four types of storm data collected during the 1969 spring season were analyzed. These observations were provided by a weather radar, a surface mesoscale network, an instrumented tower, and aircraft turbulence measurements. Individual storm motions were studied using digital

---

*Mr. Barclay was assigned to NSSL during January 1969 to January 1970, from the Commonwealth Bureau of Meteorology, Melbourne, Australia.

This work has received substantial support from the FAA under interagency contract FA68 WAI-146.

radar data for several of the major severe weather occurrences in the 1969 spring season and for several previously observed storm periods in 1967 and 1968. The tower and surface network data were extensively analyzed to determine the intensities and patterns of the squall lines ahead of three severe storms that occurred in the 1969 season. Some of the aircraft pilot reports of turbulence during penetrations through and flights around thunderstorms during the 1969 season are tabulated in appendix A.

The movement and predictability of radar observed precipitation areas have been studied by numerous investigators. Most studies have involved analysis of radar film (Ligda, 1953; Boucher, 1961; Boucher and Wexler, 1961; Newton and Fankhauser, 1964) with time intervals between data generally varying from 1/4 to 1 hour. Since digital radar data became available, it has been possible to process data much more thoroughly and rapidly. Kessler and Russo (1963a) discuss the assembly of such data, and investigated the properties of weather radar echoes using various statistical techniques. Kessler and Russo, (1963b) Noel and Fleisher (1960) and Noel (1962) have studied linear prediction using multiple regression techniques. Most of the radar data used in these studies were "digitized" manually from 35 mm film and referred to a Cartesian grid with a mesh scale of 2.5 to 5 miles.

A brief history of radar data collection at NSSL is relevant to the description of the digital radar data used in this study.

In 1967, the linear WSR-57 radar receiver with step attenuation was replaced with a log receiver and signal integrator that provided multiple contours simultaneously on the PPI. This integrator averaged the received signal at 200 range intervals of 0.65 n mi for every 2 degrees of azimuth, with output in six levels for contouring (Lhermitte and Kessler, 1965). A digital translator was then designed and constructed to record this quantized data on magnetic tape. Observation time, azimuth, and elevation in digital format were also recorded. Eighty sampling gates at range steps of 1.4 n mi were generated in the translator. These stored levels of intensity, depending on the quantizer output, were in discrete BCD integers of 1 through 6. The clocking rate of the 80 sampling gates matched the input speed of an NCR 735 buffer recorder. The 80 sampling gates occur every 2 degrees of azimuth; hence, one radar scan consists of 14,400 discrete values of intensity, ranging from approximately $Z = 10$ to $10^6 mm^6 m^{-3}$. The recording format of the NCR 735 is compatible with most computers and can be used with a data phone for long line transmissions to computers or remote Planned Position Indicator (PPI) receivers. In 1967 and 1968 the digitizing intervals were about 15 min, with the minimum time of 2.5 min between observations governed by the slow data acquisition rate of the buffer recorder (Wilk, et al., 1968).

After 1968, a continuous magnetic tape recorder was obtained that greatly reduced the sampling time so that digital data during 1969 was available at 40 sec intervals when required. The word length was increased to 121 sampling gates of 1 n mi lengths and the quantizer output modified to present 9 levels of intensity.

Cross-correlation techniques have been used by Wilson (1966) to measure the movement and predictability of radar echo patterns. These techniques were tested at the National Severe Storms Laboratory (NSSL) and found to be good for storm areas but somewhat lacking in application to the motion of individual thunderstorms.

An interesting technique for studying echoes or elements of echoes, but one which neglects details in the echo "field," is the "tracking" of individual echo centroids. The possible use of PPI centroids to track the motion of a radar echo was discussed by Boucher and Wexler (1961) but was not developed by them in detail. Since the technique can be readily programmed for a computer, routines have been developed at NSSL to compute echo centroids directly from digital radar data and to analyze the centroid motions. The automatic isolation of individual thunderstorms within an echo field serves as a data base for all the prediction characteristics obtained in this study. The velocities of the storm centers have been investigated with a view to predicting thunderstorm positions for intervals of 1 to 30 minutes.

An important aspect of position predictability is the stability of echo area. The areas of complete echoes and areas for various levels of reflectivity in these echoes have been computed for several cases that showed consistent movement. Echo predictability has been defined by linear interpolation "best fit" of echo centroid tracks, and for selected storms, the spatial and temporal variability of storm motion is summarized as a guide for identifying the areas where severe thunderstorms are likely. A scheme is outlined to state the probability that severe turbulence depicted by a chosen echo intensity will pass through a control zone of an airport or air route. Techniques to automatically process echo motion by computer were given considerable attention; however, further refinement is indicated for use in operational analysis and several possible improvements are suggested. From a statistical analysis of digital radar data, estimates of the "computer load" likely during severe weather situations are presented.

The surface network and tower data have been used as bases for space and time analyses of the maximum wind gusts. The importance of the surface wind events associated with the gust front prior to the heavy convective precipitation in squall lines is discussed.

Finally, some comments and suggestions are presented on the dissemination of "severe turbulence" information to the air traffic control system.

2. COMPUTER PROCESSING TECHNIQUES FOR DIGITAL WEATHER RADAR DATA

2.1 Echo Isolation and Echo Centroid Calculations

Techniques for identifying specific echoes from the digital "B" scan data (fig. 1) and calculating their individual motions were developed in two phases. Initially, echoes were isolated by scanning the digital field in range and azimuth and classifying contiguous areas with digits of a specified level as pertaining to one echo. These isolated echoes were identified and transferred to another magnetic tape. The area centroid of each echo was then computed and listed with the echo area. The computation of the intensity-weighted echo centroid involves combining the azimuthal centroid and the range centroid, as given by equations (1) and (2), respectively.

$$\text{Azimuthal centroid} = \frac{\sum (I \times A \times \text{azimuthal line})}{\sum (I \times A)} , \qquad (1)$$

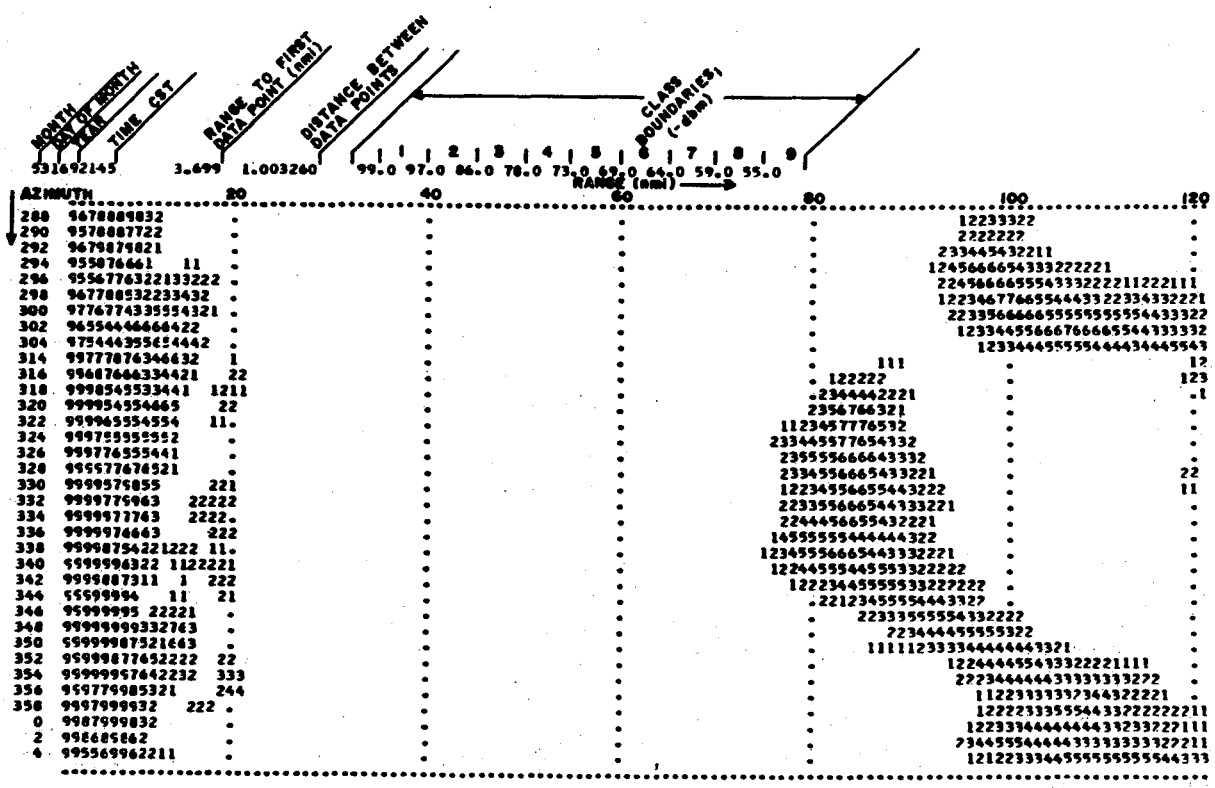

Figure 1. Portion of B-scan listing of the NSSL WSR-57 radar digital recording for the storm of 31 May 1969 at 2145 CST.

where I is the log of the intensity in the individual gates making up the echo and A is the gate area in square nautical miles.

$$\text{Range centroid} = \frac{\sum (I \times A \times \text{gate number})}{\sum (I \times A)} , \qquad (2)$$

The azimuth and range of the centroid then become,

$$\text{Azimuth} = Az_{BEGIN} + (2 \times \text{azimuthal centroid}) \qquad (3)$$

$$\text{Range} = R_o + \left(\begin{matrix}\text{range}\\ \text{centroid}\end{matrix} - 1\right) \times \begin{matrix}\text{gate}\\ \text{length}\end{matrix} . \qquad (4)$$

Az_{BEGIN} and R_o are the beginning azimuth and range of the first gate, respectively. The "2" in (3) is a consequence of the B scan data being obtained in 2 degree azimuthal increments.

2.2 Computer Matching of Radar Echoes

The identification and matching of individual storms on consecutive PPI's are prerequisite to determining their velocities and extrapolated tracks. If the interval between PPI's is large compared with the lifetime of the individual echoes or weather system being tracked, then the PPI pattern may change enough to prohibit matching, and only the statistical properties of the display can be extrapolated.

Statistically, the matching of echoes on consecutive PPI's should be possible if the echo size distributions are not significantly different (i.e., if the standard deviations of the echo sizes on both PPI's are about the same, a reasonable number of cells will match and provide a reliable velocity measurement).

The isolated storms, which have a few intense echoes, and the continuous line cases, with rapid cell growth and decay, present the most difficult patterns to match. Figures 2 and 3 show the number and size distributions of echo areas with intensity $Z \geq 10^3 mm^6 m^{-3}$ for three storms in 1968. The squall line case of May 31, 1969, which is not shown, had significantly more echoes ($Z \geq 10^3 mm^6 m^{-3}$) but contained a similar relative size distribution.

Since the number of these echoes is generally small, their sampling distribution will not be normal. To test the significance of

the differences between the standard deviations of the size distributions on consecutive PPI's, the transformation

$$\bar{\sigma}^2 = \frac{N}{N - 1} \mu^2$$

was made, where μ^2 is the sample variance, and $\bar{\sigma}^2$ is the unbiased estimate of the population variance. Fisher's "z test of significance" (Croxton and Dudley, 1939) was used to compare the variance in echo sizes from PPI to PPI.

This test, defined by

$$z = \tfrac{1}{2} \log_e \frac{\bar{\sigma}_1^2}{\bar{\sigma}_2^2} ,$$

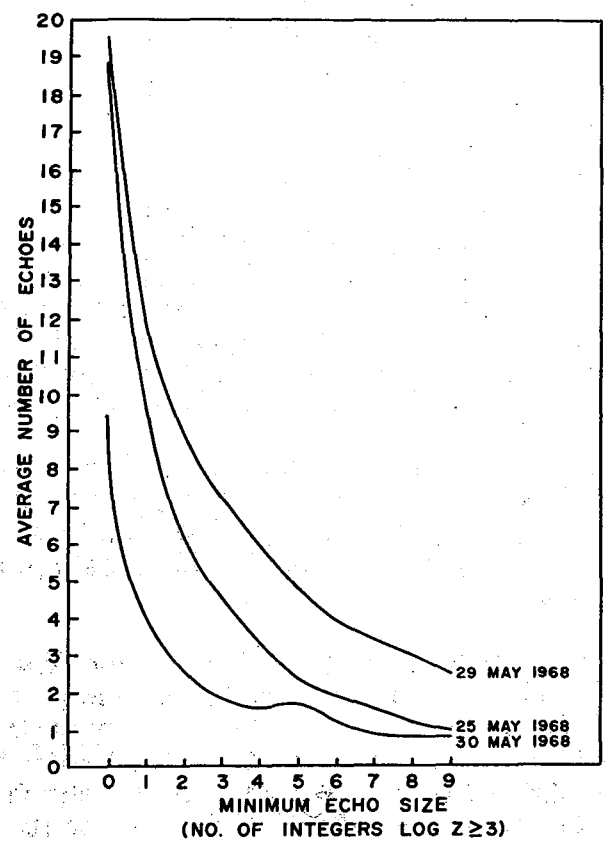

Figure 2. Number of echoes on PPI remaining after filtering out 1 integer to 9 integer echoes.

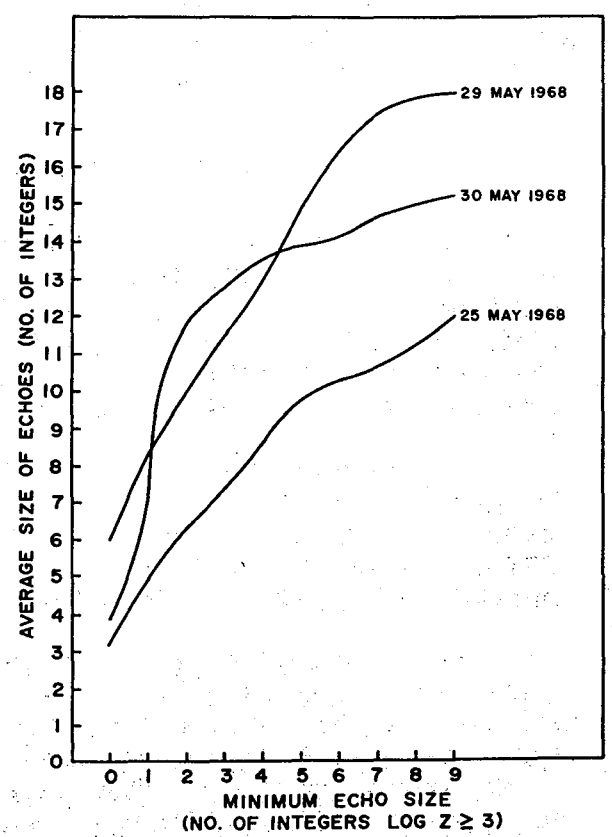

Figure 3. Average size of echoes (no. of integers) remaining after filtering out 1 integer to 9 integer echoes.

gave values of z of about 0.5 for a PPI sampling interval of 15 min, which indicate the variances of the echo distributions on the two PPI's are not significantly different at the 95 percent confidence level and are probably drawn from the same precipitation system.

Further inspection of the size distributions suggests that the rapid growth and decay of small areas cause most of the change. Of course, echoes affected by the scope boundary also confuse the pattern agreement. To illustrate the increase in confidence level when echoes with small number of digits were removed, the echo size distributions were filtered to sequentially remove cells of one digit up to cells of 9 digits, and the z values were recomputed. With all cells of 9 digits or smaller rejected, the z values approached 0.25, which indicates an increase in confidence level for the larger echoes.

To further show that matching should be possible during an entire storm period, when the criteria for pairing echoes from one PPI to the next included weighting by size, the "criterion for likelihood" test (Croxton and Dudley, 1939) was applied to 45 consecutive PPI echo size distributions for the storm of 16 April 1969. This test, which combines the echo size distribution variances of all the PPI's considered, is defined as

$$L = \frac{\left(\sigma_1^2 \times \sigma_2^2 \times \sigma_3^2 \quad ---\sigma_K^2\right)^{1/K}}{1/K\ (\sigma_1^2 + \sigma_2^2 + \sigma_3^2 \ ---\sigma_K^2)},$$

where σ_1^2, σ_2^2, σ_3^2 --- are the variances of echo size on K consecutive PPI's.

Figure 4 shows values of L obtained for each of the 9 size filters and, as with the z test, shows that weighting the larger cells will aid in matching the PPI's.

Considering the stable character of the echo statistics, it seemed appropriate to develop matching logic so that individual echo velocities could be determined automatically. Ouput from the echo isolation/echo centroid program is used in this routine, which can be run on either the IBM 360/40 or IBM 1620.

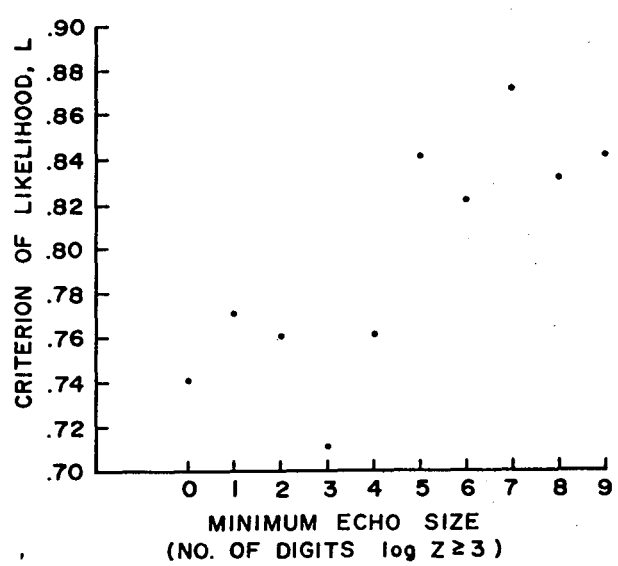

Figure 4. Criterion of likelihood test showing the increase in scope continuity with increase in minimum echo size.

Each echo is characterized by its centroid, area, and intensity, and a "reliability factor" R_F is computed for each echo at each observation considering (a) the degree of isolation from its neighbors, (b) echo area, and (c) intensity.

In essence, the larger the area of echo j, as compared to echo i, the larger R_F becomes. The premise behind the reliability factor is that a large, isolated echo should be more reliable in movement, and more easily matched than a field of small echoes. Equation (5) combines these factors in an arbitrary weighting function,

$$R_{F(j)} = \frac{D + \sqrt{d_j}}{E + \sum_{i \neq j} \frac{d_i}{F + S^2_{ij}}} \quad , \qquad (5)$$

where D, E, and F are constants chosen empirically from the analysis of actual digital data and give R_F values between zero and 250.

The summation of the log of the reflectivity times area of the digital field making up the individual echo is $d = \sum \log Z \times \text{area}$, and i and j are separate echoes observed at the same observation. In computing the reliability factor for echo j, the summation in the denominator of (5) is reiterated for all pair combinations observed at that time. S_{ij} is the distance between the centroids of echoes i and j.

Figure 5a illustrates the effect that echo area and distance between echoes have on R_F considering only two echoes.

An error (fig. 5b) is calculated for the displacement point to each echo centroid in the second of the two B scans by (6).

$$\text{ERROR} = \left(1 + K \frac{|R_{Fk} - R_{Fj}|}{R_{Fj}}\right) (DX^2 + DY^2) \quad , \qquad (6)$$

where DX^2 and DY^2 are the squares of the X and Y displacement components of the distance between the projected centroid and the actual echo centroid, and R_{Fj} and R_{Fk} are the reliability factors in the first and second B scan, respectively. The error is proportionally weighted (constant K chosen empirically) by the difference in reliability factors for the two echoes with respect to the echo from which the displacement is made. This error, therefore, increases if a large echo is matched with a smaller one, but no emphasis is given to the absolute difference in reliability factor. Hence, small differences in reliability factors for echoes with low reliability factors will be the same as a proportionally larger difference between echoes with larger reliability factors.

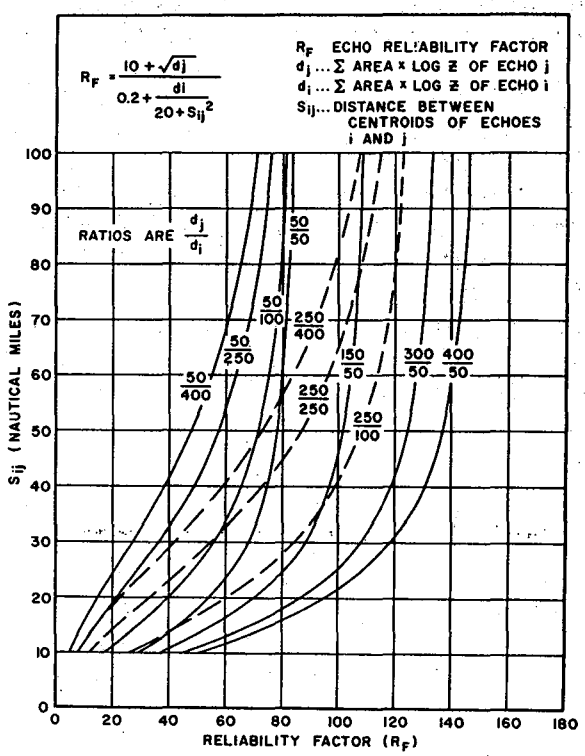

Figure 5a. Illustration of the effect on reliability factor of the distance between echoes for various ratios of echo sizes and intensities.

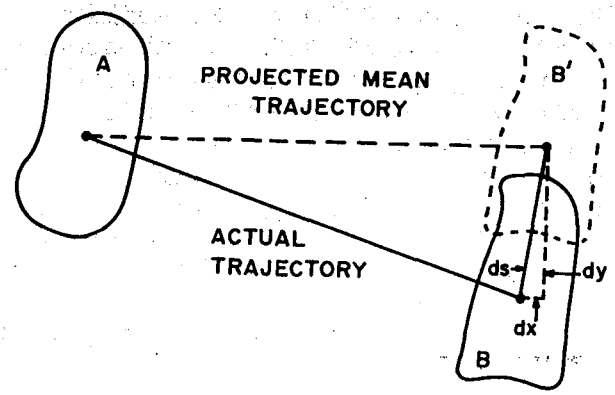

Figure 5b. x and y components of the error displacement measured during echo matching.

After the minimum errors for each displacement point to echo centroid have been computed, a "fit index" (F.I.) is calculated using:

$$F.\ I. = \frac{R_{Fk}}{ERROR + 20\ (TDX^2 + TDY^2)}\ , \qquad (7)$$

where TDX and TDY are the X and Y displacement components for the trial match of echo centroids from the first to the second B scan.

Substituting (6) into (7),

$$F.I. = \frac{R_{Fk}}{\left(1 + \frac{K\ (R_{Fk} - R_{Fj})}{R_{Fj}}\right)(DX^2 + DY^2) + 20(TDX^2 + TDY^2)}\ . \qquad (8)$$

Equation (8) gives preference to echo matching over shorter distances corresponding to short time intervals between observations.

The F.I. is summed for each of five echo displacements. These echo displacements are obtained from the matching of the echo with the highest reliability factor in the first B scan, in turn, to the echoes with the five highest reliability factors in the second B scan. If the ratio of the best to the second best fit index is greater than 3, then the displacement associated with the best fit index is used for an estimate of the pattern displacement. Each echo of the first B scan is then projected with the pattern displacement and matched with the best fitting echo of the second B scan. If the ERROR is less than a chosen value (determined empirically using known matched echoes), the match is recorded as the appropriate displacement.

3. ECHO MOVEMENT OF STORMS ANALYZED

It is noted that the motions of the echo centroids were not smooth; many minor and occasionally some major changes took place in the apparent centroid direction and speed of movement (fig. 6). The excursions from a straight line illustrate the natural variability of the weather

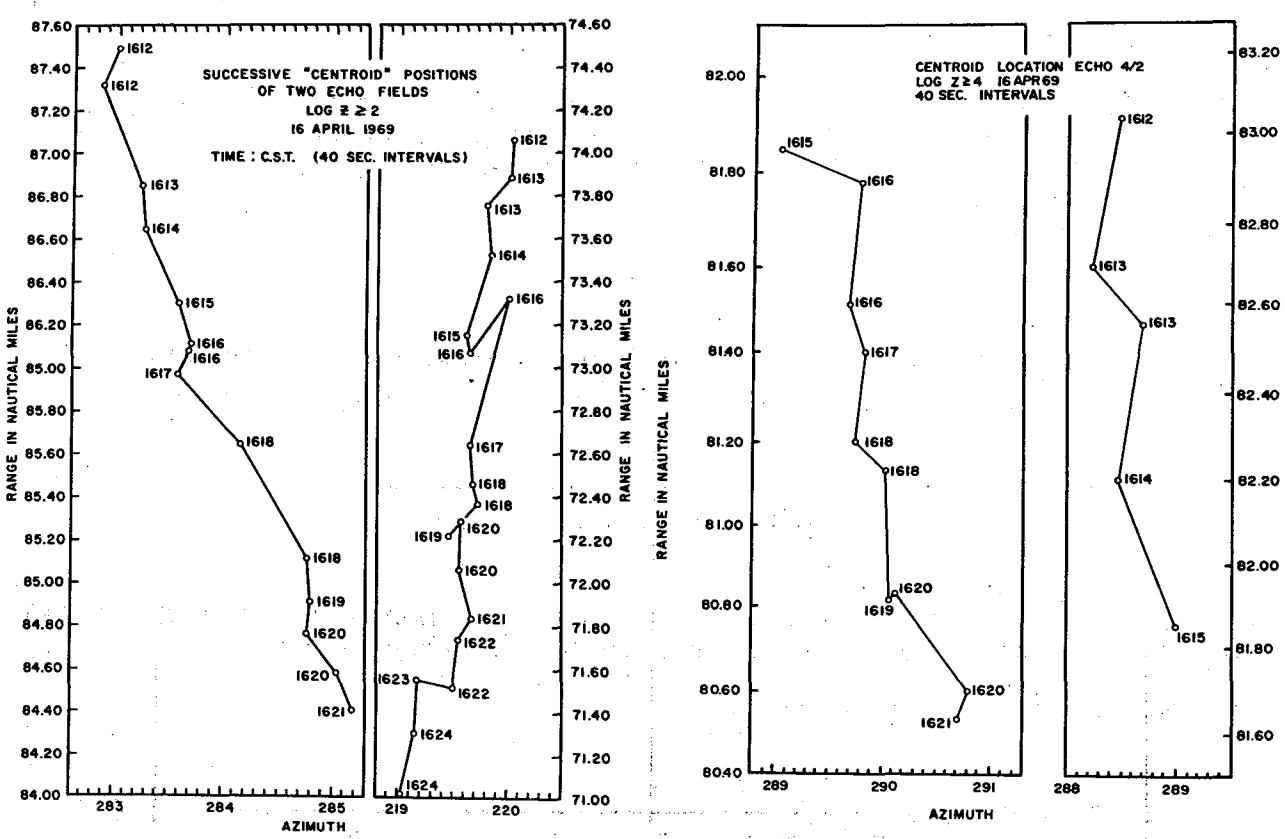

Figure 6. Echo centroid movement based on $Z \sim 10^2 mm^6 m^{-3}$ and $Z \sim 10^4 mm^6 m^{-3}$ level of intensity for observations made of the storm on 16 April 1969 at 40 second intervals.

echoes. In addition, there is a small variability caused by the electronic technique of sampling the intensity in each gate from one observation to the next (i.e., the observational accuracy of the system).

From the storms analyzed with the computer procedures outlined in the previous section, the following general conclusions were reached:

(1) Echo centroids based on the low reflectivity levels (log Z ~ 1, 2), in general, show smoother movement, but because of the large areas of these low levels, an occasional large change in area or shape, when two echoes join or separate, for example, will make a dramatic change in the echo centroid location.

(2) At the higher reflectivity levels the behavior of the echo centroid movement is variable because of cell lifetime. With a well organized frontal type storm there is good continuity in the centroid movement at the log Z ~ 4 level, but in the air mass and poorly organized frontal type storms the centroid motion is erratic.

To illustrate the possible extreme variation in centroid motion, a single-cell type severe storm (fig. 7), with which a tornado was associated, was hand digitized so that intensity and positional information was available at approximately 1 1/2 min intervals. Echo centroids for $Z \geq 10$, 10^2, 10^3, and $10^4 mm^6 m^{-3}$ are shown in figure 8. There was considerable rotation in this echo, which is illustrated by the back and forth motion of the $Z \geq 10^3$, $10^4 mm^6 m^{-3}$ centroids (fig. 8b). In this case the movement of the echo is best depicted by the $Z \geq 10 mm^6 m^{-3}$ centroid motion (fig. 8a).

An analysis of echo area showed that when motion was obtained from successive centroids, the area of the echo or portion of the area used to compute the centroid remained fairly constant. Figures 9 and 10 illustrate echo centroid path and associated echo areas.

The fact that the area remains constant is significant. The consistency of echo area is a factor in the computer analysis of echo matching.

3.1 Minimum Temporal Resolution of Echoes for Extrapolation Purposes

In an effort to determine when the irregular motion of the echo centroids was reduced to a minimum level, a study was made of the

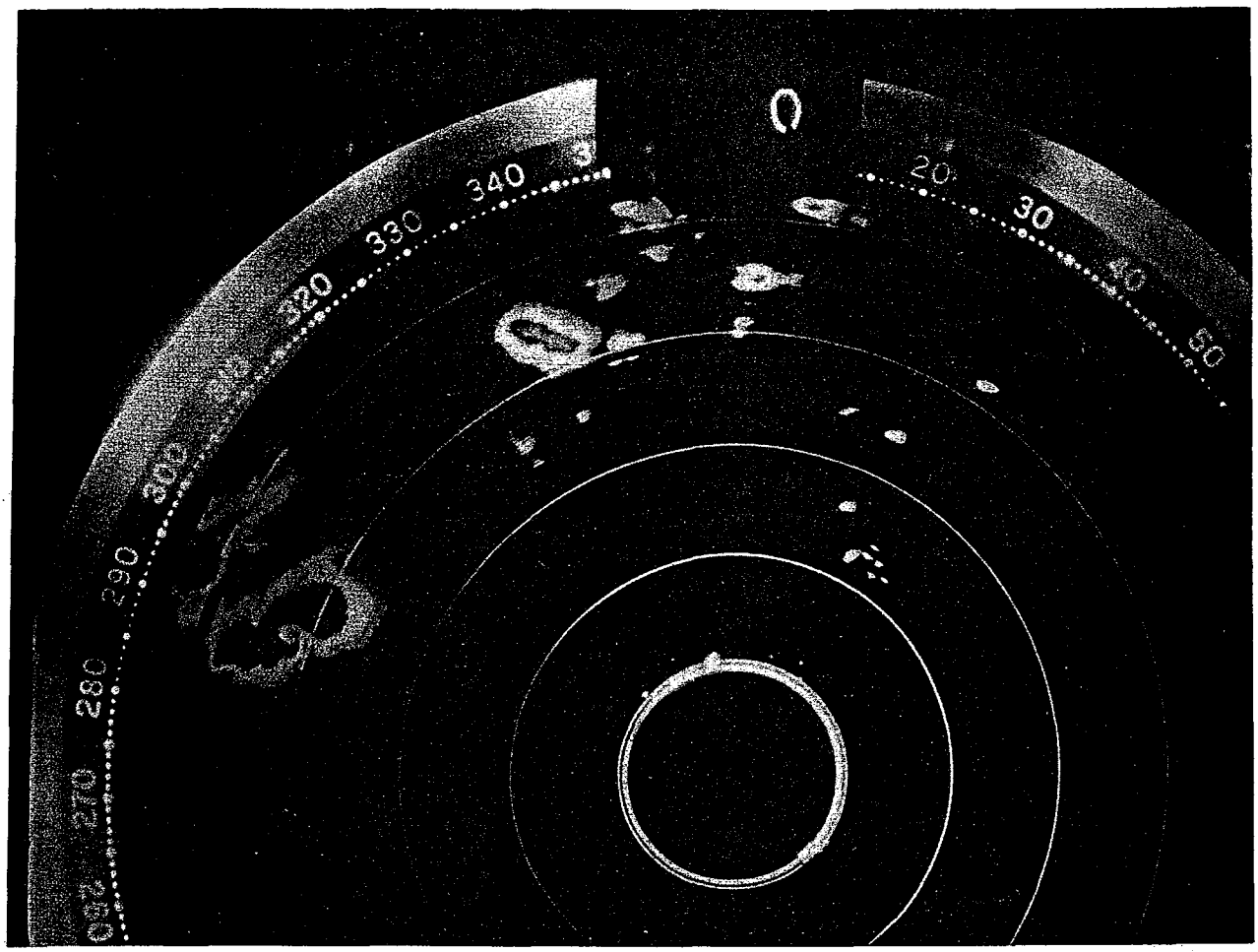

Figure 7. NSSL WSR-57 radar contoured display of the severe thunderstorm on June 10, 1967. A tornado was located at approximately 290 degrees at 85 n mi.

variation in direction and speed of successive centroid positions for echoes that showed good movement. Results are graphed in figure 11 and show that the standard deviations of speed (σ_S) and direction (σD) are reduced for observations timed at intervals greater than about 2 1/2 min. One implication of this is that even with the capability of obtaining a digital picture at 40 sec intervals, the error in using σ_S and σ_D for any echo extrapolation calculations cannot be significantly reduced by making observations more frequently than 2 1/2 min intervals.

Although movement over such small time intervals is rarely required, and in general not practical when using tracing techniques directly from the PPI, it is of some importance in this study of the extrapolation of echoes associated with severe turbulence in a terminal area for a 1 to 30 min time frame.

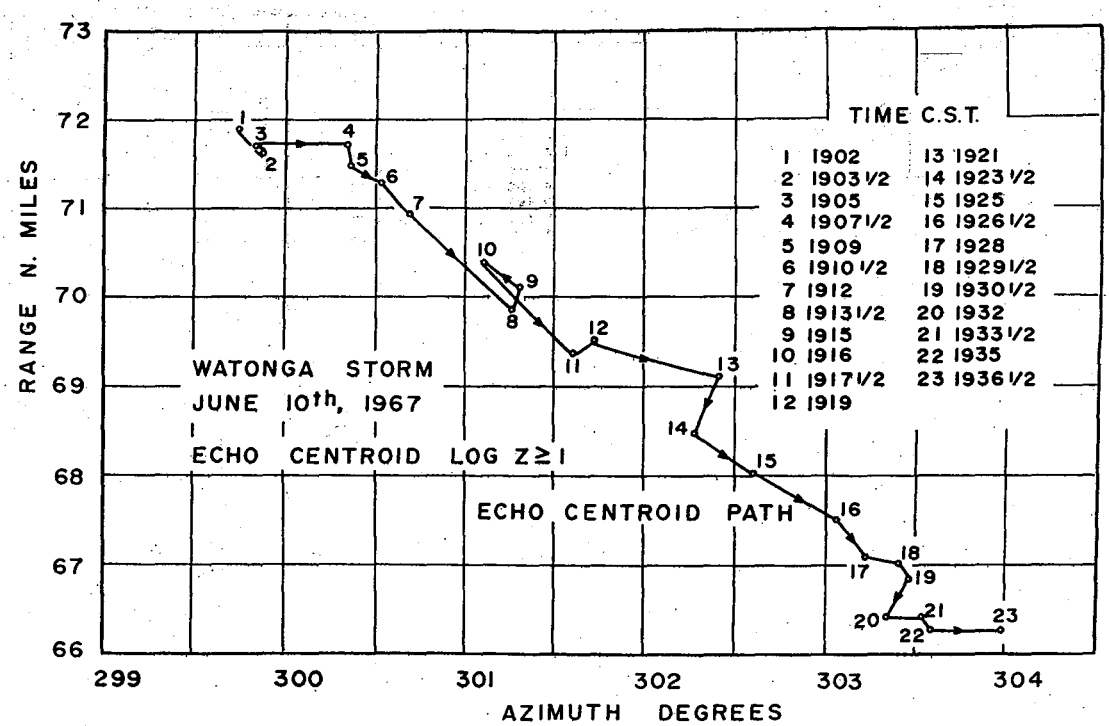

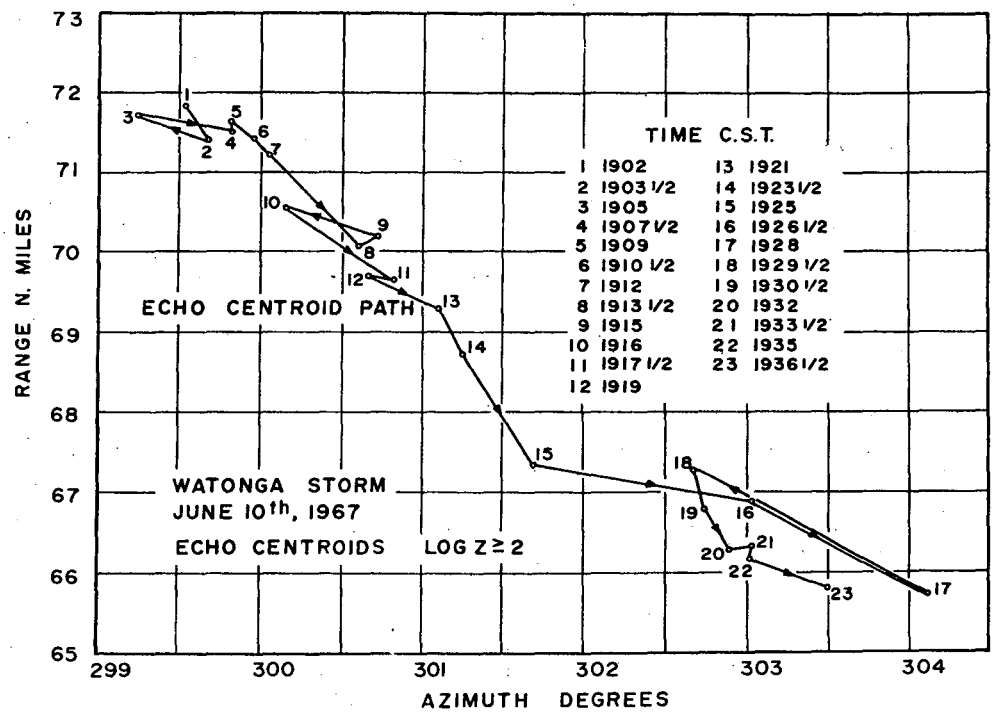

Figure 8a. Echo centroid motion for $Z \geq 10$ and $10^2 mm^6 m^{-3}$ for single cell tornadic storm (10 June 1967).

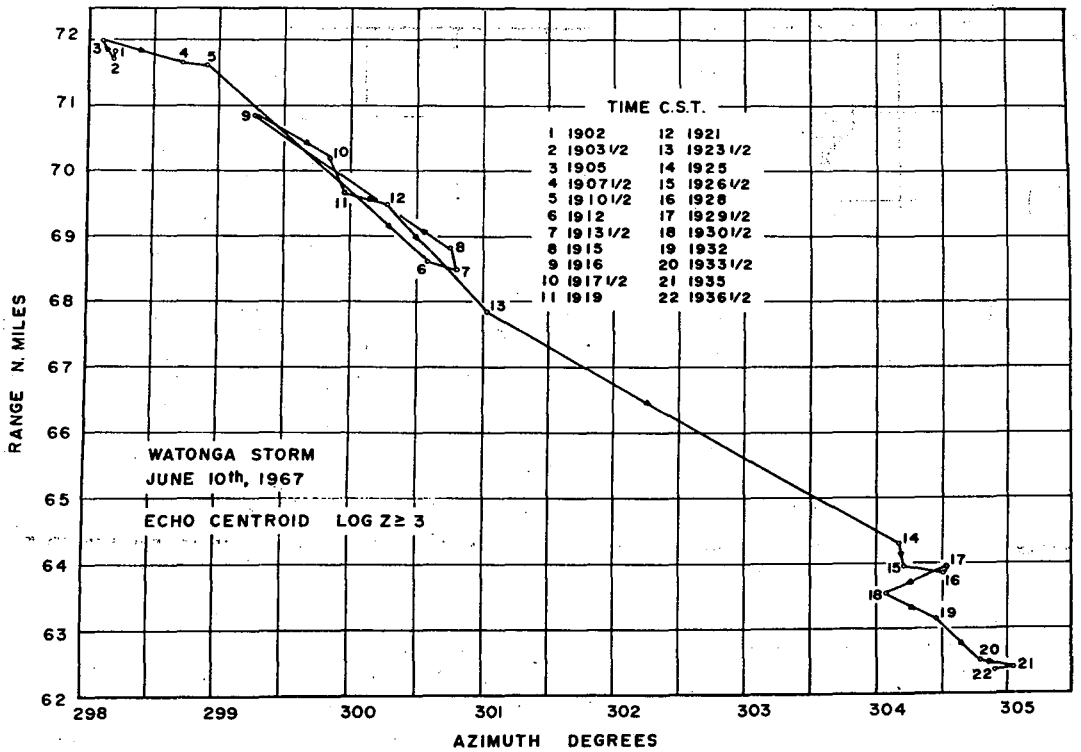

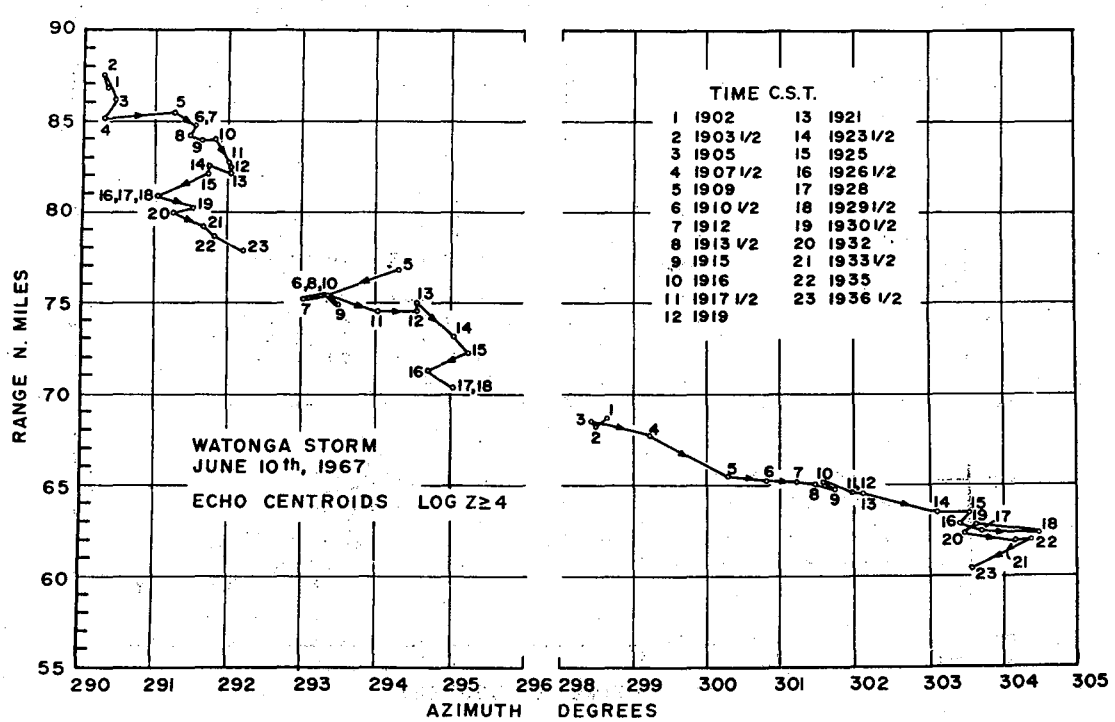

Figure 8b. Echo centroid motion for $Z \geq 10^3$ and $10^4 mm^6 m^{-3}$ for single cell tornadic storm (10 June 1967).

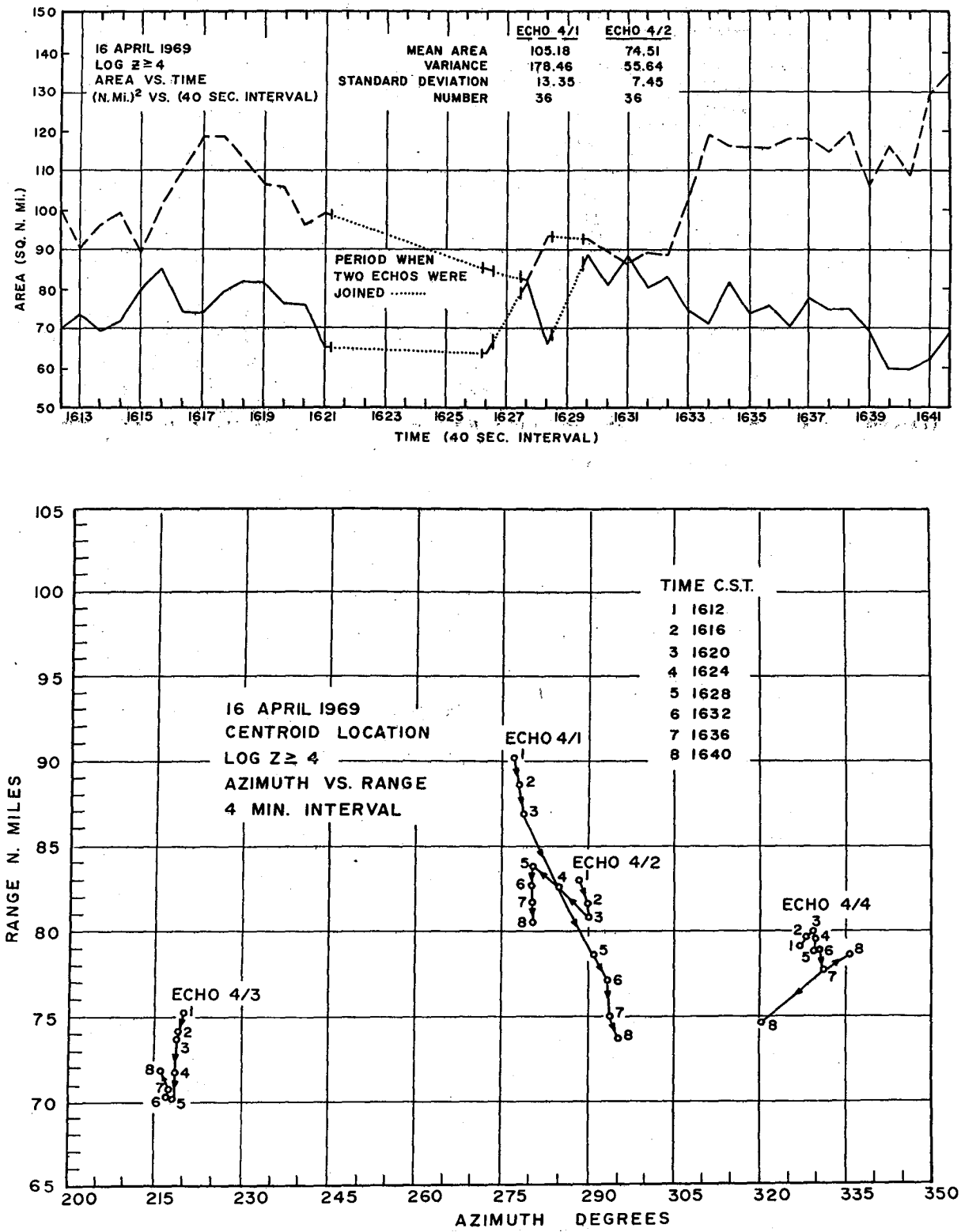

Figure 9. Comparison of echo area and echo centroid path for log Z ≥ 4 echoes observed on 16 April 1969.

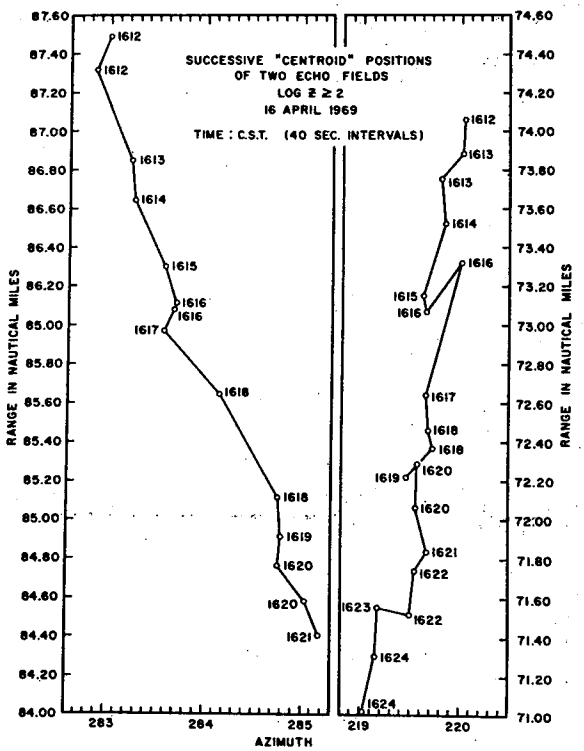

Figure 10. Comparison of echo area (below) and echo centroid path (left) for log Z ≥ 2 echoes observed on 16 April 1969.

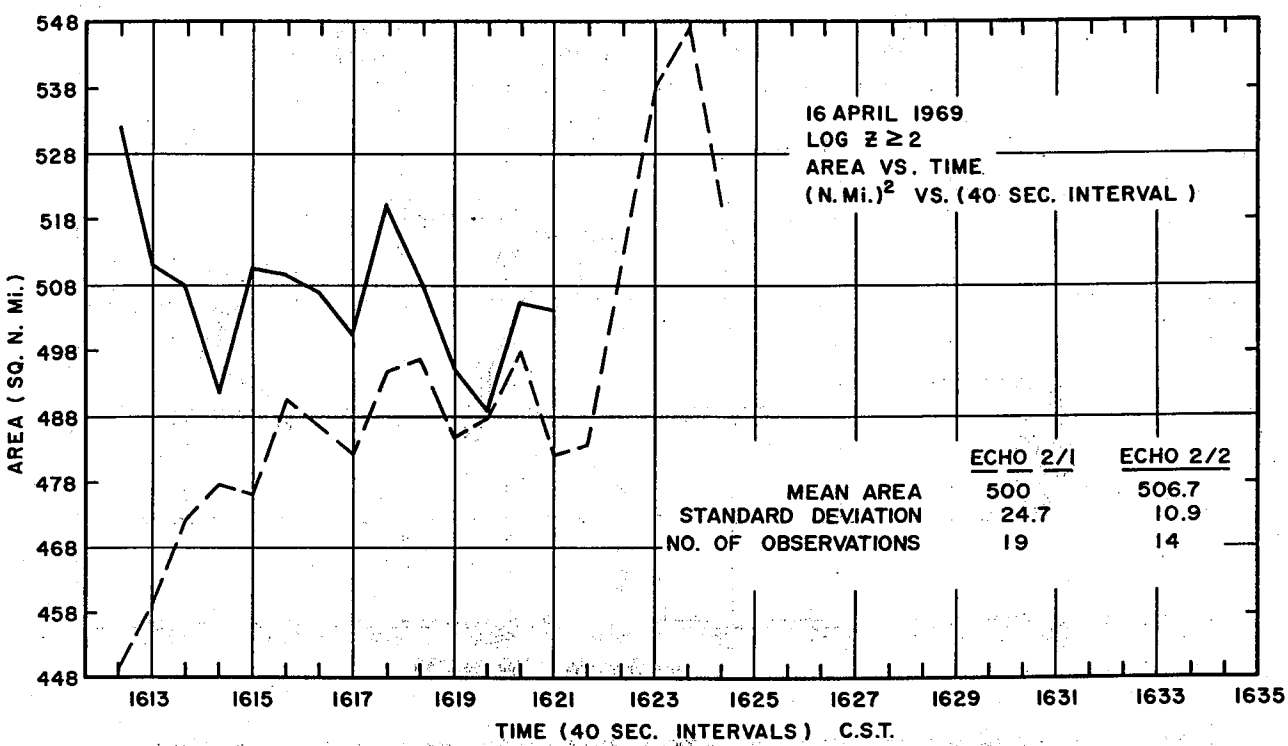

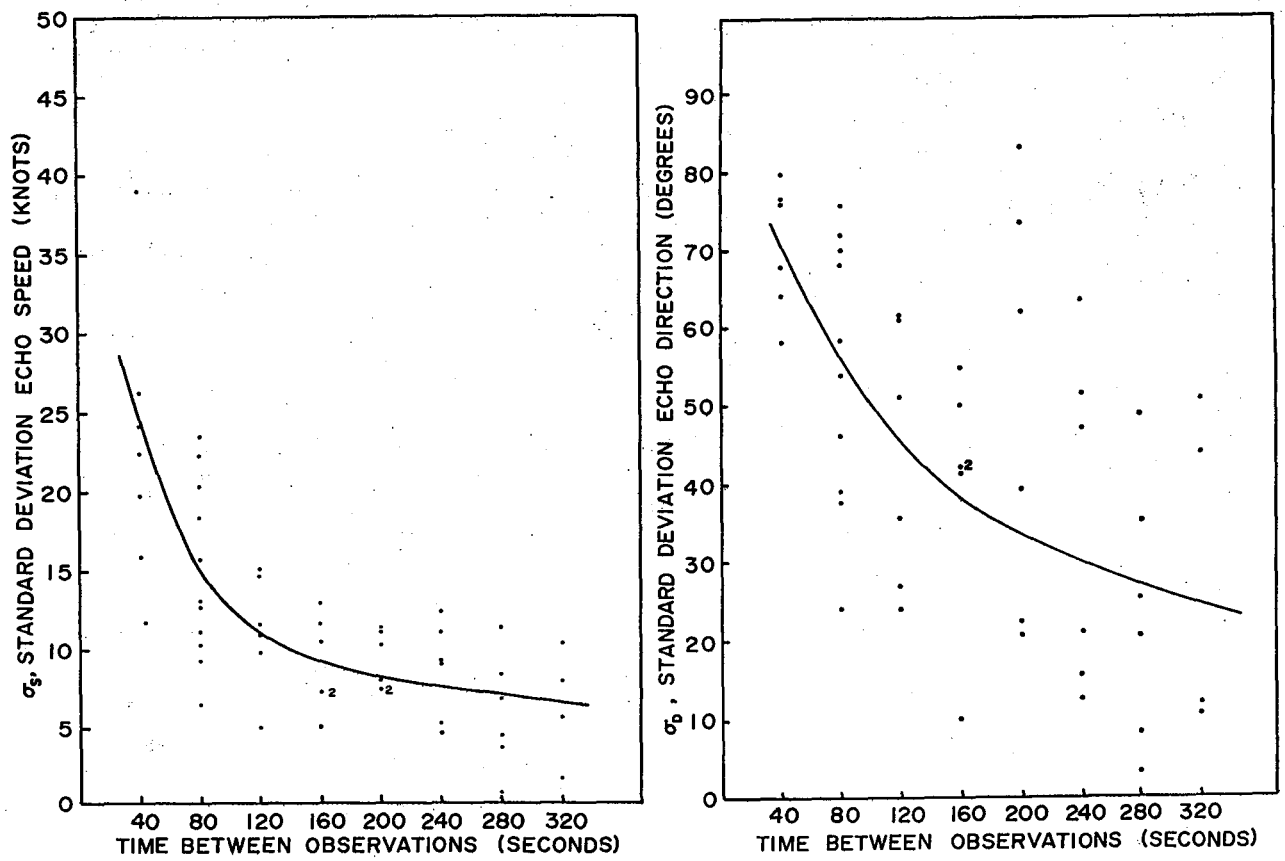

Figure 11. Standard deviation of the centroid motion speed and direction for several storms during the 1969 spring season for varying time between observations.

3.2 Extrapolation of Echo Path

Once the echo has been identified by its centroid, the next problem is the extrapolation of its path with respect to time. Observations by Ligda (1953) show that the motion of small precipitation areas can be either rectilinear or curvilinear, with divergent and parallel flow possible in both cases. For short time intervals, rectilinear motion is adequate to describe the motion of small areas.

Computer techniques were developed at NSSL to extrapolate the position of the echo centroid given the time and position of two or more centroids. The polar coordinates (r, θ) of the given centroids (the number of which can be varied) were converted to cartesian coordinates x, y, with x and y as a function of time. Linear least square approximations $x(t)$ and $y(t)$ were computed for x and y values as a function of time. These functions were used to extrapolate the position at given later times. After the x and y coordinates

are computed, they are converted to equivalent polar coordinates. The best fit equation can be used to trend the echo centroids for prediction purposes.

Figure 12 shows the actual echo centroid path of the log $Z \geq 1$ centroids and the extrapolation path for various input centroids for the tornado bearing storm discussed earlier. To assess the error of extrapolation, a program was developed which calculates the error in both time and distance of the extrapolated position in terms of the actual observed position. Figure 13 illustrates the errors measured, namely δt and δd. These errors are summed for each observation time ($\Sigma\delta t$ and $\Sigma\delta d$).

Of particular importance to the operational application of the echo path extrapolation using centroids is the problem: how long should past centroid position data be consulted in order to minimize the position and time error for future time extrapolation?

By increasing the number of input centroid positions progressively, and computing mean, maximum and standard deviation values of δt and δd for various input, the mean, maximum, and variance of the temporal and spatial errors in relation to period of extrapolation were obtained.

Graphs of the above values are plotted in figure 14 for the tornado bearing storm using log $Z \geq 1$ to compute the centroid path. It was fortuitous, in this example, that both the distance and time errors were small using the first two centroids. (The line through these two centroids closely approximated the best fit path of all the centroids.)

In this case, after eight centroid observations at approximately 1 1/2 min intervals, the mean values of the distance and time error have reached values of 0.5 n mile and 2.2 min, respectively, and after 16 observations these values were reduced to 0.25 n mi and 1.2 min.

In summary, one should emphasize that track extrapolation analysis can be operated in real time. The reflectivity threshold level representing the best motion, and the number of centroid observations that should be used to reduce the error to an acceptable value can be programmed for determination by the computer.

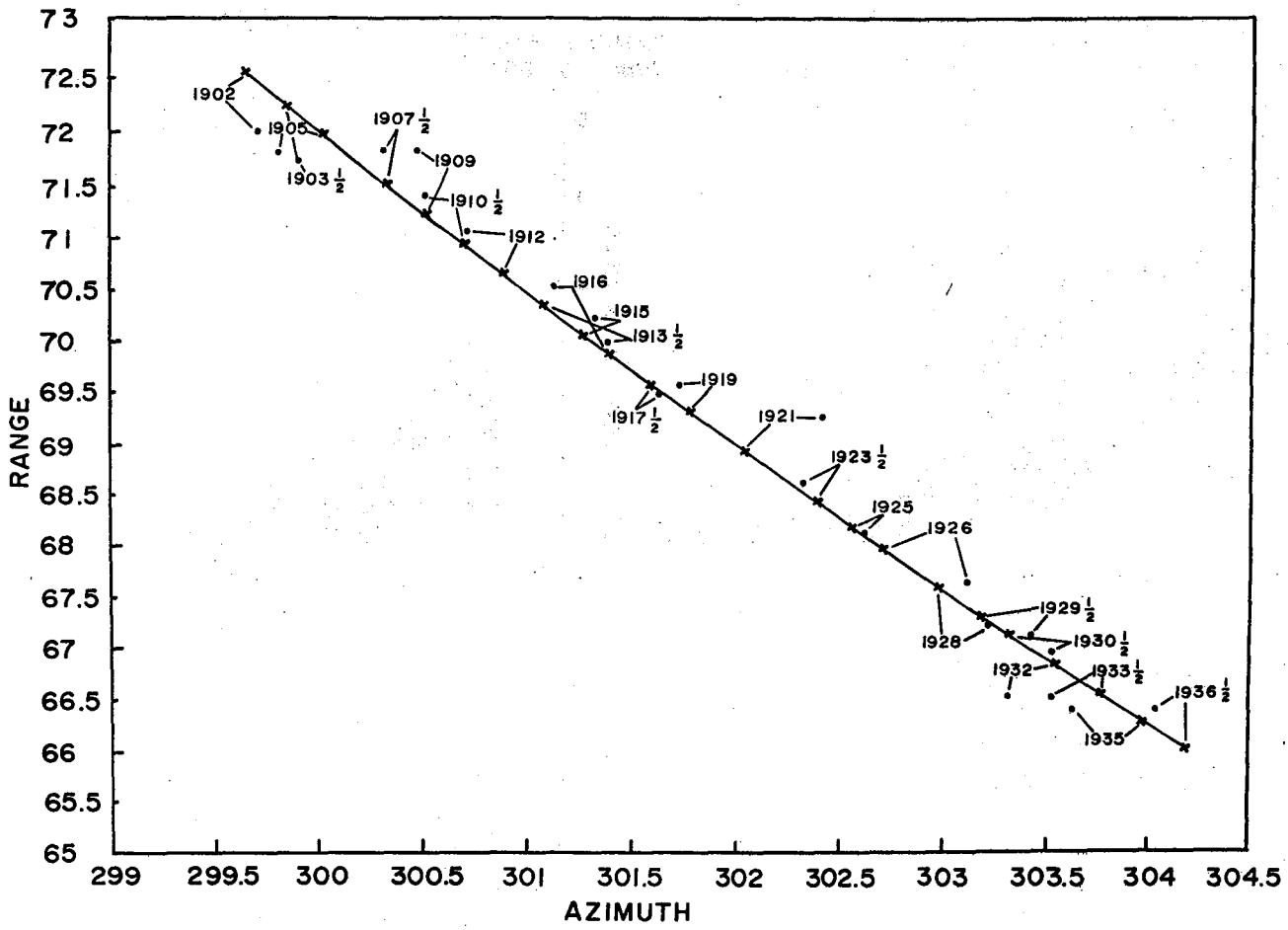

Figure 12. Actual centroid locations and "best fit" path for the severe storm echo on 10 June 1967.

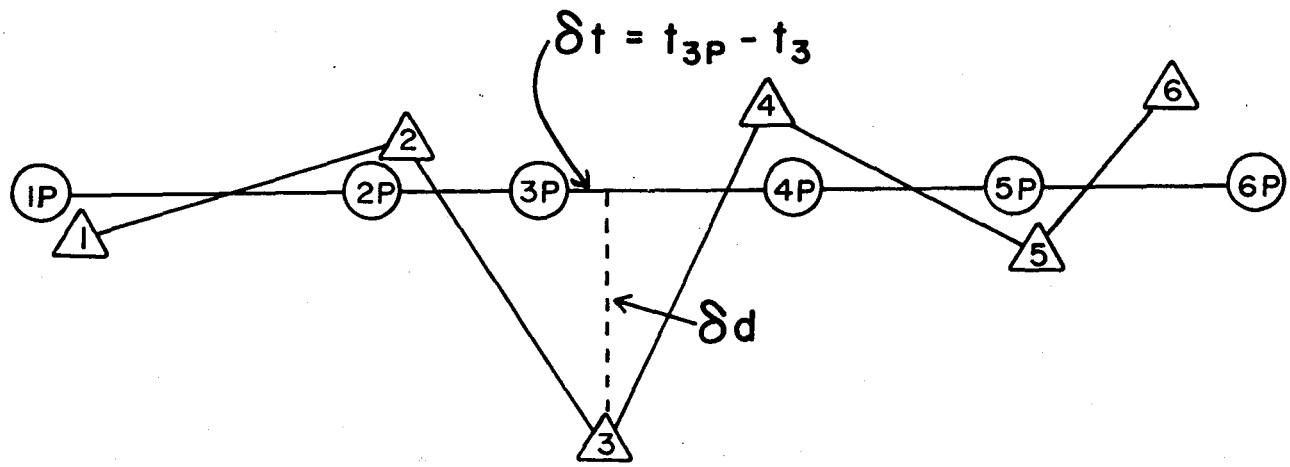

Figure 13. Illustration of the centroid locations and the determination of the time and distance errors in linear extrapolation. $\triangle 2 = t_2$ actual echo centroid path at times $t_1, t_2, \ldots t_6$. $(2P) = t_{2P}$ best fit echo centroid path at times $t_{1P}, t_{2P}, \ldots t_{6P}$.

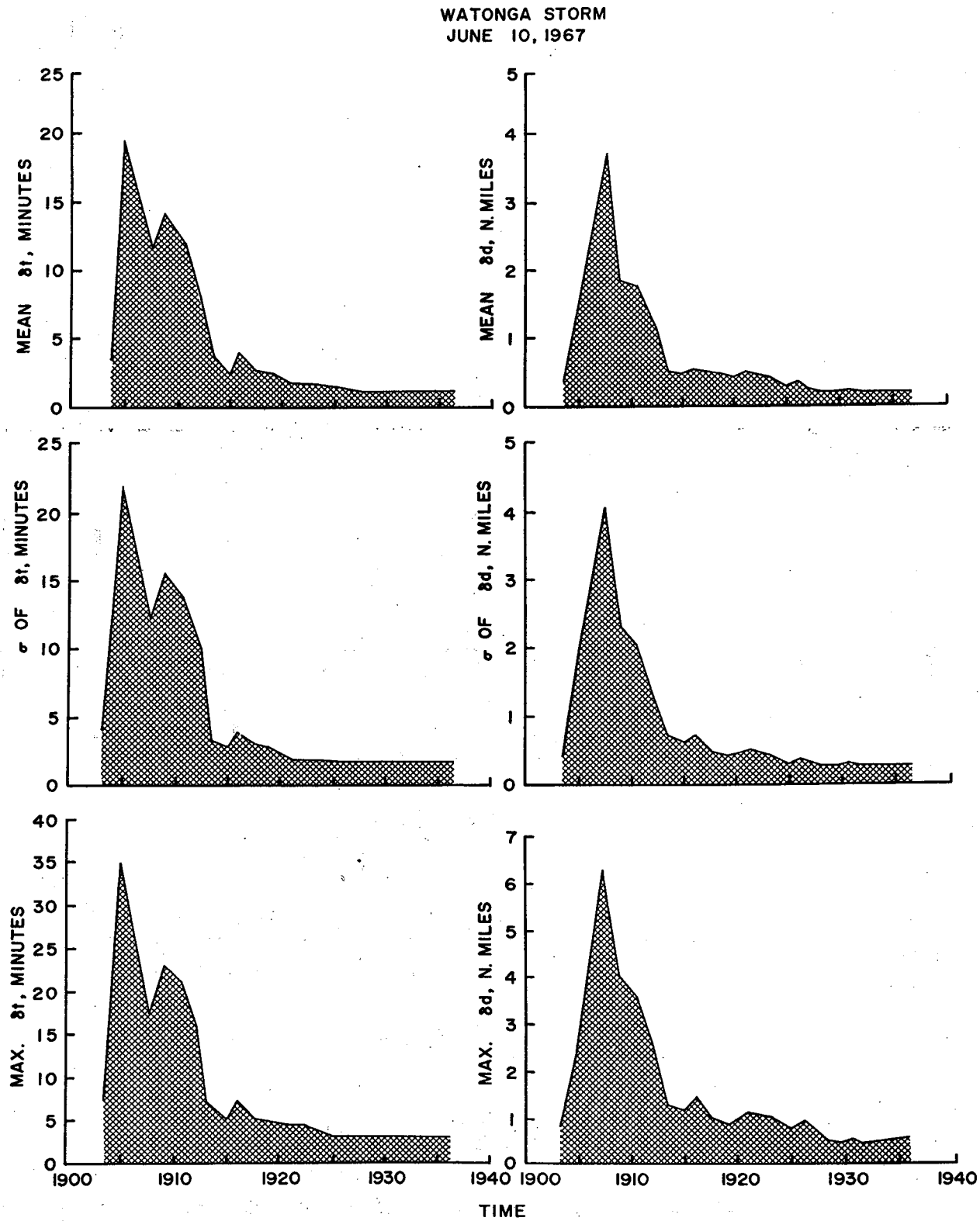

Figure 14. Tornadic storm, 10 June 1967. Mean, maximum and variance of temporal and spatial errors of linear extrapolation for period of extrapolation.

3.3 Application of Cell Track Extrapolation

Newton and Fankhauser (1964) suggested a semi-objective approach to forecasting the likelihood of thunderstorm occurrence at a specific point (such as a point on an airway or an air terminal) lying in the general region of the projected path of an existing thunderstorm. This method of probability forecasting uses the mean echo direction and the standard deviation, σ_d, derived from a study of many similar storms. Figure 15 shows the geometrical relationship among the angle σ_d, an echo core of diameter D, and a point distance R downstream. As illustrated, $R \approx 28D/\sigma_d$ where the standard deviation of direction, σ_d, is in degrees.

A modification of this technique uses the distance and time errors obtained from the linear approximation of the centroid motion of the individual echo (fig. 14). Maximum initial values of δt and δd (corresponding to 3 input centroids) for extrapolation over a 30-minute time period, are about 30 minutes and 6 n mi. Assuming normal distribution of the echo speed variation from centroid to centroid position, there is a 68 percent chance that the error in timing the arrival of the thunderstorm at point P is less than 30 minutes. If echo centroid directions are distributed normally, the direction of movement should be within the limits $\pm\sigma_d$, 68 percent of the time. A value of σ_d corresponding to the 6 n mi error (δd) would be approximately 22 degrees over a distance of

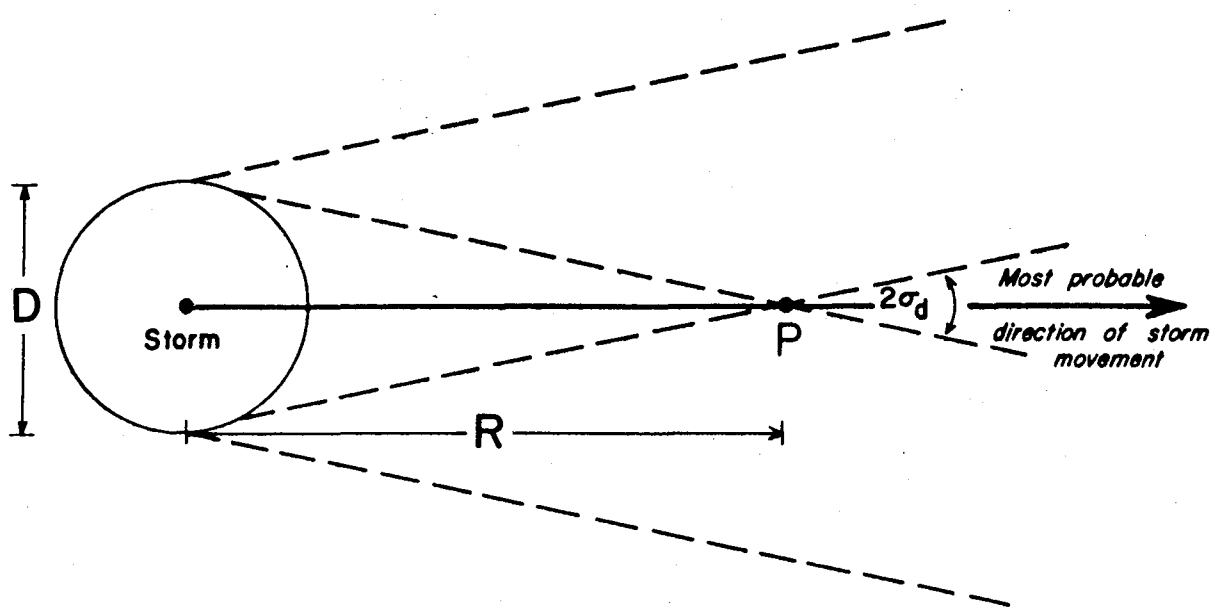

Figure 15. The standard deviation of storm direction is σ_d, and there is a 68 percent chance that a portion of the model storm will pass over point P. The percentage is larger for points interior to the dotted region between the storm and P, less for points at greater distance than R. (After Newton and Fankhauser, 1964.)

15 mi (a likely distance moved in approximately 30 minute movement prediction time). When σ_d is 22 degrees, the prediction distance R is approximately 1.3 times the diameter D.

As shown in figure 14, both δt and δd decrease as more centroid positions are added. In this example, after 12 input centroids, the maximum errors in extrapolation over the next 15 minutes are about 5 minutes and 1 n mi. However, this represents the final "degree of fit" to a linear path after most position data are available.

4. DIURNAL VARIATION OF SEVERE WEATHER

The extent of operational analysis of echoes for such purposes as cell track extrapolation is sensitive to the load imposed on the computer in handling all the data. Also the frequency of this load is to be considered. The marked diurnal variation of severe storms has been known and studied for many years. House (1963) points out that the frequency of tornadoes in the United States is strongly correlated with solar insolation (i.e., about 50 percent of the tornadoes in the past four decades have occurred between 3 and 8 pm). There is some sectional variation; for example, Oklahoma and Kansas experienced 62 percent of their tornadoes in this 5-hour period compared to only 36 percent in the region from Florida to Mississippi. Although no definite cause of the relatively large number of nocturnal occurrences in the Southeastern U.S. is known, recent studies (Pitchford and London, 1962) link these severe thunderstorms to the nighttime intensification of the low-level jet. Whatever the cause, the diurnal distribution of severe thunderstorms is an important consideration for radar operations and data processing systems. Automatic weather depiction, such as that planned for the National Airspace System (NAS), will obviously result in highly varying data loads on the computer and can be a major consideration in system design.

An insight into the magnitude of this problem is obtained from a review of a year's radar data (1966) collected at NSSL. Analysis routines were developed to give percent of echo coverage by intensity for each hour. These data were further simplified for this project by considering only those reflectivities equal to or greater than $10^3 mm^6 m^{-3}$. This was done so the coverage would correspond to that expected on the less sensitive Air Traffic Control (ATC) radars (Wilk et al., 1965).

Figure 16 shows the number of days versus the percent of echo detected by the NSSL WSR-57 weather radar that is equal to or greater than $10^3 mm^6 m^{-3}$. These percentages indicate the amount of the echo displayed by the WSR-57, which is also displayed by the less sensitive ATC radars operating with MTI and circular polarization.

The total number of days on which intensities equal or exceeded $10^3 mm^{6m-3}$ occurred are shown under the time. The maximum number of occurrences (55 days) was at 1500 CST, with a strong secondary maximum (53 days) at 0300 CST. The minimum number of occurrences (31

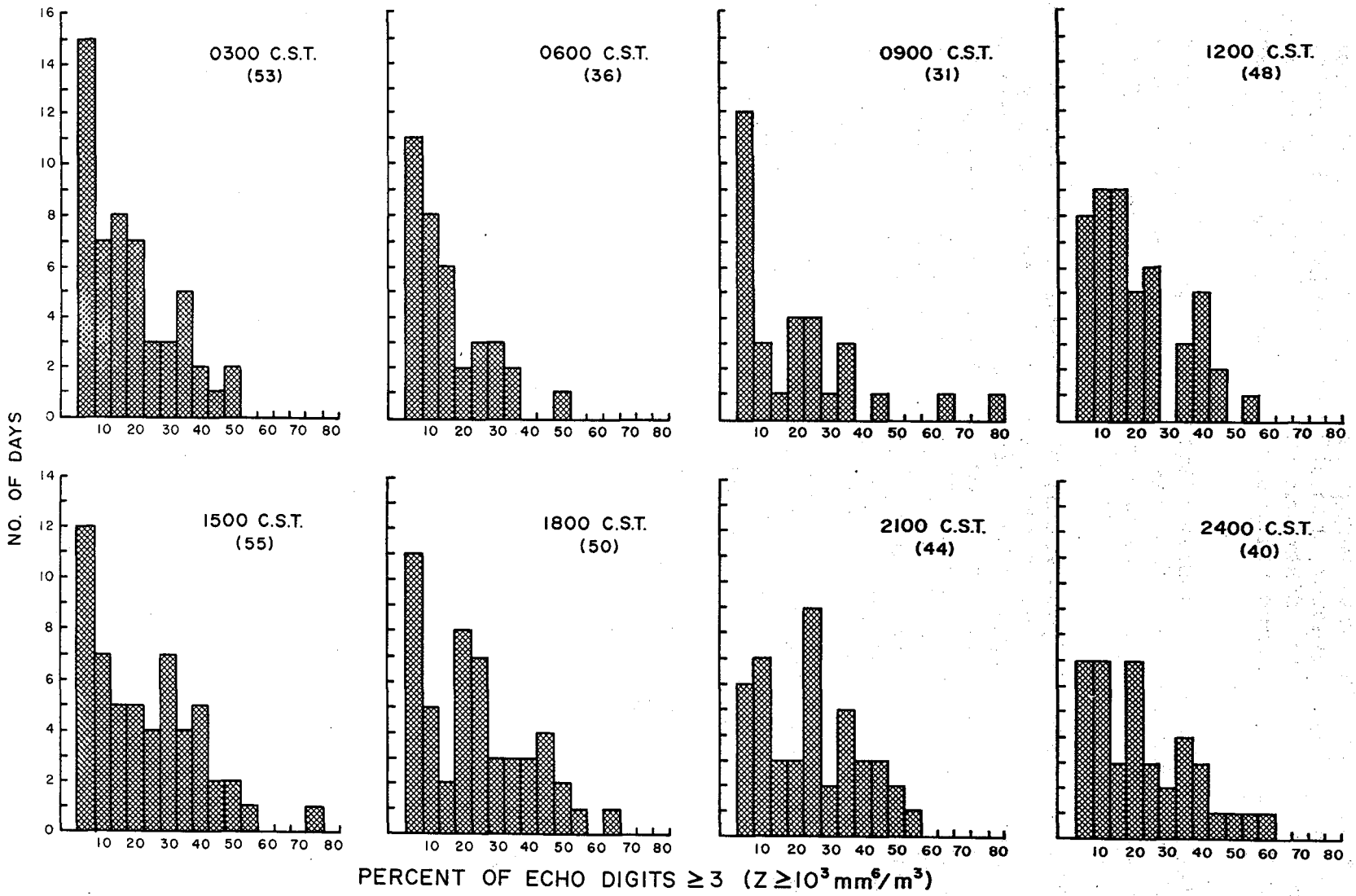

Figure 16. Distributions by time of day of the percent of echo intensity integers which equal or exceed $10^3 mm^6 m^{-3}$.

days) was at 0900 CST. The average percentage of the WSR-57 radar echo area equal to or greater than $10^3 mm^6 m^{-3}$ maximizes at 2100 CST; however, the shape of the distribution remains similar for all times of day, and the most common value of echo area $\geq 10^3 mm^6 m^{-3}$ is less than 10 percent.

The distributions of hourly coverage are typically noisy and reflect the importance of a few intense storm periods on the annual distribution. In fact, most of the severe weather events in Oklahoma during 1966 occurred on only 31 days.

ATC radars generally show only those storms of at least moderate intensity, and do not as yet have contoured displays to discern between moderate, strong, and very strong echoes. Because of this limitation, it is important to determine the agreement between the moderate threshold and severe weather. Figure 17 shows the severe weather events as reported by surface observers, plotted against the percentage of radar echo area equal to or greater than $10^3 mm^6 m^{-3}$ and according to time of day. As expected, there is a preference for severe weather to occur between 1600 CST and 2200 CST. This corresponds to the 1500 CST peak in occurrence of $Z \geq 10^3 mm^6 m^{-3}$ echoes. There is a poor correlation between the percentage coverage of moderate intensities and the number of severe weather events (i.e., the range of the percentage coverage

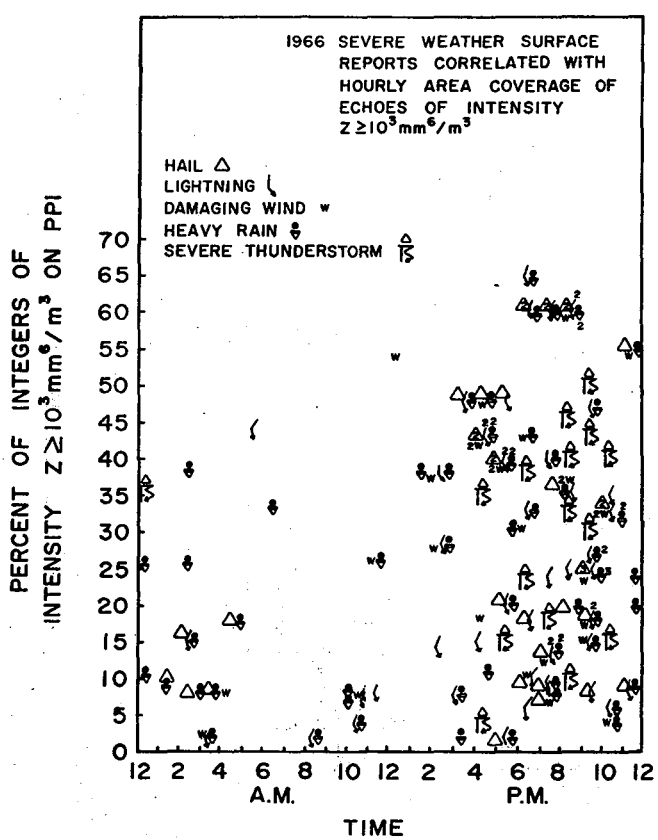

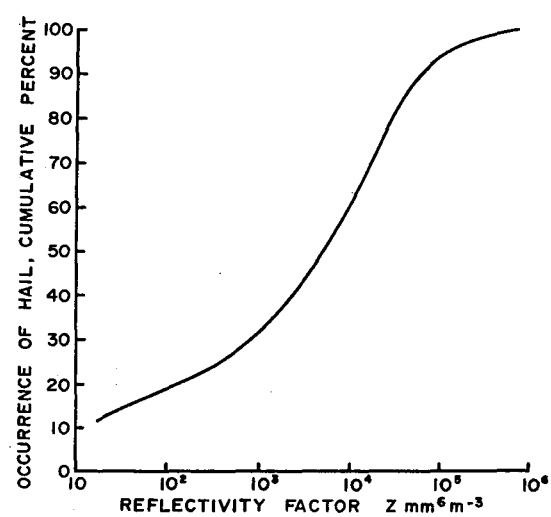

Figure 17. (left) Severe weather events and the corresponding percent of echo intensities which equaled or exceeded $10^3 mm^6 m^{-3}$ by time of day.

Figure 18. (above) Cumulative percent of hail occurrences versus WSR-57 radar echo intensity measurements.

of $10^3 mm^6 m^{-3}$ is broad, showing that with or without severe weather the amount of $10^3 mm^6 m^{-3}$ echoes relative to the total echo varies greatly and is not an indication of the storm severity). The coverage of $10^3 mm^6 m^{-3}$ echo is not related to the existence of $10^5 mm^6 m^{-3}$ cores, which are well correlated to severe weather events (Ward et al., 1965). The agreement between maximum cell intensity and surface hail reports (fig. 18) shows the cumulative frequency of hail reports against radar reflectivity factor measured at the position of the surface hail report.

5. SURFACE WIND GUSTS ASSOCIATED WITH SEVERE STORMS

The intensity of the radar echo provides a quantitative measure of the precipitation rate and a qualitative indication of hail. However, little information can be derived about the extent and magnitude of wind gusts. This is a serious limitation, since the cold air outflow from severe storms spreads horizontally for several miles and can produce sudden changes in wind speed and direction far in advance of the radar echo. Fujita (1963) summarizes numerous mesoscale studies that document the complexity of the surface pressure, temperature, wind, and precipitation fields associated with thunderstorm systems. The Browning-Ludlam steady-state model of convection (Browning and Ludlam, 1962) and the study by Newton and Newton (1959) of the dynamical interaction of the storm with its environmental wind field have suggested that downdrafts are intensified and steadied by the vertical transfer of fast moving air downward to the surface. Although radar observations are used intuitively to support these and other theories of air motion, there is, as yet, no quantitative method for deducing the air flow associated with the echo intensity fields.

Occasionally, radar detects the boundary (high density gradient) line on the cold air interface. These "thin" lines are coincident with the wind shift and provide reliable information about its motion (Bigler, 1959). Until radar has the capability of routinely detecting and displaying the horizontal field of motion, we must rely generally on surface wind observations to delineate hazardous gust lines. The following sections describe the surface wind conditions associated with three squall lines observed in 1969. The radar data for two of these storms were used in the echo motion study discussed earlier.

For the 1969 severe storm observational program, NSSL installed and operated a 29-station network in an 800 square n mi area to the southwest of Oklahoma City. These field sites were equipped with cup anemometers, hygrothermographs, microbarographs, and raingages. The data were recorded on strip charts as analog traces with a time resolution of 1 to 2 min. The anemometer chart speed was 3 in. per hour and recorded a severe storm gust 'event' typically as shown in figure 20. These records were reduced manually by tracing the envelope of the maximum and minimum values and digitizing the smoothed traces at 1 min. intervals over the period of interest. The envelope values were then

averaged to find the mean, and the differences were taken as a measure of the variance.

Within the gust front, the 1-min mean and variance are strongly related. Figures 20, 21, and 22 illustrate this relationship for the storm of 29 May 1968. The stations show considerable variation in scatter, which may be caused by site exposure. Stations that were suspect were relocated in 1969 for the current study. Although equal station spacing was desirable for areal analysis, the sites were selected primarily by the quality of exposure.

An objective analysis technique developed by Barnes (1964) was used to space interpolate the 5-min running average of the 1-min mean values of the maximum wind speed data over a fine grid mesh within the mesonetwork. This technique assumes the distribution of the observed parameter is representable by the summation of an infinite number of independent sine waves, and that the interpolated value at a grid point is determined by the summed influence of all surrounding observations weighted according to their distance from the grid point. The weight function is

$$W = \exp(-r^2/c) \quad , \tag{9}$$

where r is the distance from the observation site, and c is a constant that determines the rate at which the influence of the datum decreases with distance. The interpolated value at grid point (x,y) is given by

$$g(x,y) = \sum_{i}^{N} W(r_i)\ V_i / \sum_{i}^{N} W(r_i) \tag{10}$$

where V is the wind speed and N is the number of observations.

Usually, application of such a weighted averaging technique considerably smooths small scale variations (small in relation to the spacing between stations). However, it has been shown that an iterative procedure can be used to obtain an interpolated field that fits the observed data to any degree of precision desired (Barnes, 1964). The degree of fit is determined from considerations of the accuracy of the observations and the application of the analysis. If the data are relatively accurate and one wishes to depict the smallest details of the distribution (i.e., waves twice the length of the average station spacing), then a close fit to the observed data is required.

In the present analyses, variations with wave lengths of twice the station spacing (12 n mi) are smoothed to two-thirds their indicated amplitude, while waves three times the length of station spacing (18 n mi) are represented to about 90 percent of their amplitude.

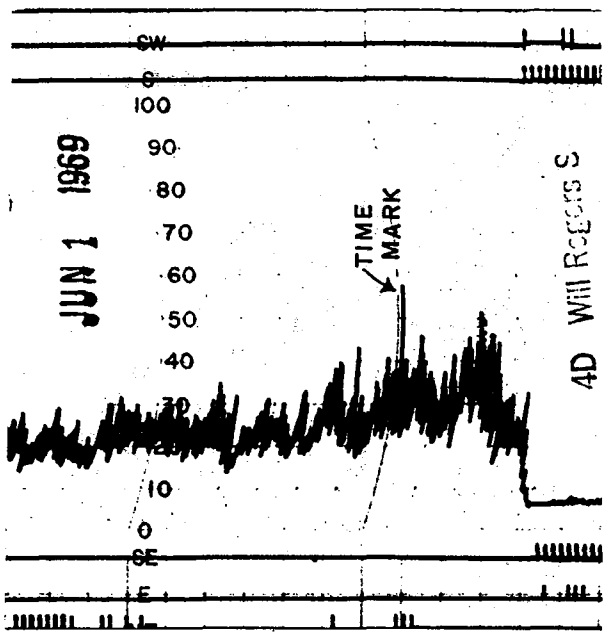

Figure 19. Surface wind velocity record, 31 May 1969, Will Rogers International Airport, Oklahoma City.

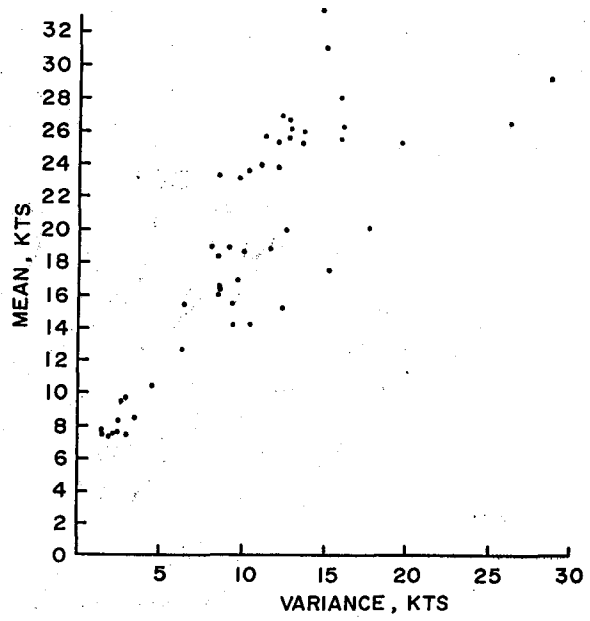

Figure 20. Data for Station "A" showing relation between mean wind speed and speed variance during gust front of 29 May 1968.

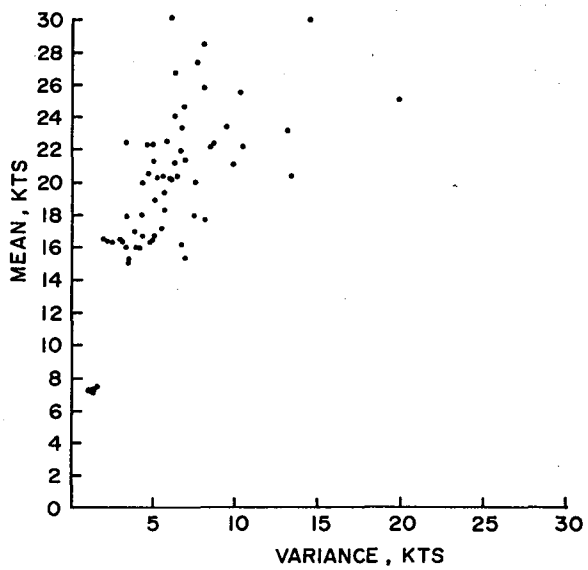

Figure 21. Data for Station "B" showing relation between mean wind speed and speed variance during gust front of 29 May 1968.

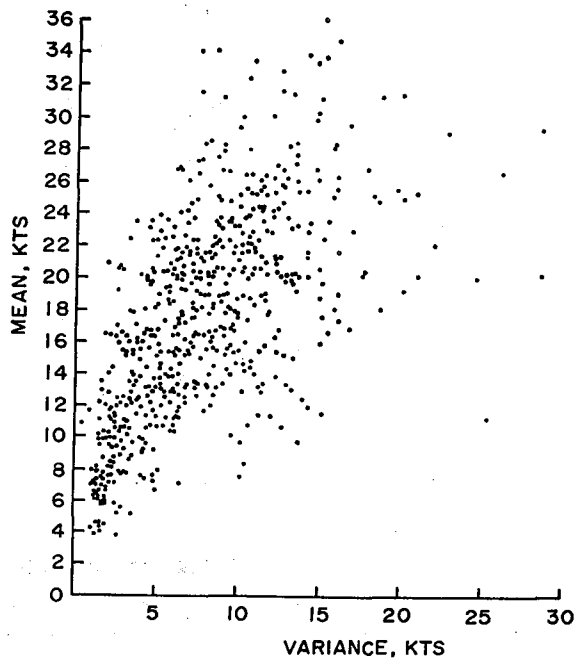

Figure 22. Data for all stations showing relation between mean wind speed and speed variance during gust front of 29 May 1968.

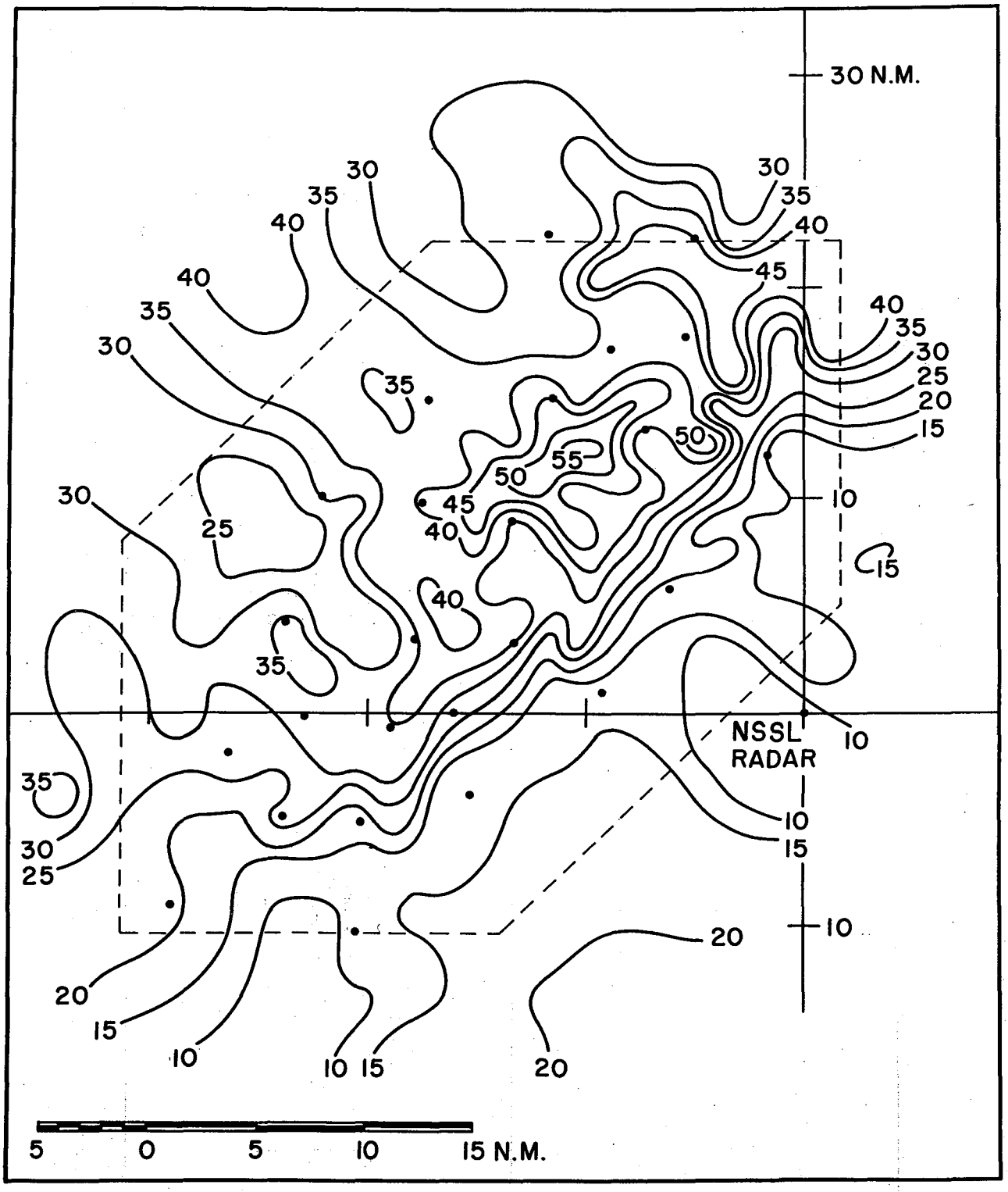

Figure 23. Subjective analysis of the wind speed field, 2342 CST, 31 May 1969. Field was obtained by time to space conversion using the wind shift line velocity of 315°/38 kts.

This is illustrated by considering a time-space analysis of a typical trace recorded during the strong gust front on 31 May 1969 (fig. 19). The time between the wind shift and the maximum gust is about one-half the period of the gust front disturbance. The wave length is defined as

$$\lambda_{n\ mi} = V_s P/60 \quad ,$$

where V_s is the translational velocity in knots and P is the period in minutes. For an average period of 34 min (fig. 19) and a translational velocity of 38 knots, the wave length is about 22 n mi. This distance corresponds to about three and a half times the station spacing and should result in a gust amplitude smoothing of about 10 percent in the Barnes' objective interpolation. This logic was tested by comparing a 'hand' analysis (fig. 23) of a time to space conversion with the analysis by the objective technique. The two sets of grid overlay values were plotted, as shown in figure 24; comparison of the 'best fit' and the 1:1 line confirm that the high values are smoothed about 10 percent by the objective technique.

In the first analyses, the times of the gusts were used as input. Three major squall lines that occurred on April 16, April 26, and May 31 were analyzed in this manner. In addition, the May 31 case was analyzed in detail to study the temporal development and motion of the gust front.

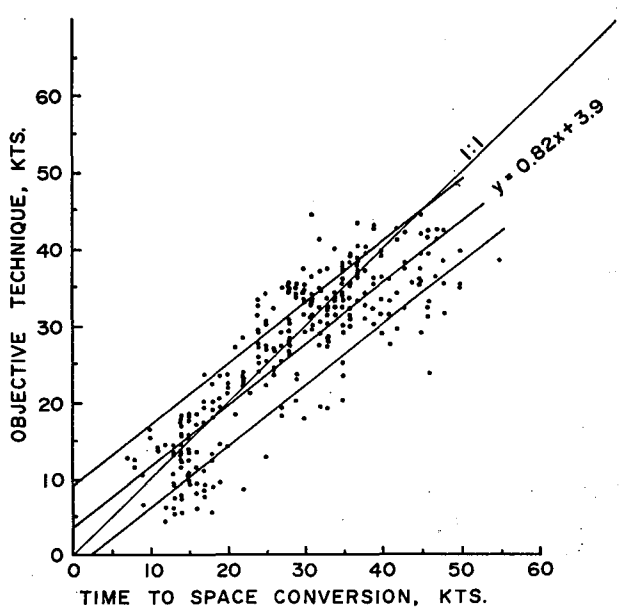

Figure 24. Comparison of space interpolated values of the wind speed between the Barnes' objective technique and the time-space conversion technique.

5.1 Gust Characteristics

The storm of the 16th was an organized squall line with several strong centers of convection easily located on the WSR-57 radar displays. Figure 25 shows the horizontal sections at 0, 1, and 2 degree antenna tilt. Initially, the boundary of the cold air was in juxtaposition with the leading edge of the echo and then gradually accelerated ahead of the storm as it moved through the network.

The squall line on April 26 was similarly well organized, as shown in figure 26. The perturbation marked by the arrow is probably a tornado cyclone. An associated funnel caused considerable damage near Chickasha, Oklahoma, at 1702 CST. There were at least two damaging funnels reported in the squall line, but the high winds covered a very small area; since they were not detected by the mesonetwork, this did not affect the analysis of the mesoscale data.

The squall line of May 31, illustrated in the radar display in figure 27, differed from the other two cases in that it occurred near midnight, had less intense precipitation, and was not as well organized (as displayed by the radar). The surface wind gusts, however, were more severe and better organized than in the other two cases. The cold air outflow was ahead of the precipitation (marked by the arrow on figure 26) when it entered the network. The gust front had moved well in advance of the echo by the time it reached Oklahoma City.

The overlay grid used in the objective analysis is superimposed on the network map shown in figure 28. The 20 x 20 matrix covers the 800 sq mi area of the network with a mesh size of 1.7 n mi. The interpolated grid values were used to determine the areal probability histograms shown in figures 29, 30, and 31. On April 16 about 38 percent of the area experienced gusts of a magnitude between 35 to 40 knots. On April 26 the range of gusts was similar, but the 30 to 40 knot interval was even more dominant, covering nearly 75 percent of the area. The data for the May 31 storm showed higher maximum values but again the 35 to 40 knot interval was most common. In degree of severity (over the network) the storms are ranked in the order of the 26th, 16th, and 31st, having corresponding 10 percent probability values greater than 40, 45, and 50 knots, respectively.

It is important to note that these wind speed values are 5-min averages of the smoothed envelope. There were many 'spikes' in the wind traces which exceeded these values by 5 knots. Another 5 knots of suppression results in the objective analysis, so that local excursions of the order of 10 knots occurred instantaneously throughout the network, and the probability of singular values should be adjusted accordingly.

The gust front on May 31 was especially interesting because of its continuity in time and space. The gust records for the 29 stations were 'digitized' over the same 90 min interval, and the 5-min running averages were then objectively analyzed. (The 5-min wind speed maps

(c)

(b)

(a)

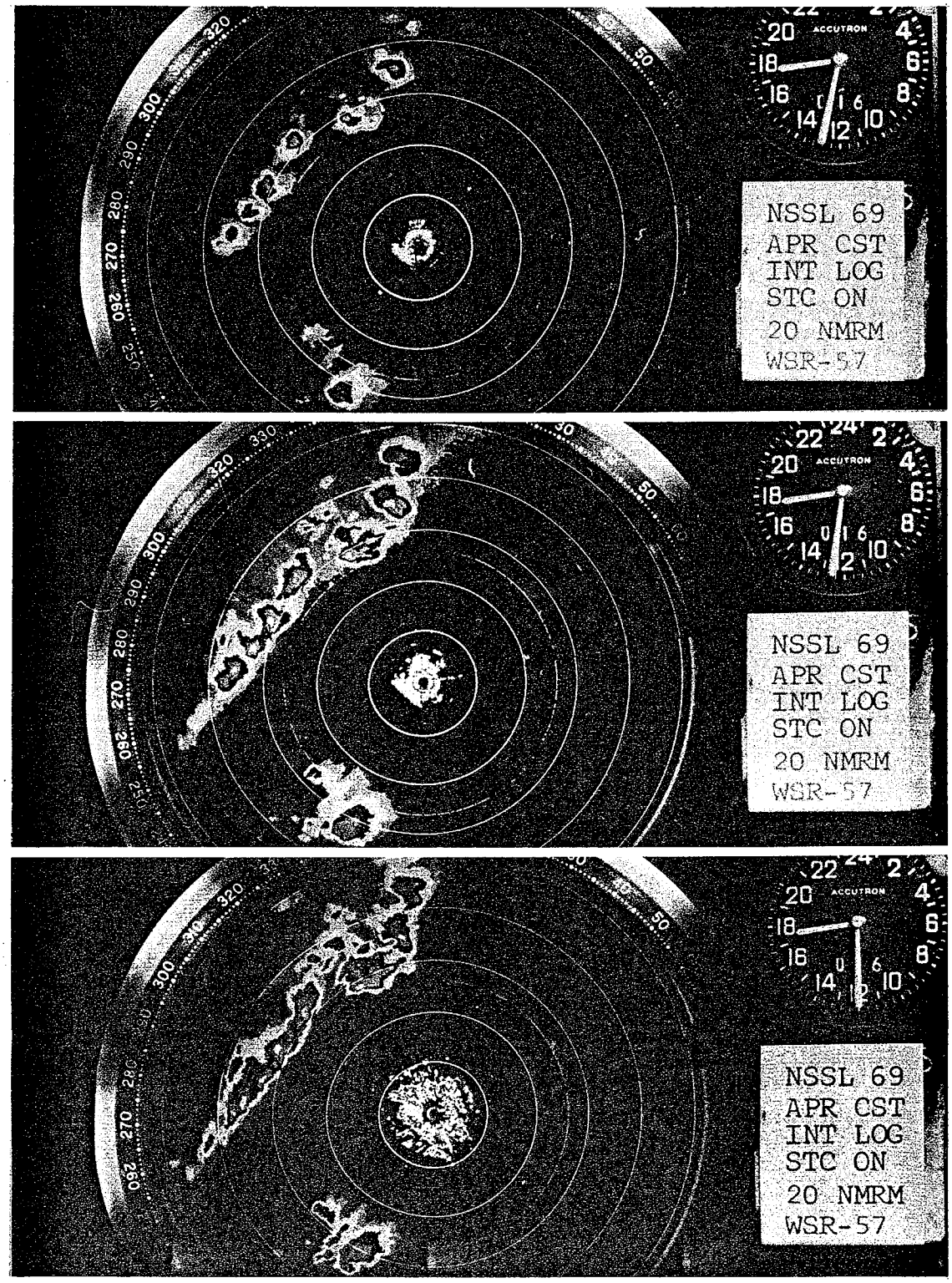

Figure 25. WSR-57 radar contoured 100 n mi. display for 16 April 1969. The first intensity level, $Z = 10 mm^6 m^{-3}$; bright cores, $Z = 10^5 mm^6 m^{-3}$. (a) antenna tilt is zero degrees (mean beam altitude of 2400 ft at 60 n mi.) (b) antenna tilt is one degree, (beam altitude of 8700 ft at 60 n mi.) (c) antenna tilt is two degrees, (mean beam altitude of 15,200 ft at 60 n mi.)

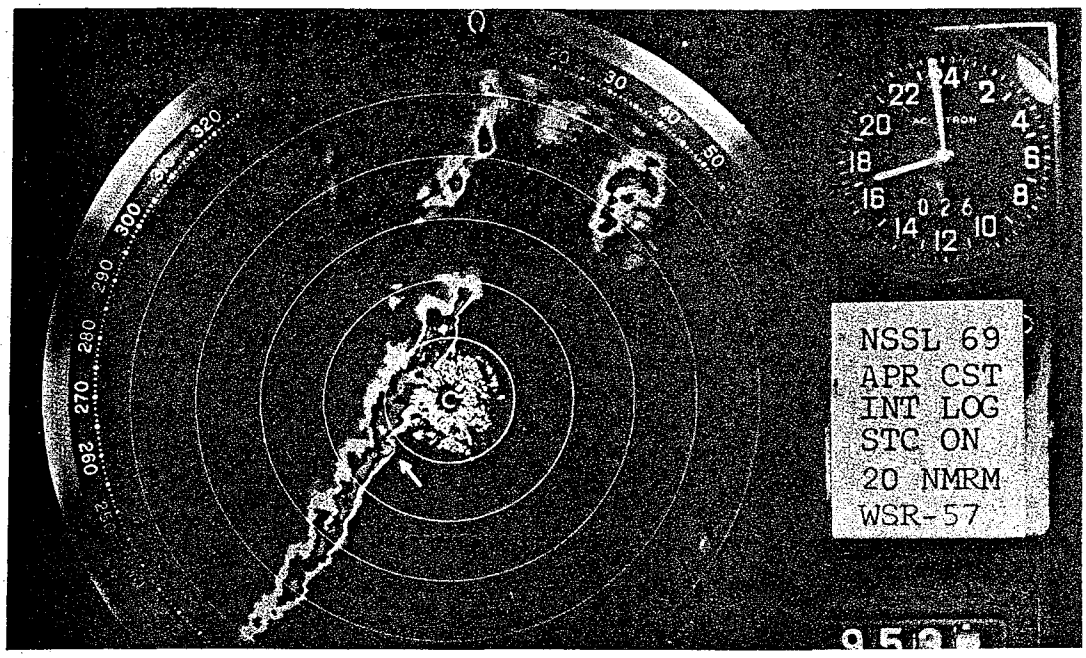

Figure 26. WSR-57 radar contoured display for 26 April 1969. Range marks are 20 n mi. The intensity levels are approximately 10 db steps and correspond to radar reflectivity factor (Z) values from 10 to $10^5 mm^6 m^{-3}$. The arrow points to a small scale circulation probably associated with a reported funnel.

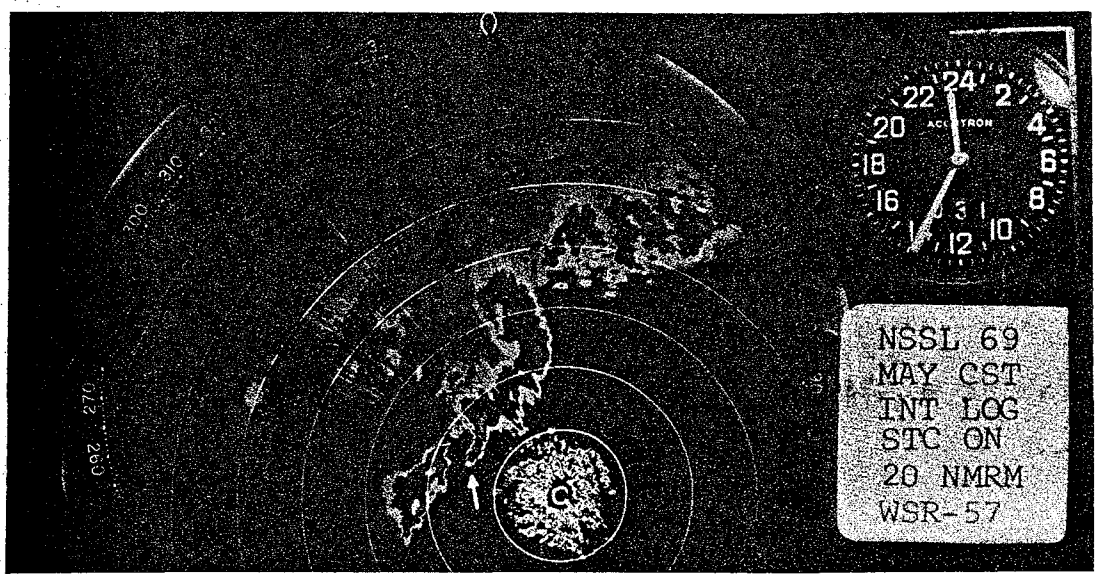

Figure 27. WSR-57 radar contoured display for 31 May 1969. Range marks are 20 n mi. The arrow marks the precipitation best correlated with the orientation and motion of the strong gust front.

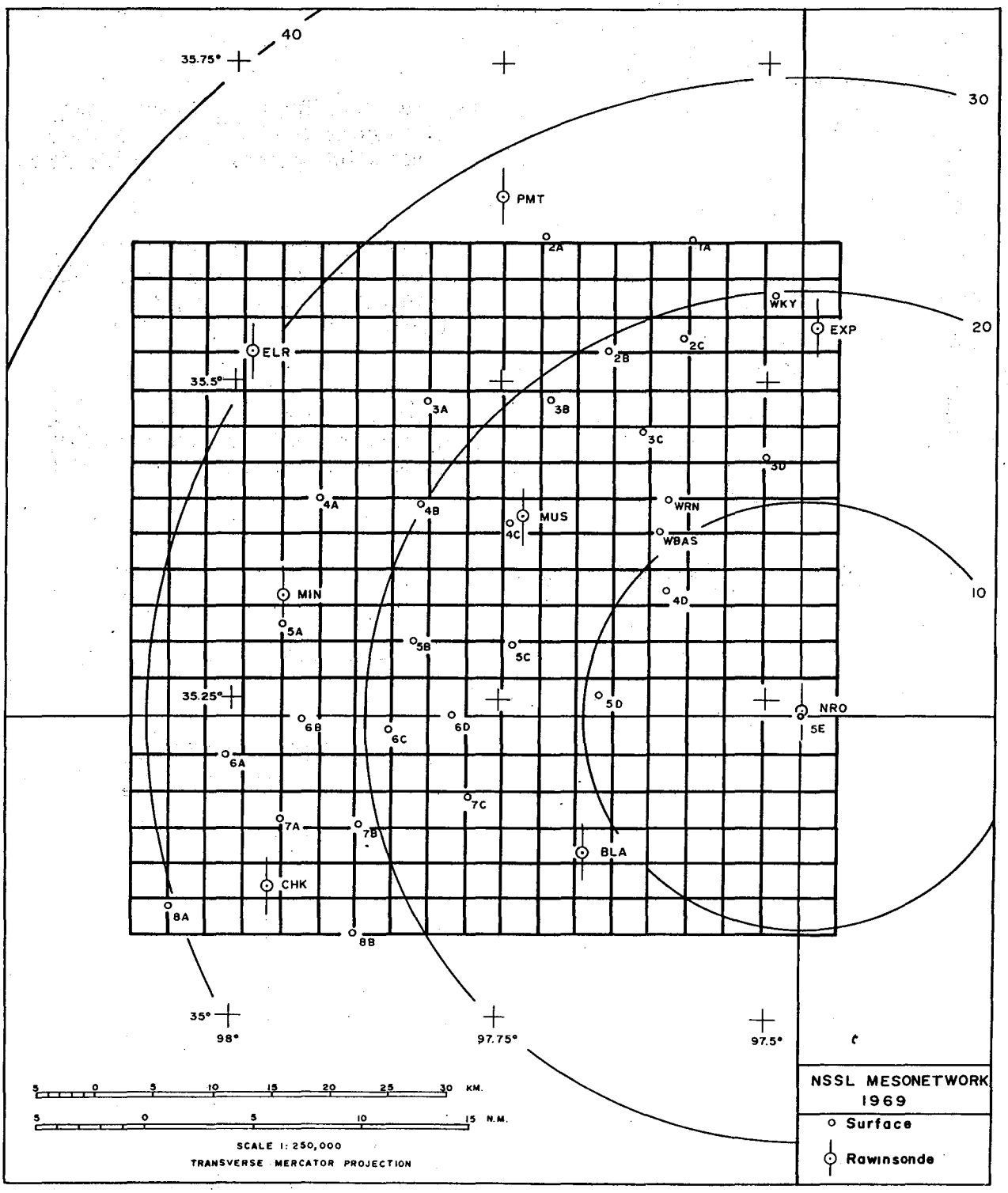

Figure 28. NSSL surface network and objective analysis grid.

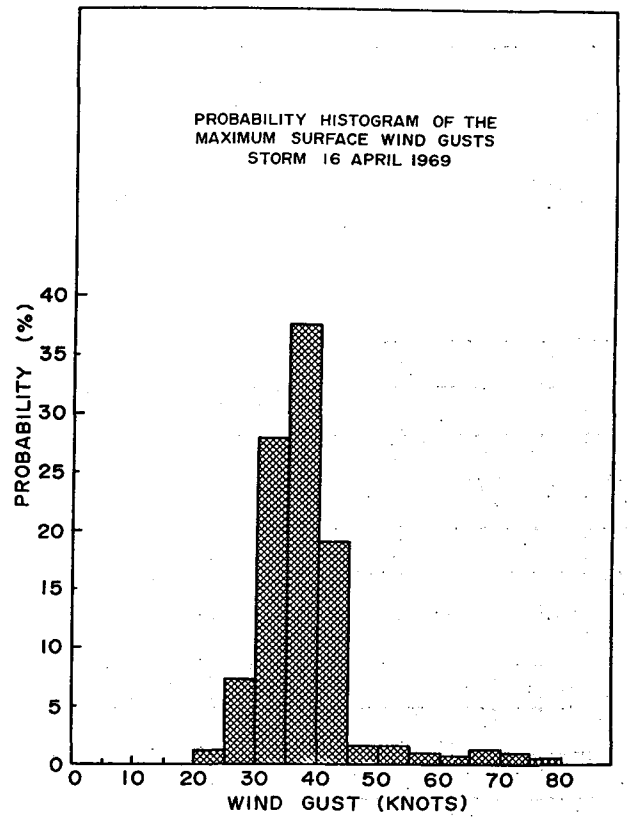

Figure 29. (left) Probability histogram of the maximum surface wind gusts, 16 April 1969.

Figure 30. (below, left) Probability histogram of the maximum surface wind gusts, 26 April 1969.

Figure 31. (below) Probability histogram of the maximum surface wind gusts, 31 May 1969.

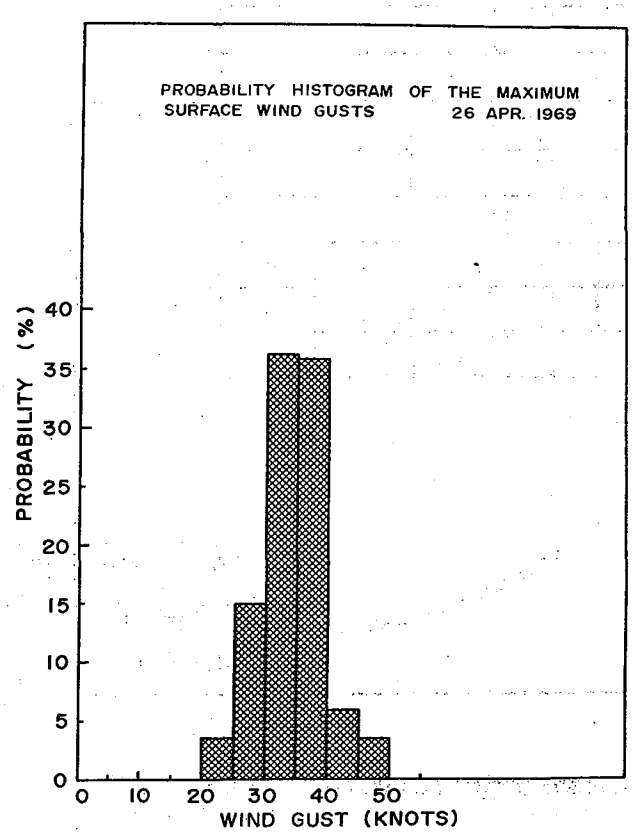

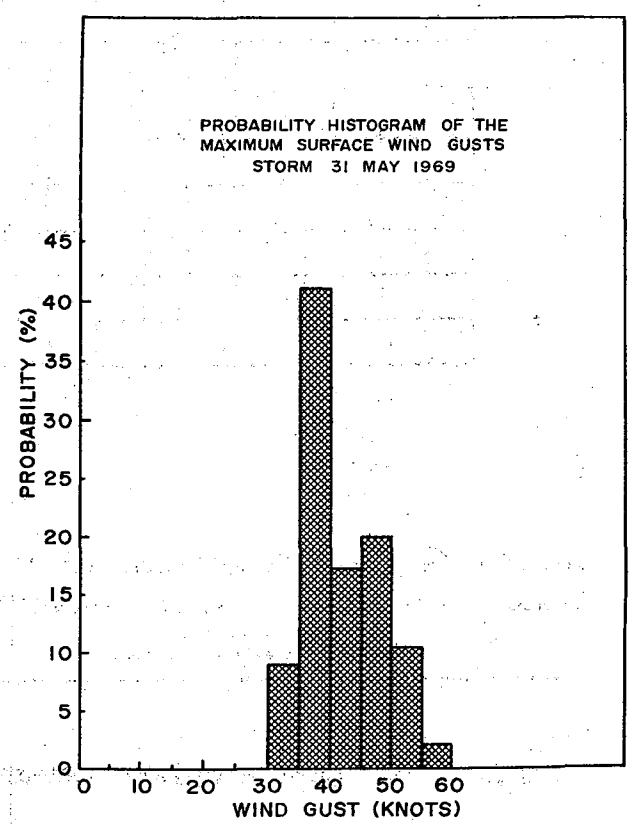

for a 25-min period are shown in appendix B). Changes in the frequency distribution of maximum wind gusts in the network area during the gust front passage are shown in figure 32 (see also figs. 33 through 36). At 2327 CST, the network was under the pre-squall southerly airflow with over 50 percent of the area experiencing gusts between 10 and 15 knots. By 2332 CST, the gust line was entering the western edge of the network, and, by 2342 CST, a bimodal distribution was evident, with 30 percent of the area exceeding 40 knots. The network was most affected by the gust line at 2357 CST, with over 70 percent of the area experiencing sustained gusts in excess of 30 knots. After 0030 CST, the gust spectrum again narrows to reflect the 'cold air mass' environment and the mean gust speed has subsided to less than 30 knots.

Figures 34 and 35 are objective analyses of the wind speed and direction at 2332 CST. By mentally overlapping these fields, one can see the band of strong shear about 4 miles in width, that constitutes the gust hazard to aviation. A plot of the directions of the gusts versus magnitudes in the overlap area (fig. 33), shows the strong veering that occurred as the average gust speed increased. First and second degree "best fit" functions were obtained as a possible operational guide to prediction of cross wind magnitudes. Obviously, the degree of fit will vary from storm to storm, but these data suggest that real time analysis of this type are practical.[1]

The thunderstorm project and later studies (Fujita, 1963) have shown the passage of the discontinuity with the cold air outflow is characterized by a sequence of pressure rise, wind shift, maximum gust, temperature fall, and rain, in chronological order. This is typical of the squall lines observed in 1969.

The distributions of times between wind and rain events as recorded at the 29 stations are shown in figures 37 and 38 for the storms of April 16 and May 31. On the 16th, the differences between wind shift and rain were small at the start but increased to as much as 50 min (which resulted in the skewed distribution). On the 31st, none of the stations experienced a difference less than 20 min, with the mean being greater than 30 min. The gust fronts with both storms were preceded by a sudden pressure rise. Figures 39 and 40 show average differences of 5 to 6 min and 2 to 3 min for the 16th and 31st storms, respectively. The magnitudes of the rises were much larger on the 31st, ranging from 0.17 to 0.27 inches. This corresponds to an average change in altimeter of about 200 ft.

5.2 Wind Shear and Aircraft Operations

Surface weather hazardous to aircraft operations, particularly during flight at our near terminals, includes strong winds, strong wind shear, and gustiness. The vertical distribution of the rapid

[1] Y. Sasaki, University of Oklahoma, has applied variational techniques to the objective analysis of this case (unpublished manuscript, 1970).

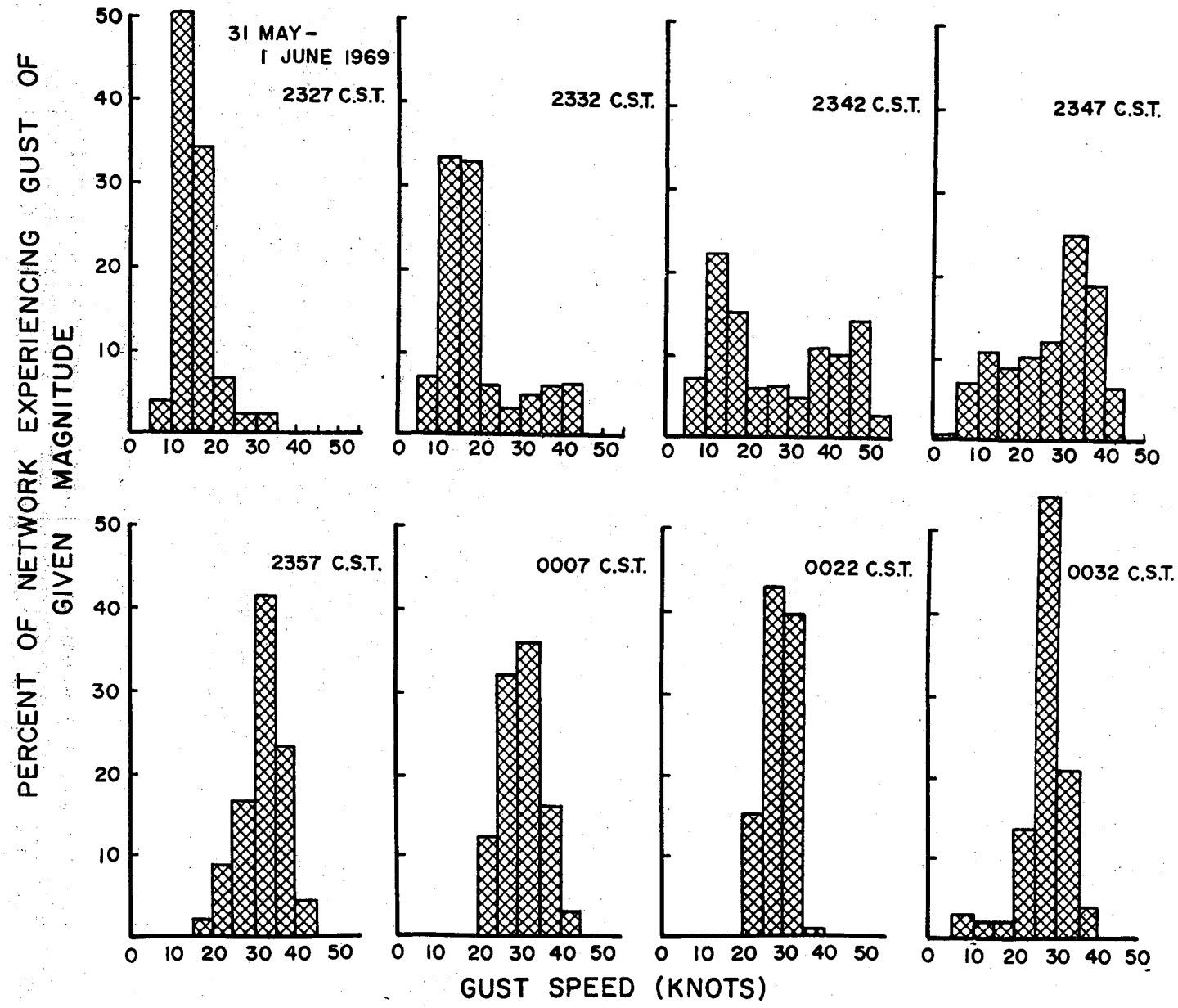

Figure 32. Probability histograms of the maximum surface wind gusts, storm of 31 May 1969.

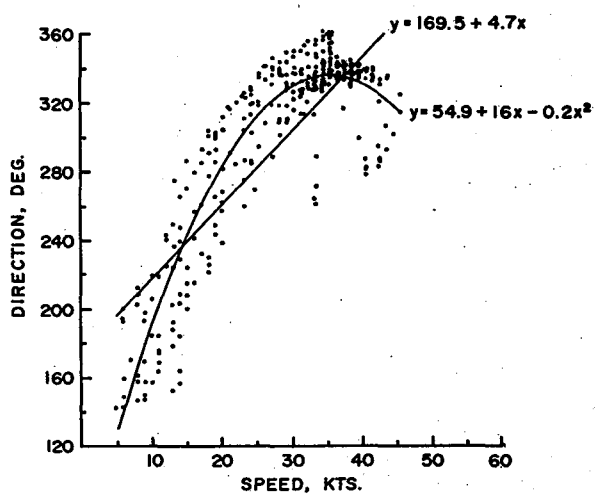

Figure 33. Relation between wind speed and direction during gust front, 31 May 1969.

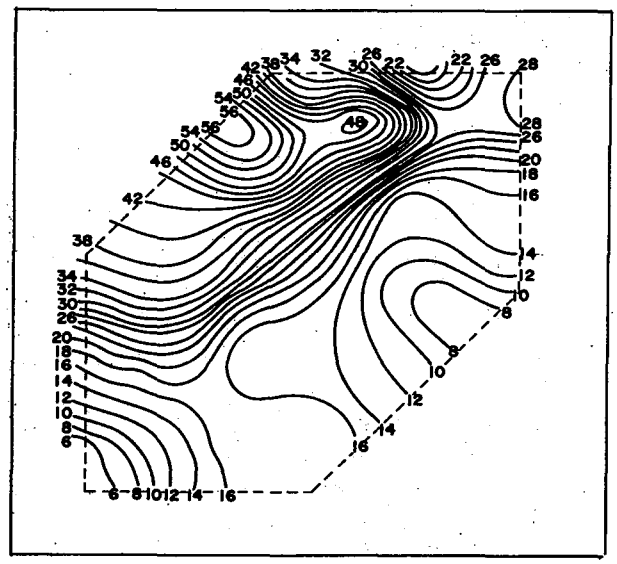

Figure 34. Wind speed analysis obtained by Barnes' technique for 2332 CST, 31 May 1969.

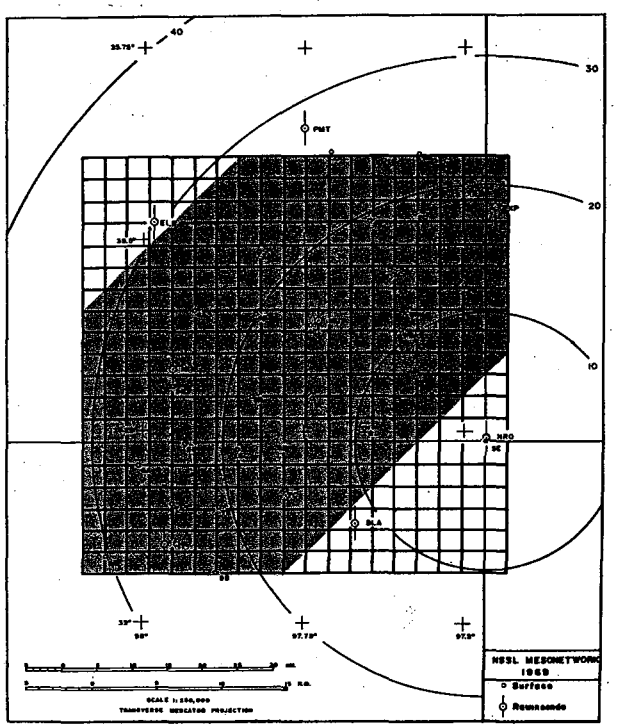

Analysis Area

Figure 35. Objective analysis grid.

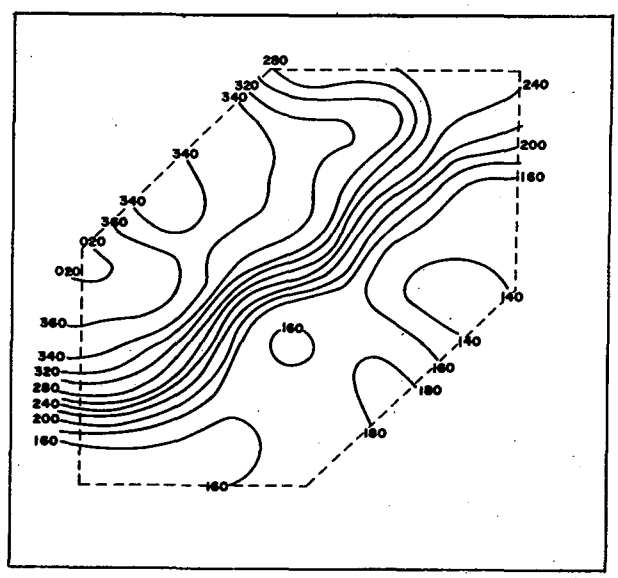

Figure 36. Wind direction analysis obtained by Barnes' technique for 2332 CST, 31 May 1969.

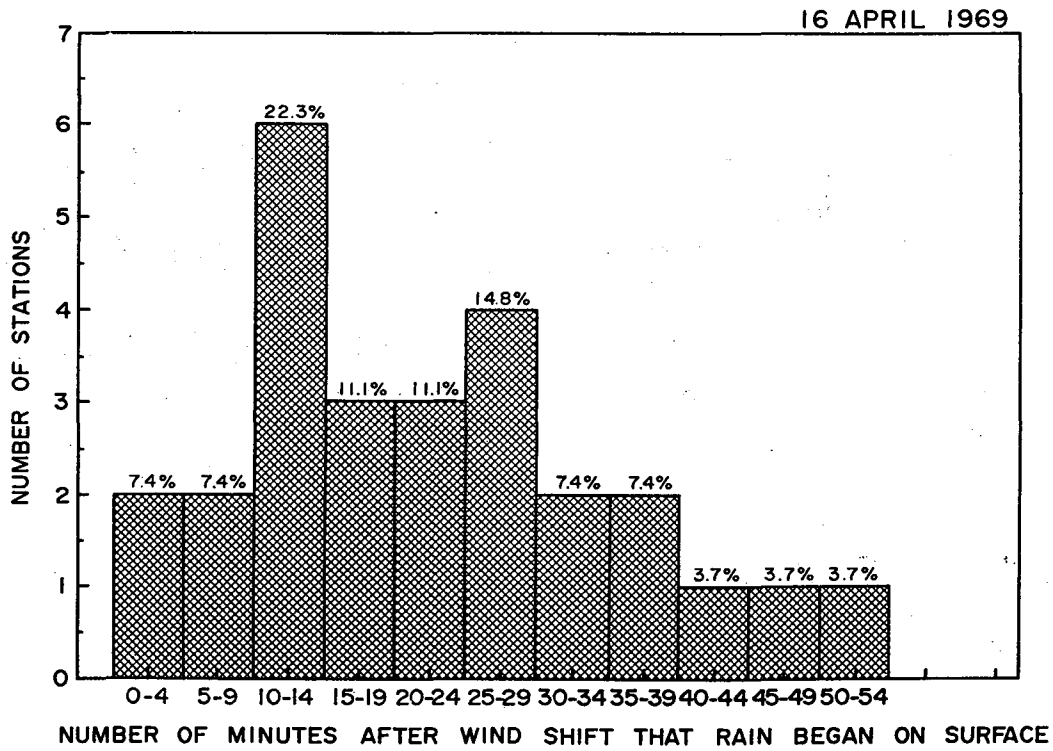

Figure 37. Frequency distribution of time differences between wind and rain events on 16 April 1969.

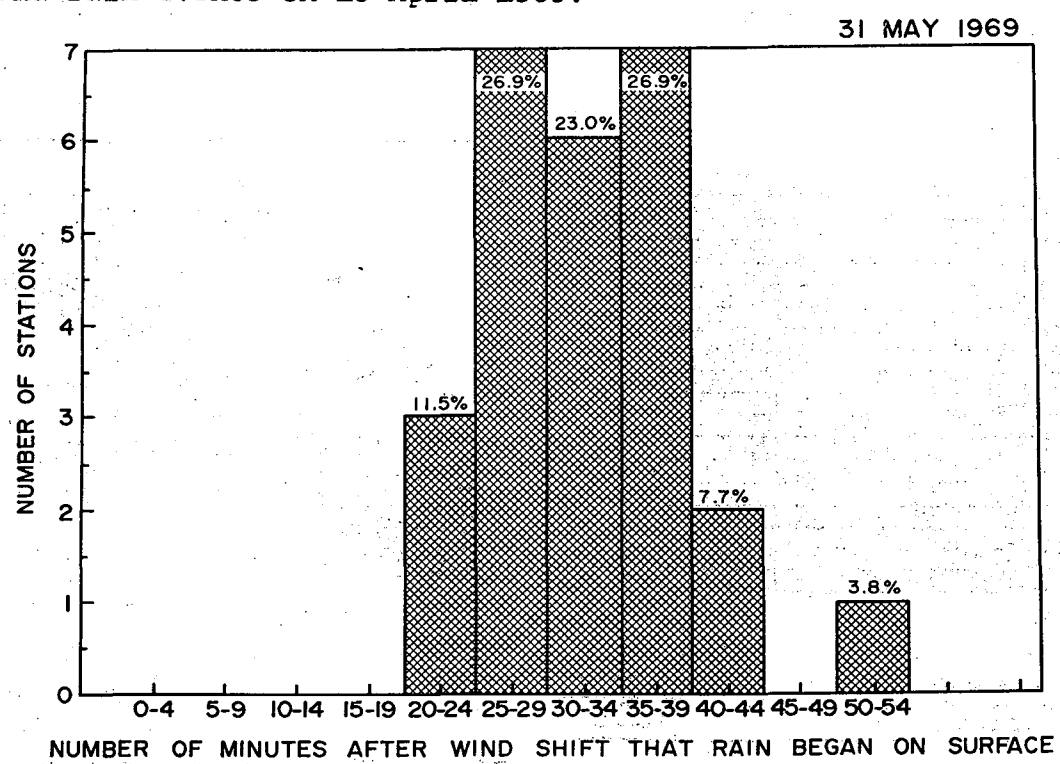

Figure 38. Frequency distribution of time differences between wind and rain events on 31 May 1969.

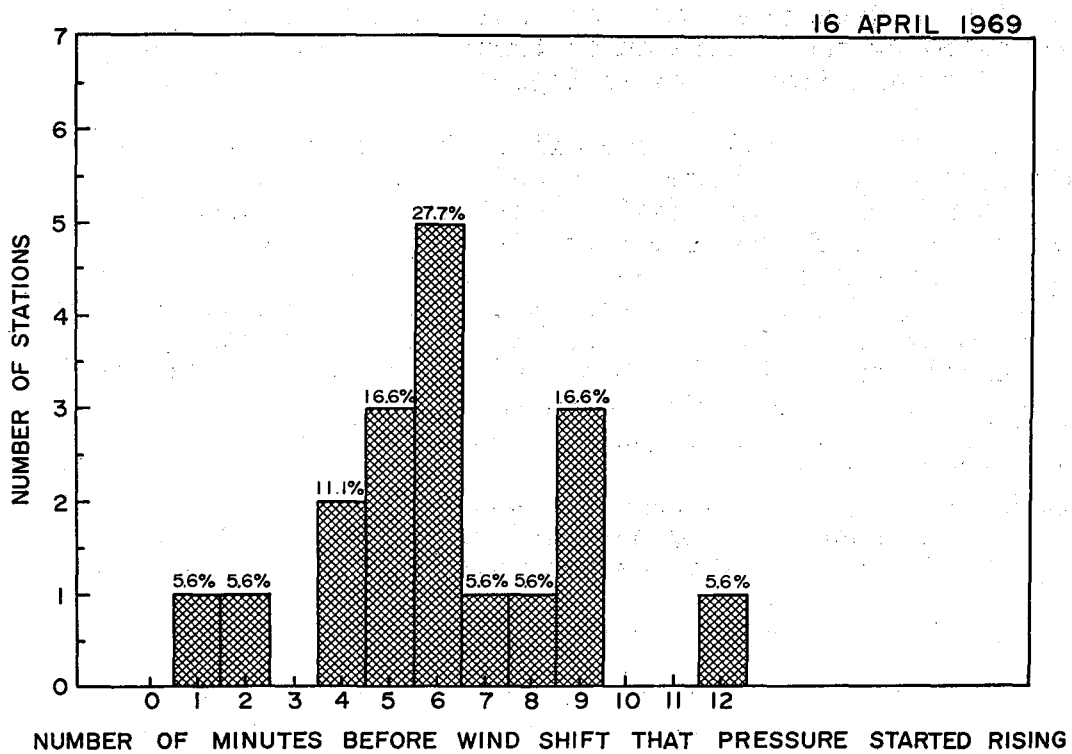

Figure 39. Frequency distribution of time differences between wind and pressure events on 16 April 1969.

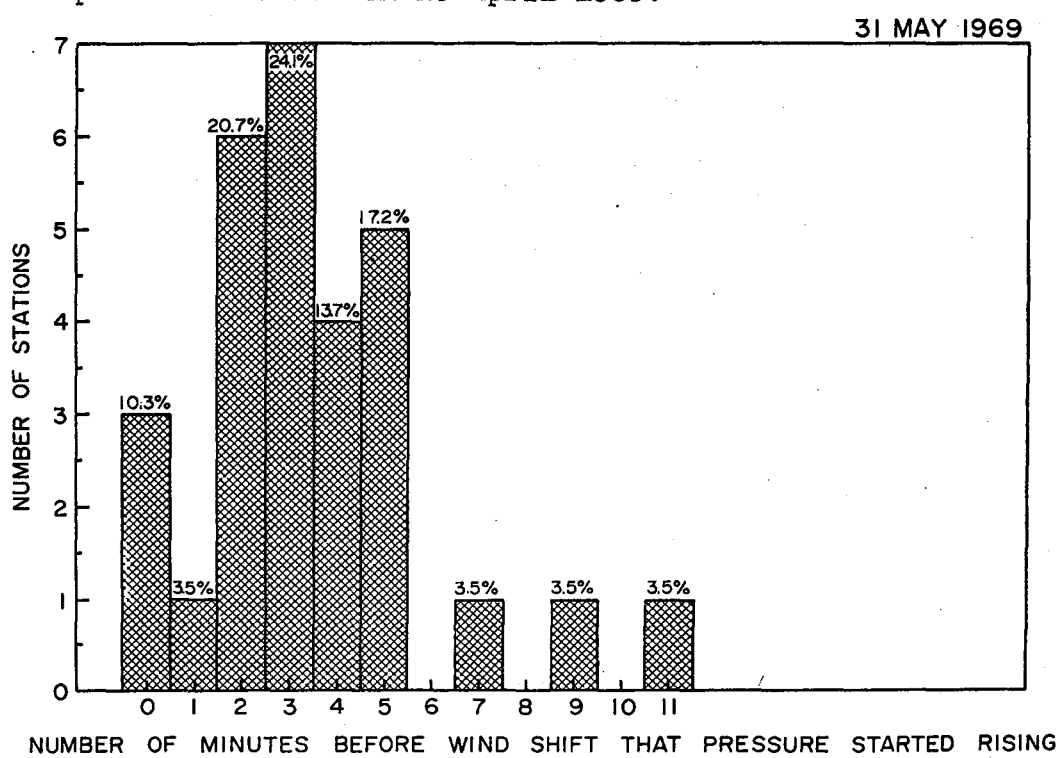

Figure 40. Frequency distribution of time differences between wind and pressure events on 31 May 1969.

changes in both direction and speed which occur along wind shift lines is illustrated by the instrumented tower wind readings during the 31 May 1969 squall line shown in figure 41.

Browne (1961) discusses the effect of wind shear on airspeed of aircraft. Traversing a strong wind shift line on a landing approach can affect landing precision; landing short if the pilot underestimates the shear associated with the line, and landing long if he overestimates the shear. The aircraft can encounter considerable "buffeting" caused by the turbulent energy associated with strong wind shear. Traverse of a wind shift line can also cause an aircraft to stall because of a sudden decrease in airspeed. Since the wind usually changes in a cyclonic sense within the narrow wind shift zone, the problem may be amplified during a left turn of an aircraft, whose course is changed to avoid thunderstorms. For example, a rapid drop in airspeed may be accompanied by a sudden increase in bank angle owing to the pressure of the side component of the new wind on the aircraft wing; downdraft outflow of cold air may also be encountered.

Because vertical wind shear and associated ustiness are important to aircraft operations, we have taken a preliminary look at this problem using the NSSL instrumented tower data. Singer and Smith (1953) discuss in considerable detail the relationship of gustiness to other meteorological parameters such as lapse rate, wind speed, radiation and cloud cover, and concluded that gustiness (fluctuations of horizontal wind speed and direction) is most closely related to lapse rate.

Wind shears were computed from the NSSL instrumented tower data for levels 1, 2, and 3 for April and May 1967. These levels are at heights of 146 ft, 296 ft, and 581 ft, respectively.

Five-minute average winds were obtained at hourly intervals. A reasonable representation of the wind speed profile in the boundary layer (up to approximately 1000 ft) is given by the power law,

$$\overline{V} = \overline{V}_1 \left(\frac{Z}{Z_1}\right)^{\alpha} \quad , \tag{11}$$

where α is a non-dimensional exponent that depends on the thermal stability and normally lies between 0 and 1. $\overline{V}$ and $\overline{V}_1$ are the averaged wind speeds at heights of Z and Z_1, respectively. Horizontal shear is represented by

$$S = \frac{\partial V}{\partial Z} = \frac{\alpha \overline{V}_1}{Z_1^{\alpha}} Z^{(\alpha-1)} \quad , \tag{12}$$

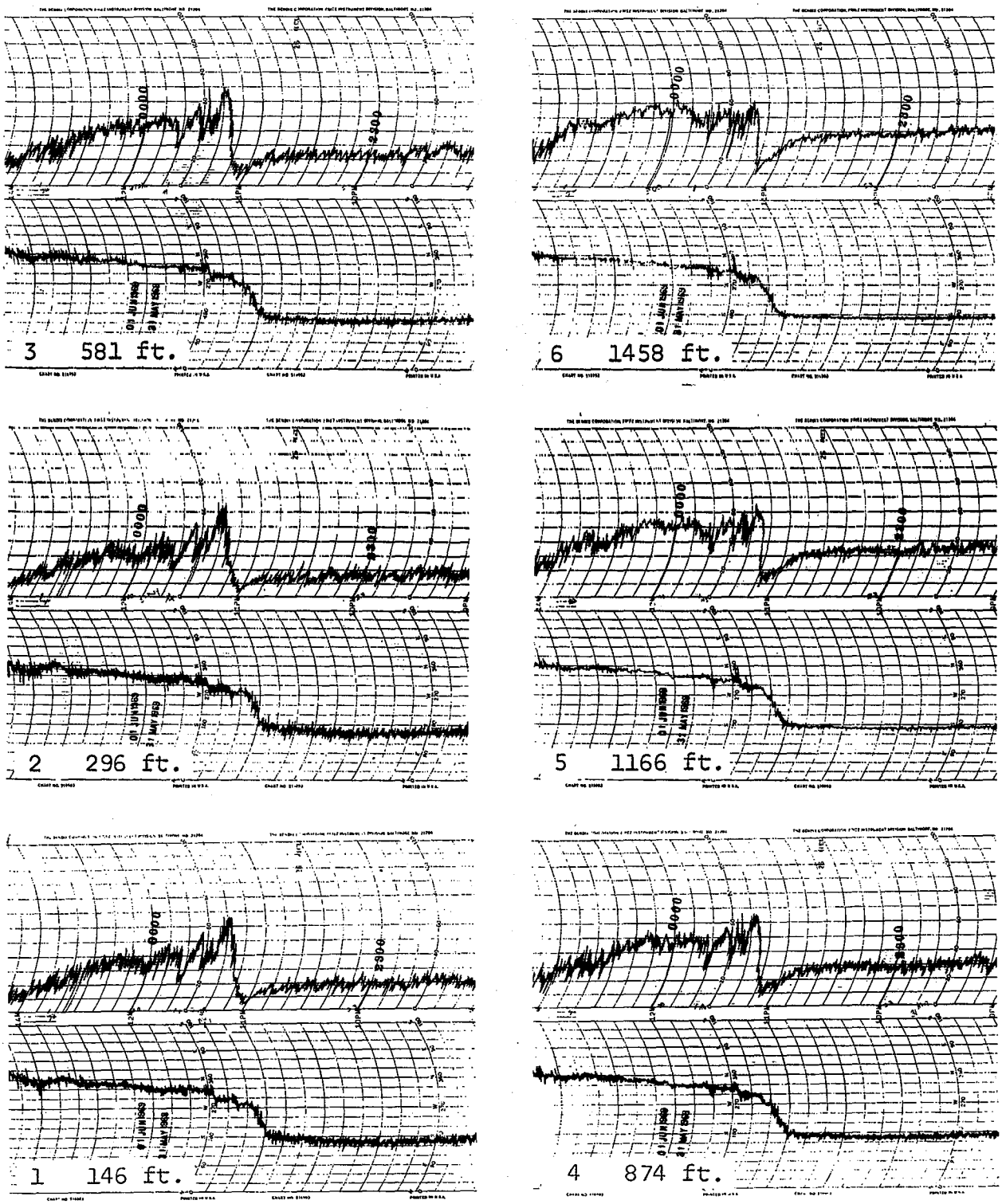

Figure 41. Bendix Aerovane wind velocity records obtained at 6 levels on the WKY TV Tower at Oklahoma City on 31 May 1969. The upper and lower traces are wind speed and direction, respectively. Fine lines are 10-min divisions and speed is in knots.

De Marrais (1959) has treated the behaviour of α with stability: α tends toward unity when the air is very stable and becomes small under the influence of turbulence accompanying unstable lapse rates.

The NSSL results for April and May 1967 are graphed in figure 42 which reproduces the general trend of De Marrais' results. In unstable conditions (super-adiabatic lapse rate) the wind is highly turbulent, and there is a rapid exchange of momentum between levels. A few feet above the ground, wind speed tends to become uniform with height. Under these conditions, α approaches zero. Under more stable conditions vertical exchange of momentum is reduced and the wind profile exhibits an increase of speed with increase in height. With temperature inversions, α approaches 1 and strong wind shear conditions exist.

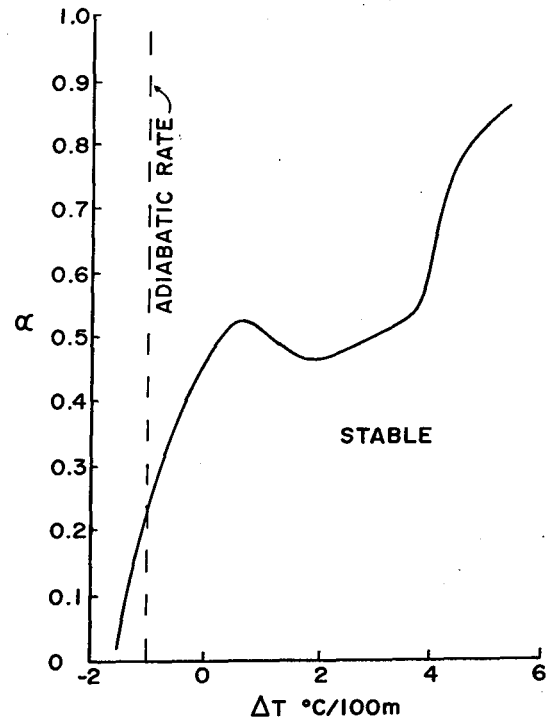

Figure 42. Power law exponent (α), versus temperature lapse rate (ΔT), degrees C per 100 m for averaged hours data collected in April and May 1967.

The application of this simplified analysis of the parameter α to airport operations appears feasible when vertical shear regimes are identified. It would require two-level wind and temperature measurements and real time solution of the power law and shear equation. Climatological data for α, as shown in figure 42, would aid in lapse rate and surface roughness normalization. Additional research is needed to relate α to turbulence experienced by aircraft.

6. SEVERE TURBULENCE ADVISORIES FOR AVIATION OPERATIONS

There are many significant problems associated with supplying practical severe weather information to the aviation services. En route flying generally permits time to monitor aircraft weather radar, navigation aids, and the regularly issued weather information, allowing adverse weather to be circumnavigated. This is altered at the commencement and end of a flight where traffic patterns are designated. Near airports, thunderstorms cause traffic congestion and sometimes close airports for extended periods. Provisions are required for timely severe turbulence warnings for both air traffic control and pilots during these periods.

Experience in Australia with the Joint Approach Control Meteorological Advisory Service (JACMAS) has shown that air traffic controllers can be assisted in advising pilots of routes free of severe turbulence on the approach and take-off phases of operation (i.e., they are given the precise location of severe weather in the controllers frame of reference). This reference is that of air routes and distances as used on the Air Traffic Control Center (ATC) bright display. Areas of likely severe turbulence are actually displayed on a closed circuit TV screen above each ATC bright display.

It is essential to have continuity in the presentation of likely severe turbulence areas (this involves a degree of interpretation, predictability, and consistency in presentation) so the controllers will have confidence in the information; it must be current, accurate, and updated regularly, as warranted by changing circumstances. A major difficulty, therefore, is the preparation and dissemination of the severe weather information. It is firmly established that severe turbulence (and hail) is associated with high radar reflectivity. Turbulence, but not necessarily severe turbulence, may be encountered outside high reflectivity areas (FAA Circular, 1968). There has been a considerable amount of work associating radar reflectivity and turbulence experienced by aircraft, with varying assessments as to how far away from the high reflectivity echo turbulence may be experienced (Burnham and Lee, 1969).

Currently, JACMAS operations in Australia (Barclay, 1968) define the severe turbulence area as the $Z = 10^5 mm^6 m^{-3}$ radar echo area plus a 5-mile "buffer" area around it, provided the echo has reached a height associating it as a storm likely to produce severe turbulence. Echo structure is also considered and potentially severe turbulent areas such as those between adjacent strong echoes or associated with tornadic hook echoes or hail "fingers" are also marked for avoidance. The controller operates around this area, routing aircraft up to but not through them. Hence, the meteorologist provides a degree of interpretation and modification to the observed $Z = 10^5 mm^6 m^{-3}$ echo area and provides a 10 min prognosis to cover expected movement. This information is passed to the ATC using closed circuit TV, with air routes and distances marked for direct reference with the controllers bright display.

Another phase of the Australian system that needs to be vigorously explored, is the "self-help" to pilots obtained by the broadcast on navigational aids of continuously updated areas likely to contain severe turbulence; advisories which are referenced to designated air routes and distance from the airports.

Efforts must continue to provide controllers and pilots with improved severe weather information. Practically, the type of information required is the location and prediction of likely severe turbulence areas so that controllers can provide pilots with a passage

through non-severe turbulence areas. Information must be given to allow them to plan how many aircraft may take off and land before a thunderstorm reaches the airport and then where to hold and vector incoming aircraft until approaches clear again.

Another important factor is the interpretation and use of weather echoes, as displayed on the controller's radar. The air traffic control radars normally use receivers of limited dynamic range. This range is further reduced by the scan conversion used for remote "bright displays." Gradations in intensity important for weather echo interpretation are therefore not displayed. Only the echo shape and areal coverage are available. The Moving Target Indicator (MTI) circuit, which eliminates fixed ground targets while allowing detection of moving aircraft, and circular polarization, which rejects the return from spherical precipitation particles, combine to produce an uncertainty in the threshold of the displayed precipitation echo.

6.1 V.O.R. Dissemination

During the late spring of 1969, an attempt was made to provide real time severe turbulence advisories by extracting data from the NSSL WSR-57 radar and disseminating it to the Wiley Post Flight Service Station (FSS). The technique was a simplified version of the operations in Australia described by Barclay (1968). Its purpose was to relay precise positional information of severely turbulent areas of thunderstorms to the FSS for dissemination to pilots over the VOR system.

Two 1-hour tests were conducted in which observations were given to the FSS at approximately 10 min intervals. Positional information of likely turbulent areas was extracted from the radar in VOR direction and range coordinates, the message compiled in the format below, and telephoned to the VOR controller.

Message Format VALID TO TTTT Z SEVERE TURBULENCE ADVISORY

AREA AA MILE DIAM CENTERED RR MILE DDD DEG OKC

LINE LL MILE WIDE CENTERED RR MILE DDD DEG OKC

Affect (air route identification) and (air route) etc.

The difficulties encountered during the very brief experiment were largely organizational ones. On both occasions the radar at NSSL was being used for "chaff" tracking with frequent changes in antenna elevation angle making access to the radar for systematic echo analysis difficult. No video map overlay was available to conveniently read off the VOR direction and distance, and the radar room telephones were being shared with other projects that caused frequent delays in communication with the FSS.

The scheme is obviously feasible and should be beneficial to pilots, particularly light aircraft pilots, but further experimentation should be done at an operational radar station where normal radar operations allow the experiment to proceed smoothly and quickly. The reaction of pilots to this kind of service might be evaluated with the help of the FSS VOR controllers and ARTC personnel.

7. CONCLUSIONS

This study has shown that the radar echoes associated with severe squall lines usually have a regular motion that can be extrapolated for at least 30 min. The accuracy of the extrapolation can be estimated by computer in real time. Large isolated storms can be identified automatically in the computer and used as a base for matching consecutive PPI displays for velocity computation.

The minimum time interval in digital radar data sampling necessary for deriving storm velocity is about 2 to 3 min. The optimum signal threshold for defining storm 'cores' for tracking varies with the storm. In general, isolated cells are best tracked with a threshold of $Z = 10^3$-$10^4 mm^6 m^{-3}$. Cores in squall lines show better consistency with a threshold of $Z = 10^2 - 10^3 mm^6 m^{-3}$. The data suggest that vertical averaging of centroid positions obtained with an antenna tilt sequence may greatly improve core identification between PPI's. Automatic identification of large, stable storms on adjacent PPI's is possible if the size and degree of isolation are considered in pairing. Complete automation may not be practical, however, because of the lengthy computer computation required and the need for additional meteorological information to define the probable hazard for each storm. It is very likely that the optimum configuration will involve a trained meteorologist who has access to real time processing and control of a variable degree of processing.

A technique is suggested for the extrapolation of arrival of a thunderstorm core into a control zone of an airport. The degree of confidence in the extrapolated path is measured in terms of timing and distance errors.

Analyses of the wind fields associated with several severe squall lines show narrow zones (few miles in width) of high winds that exhibit increased variance and strong veering as the mean wind speed increases. The gust fronts are accompanied by temperature and pressure changes that may significantly alter the local altimeter setting.

The gust zone propagated with, or ahead of, the radar echo. Although the speed and intensity of the gust line was not related to the radar echo in any obvious way, it moved with continuity and was detected throughout the NSSL network of 29 stations.

The study has shown that the applications of both radar and surface observations in real time analysis and prediction of severe weather can be greatly improved by the speed and objectivity of a digital computer. Because of the diurnal variation of severe weather in the central United States, the maximum computer load will occur between 1600 and 2200 hours, with a secondary maximum centered at 0300 hours.

One of the most serious problems associated with aviation operations is the interpretation of severe weather events. The intensity and height of the radar echo is evidence of the relative magnitude of the convection, but the computer analyses must be augmented by knowledge of the stability, moisture content, and airflow (convergence and shear) in the storms environment. It has been demonstrated repeatedly that high reflectivity is indicative of hail and turbulence and that a geographical area covered by an echo of corresponding intensity should be circumnavigated by air traffic.

The most serious limitation of non-coherent radar measurements is in the interpretation of the wind hazard associated with severe storms. Research is needed to develop technology for detecting, identifying, and extrapolating low level shear and gust zones, which constitute a hazard to aviation. Until this is done, excessive areas around severe storms must be declared suspect and avoided by air traffic.

8. ACKNOWLEDGMENTS

The authors are grateful for the assistance of Mr. J. T. Dooley and Mrs. Kathryn Gray in the collection and processing of the data used in this report. Mr. Ernie Marion contributed substantially to the echo centroid and tower analysis, and Mr. Thad Smith developed the computer routines for echo centroid matching. Messrs. Kenneth Crawford and Leslie Lemon assisted in the analysis of the surface data, and Mr. Charles Clark aided in the preparation of the manuscript.

Dr. Stanley Barnes and Dr. Edwin Kessler provided important guidance concerning theoretical aspects of the study.

REFERENCES

Barclay, Peter A., 1968: An operational system for the avoidance by aircraft of severe convective turbulence, Proc. 13th Radar Meteorol. Conf., pp. 438-441.

Barnes, Stanley L., 1964: A technique for maximizing details in numerical weather map analysis, J. Appl. Meteorol., 3, pp. 396-409.

Bigler, S. G., 1959: Some non-precipitation echoes as observed by CPS-9 radar, Scientific Report No. 1, Contract AF 19(604)3864, Texas A&M College, 27 pp.

Boucher, Roland J., 1961: The motion and predictability of stratiform precipitation, Scientific Report No. 7, Contract No. AF 19(604)5204, Allied Research Associates, Inc., Boston, Mass., 25 pp.

Boucher, Roland J. and Raymond Wexler, 1961: The motion and predictability of amorphous fields of precipitation, Scientific Report No. 8, Contract No. AF 19(604)-5204, Allied Research Associates, Inc., Boston, Mass., 32 pp.

Browne, J. A., 1961: Wind shear effects on airspeed, World Airlines, Inc., Meteorol. Dept., Tech. Bulletin No. 61-3.

Browning, K. A. and F. H. Ludlam, 1962: Airflow in convective storms, Quart. J. Roy. Meteorol. Soc., 88, pp. 117-135.

Burnham, J. and J. T. Lee, 1969: Thunderstorm turbulence and its relationship to weather radar echoes, J. of Aircraft, 6, No. 5, pp. 438-445.

DeMarrais, Gerald A., 1959: Wind speed profiles at Brookhaven National Laboratory, J. of Meteorol., 16, pp. 181-189.

Croxton, Frederick E. and Dudley J. Cowden, 1939: Applied General Statistics, Prentice-Hall, Inc., New York, N.Y., pp. 344-348.

Federal Aviation Administration Advisory Circular AC No. 00-24, 1968: Thunderstorms, Washington, D. C., 6 pp.

Fujita, T., 1963: Analytical mesonmeteorology: a review, Meteorol. Monographs, 5, No. 27, Severe Local Storms, pp. 77-125.

House, Donald C., 1963: Forecasting tornadoes and severe thunderstorms, Meteorol. Monographs, 5, No. 27, Severe Local Storms, pp. 141-156.

Kessler, E. and J. T. Russo, 1963a: A program for the assembly and display of radar echo distributions, J. Appl. Metorol., 12, No. 5, pp. 582-593.

Kessler, E. and J. T. Russo, 1963b: Statistical properties of weather radar echoes, Proc. 10th Weather Radar Conf., Am. Meteorol. Soc. pp. 25-33.

Ligda, Myron G. H., 1953: The horizontal motion of small precipitation areas as observed by radar, Technical Report No. 21, MIT, Dept. of Meteorol., Cambridge, Mass., 60 pp.

Newton, Chester W. and James C. Fankhauser, 1964: Movement and development patterns of convective storms, and forecasting the probability of storm passage at a given location, National Severe Storms Project Report No. 22, 53 pp.

Newton, Chester W. and James C. Fankhauser, 1963: Severe storm detection and circumnavigation, FAA Contract ARDS-A176, NSSP Project 1963, Washington, D.C., Unit IV-A, 181 pp.

Newton, Chester W. and H. R. Newton, 1959: Dynamical interactions between large convective clouds and environment with vertical shear, J. Meteorol., 16 pp. 483-493.

Noel, T. M. and A. Fleisher, 1960: The linear predictability of weather radar signals, Research Report 34, Weather Radar Research, MIT, Dept. of Meteorol., Cambridge, Mass., 46 pp.

Noel, Thomas M., 1962: The linear predictability of precipitation, Research Report 35, Weather Radar Research, MIT, Dept. of Meteorol., Cambridge, Mass., 49 pp.

Pitchford, K. L. and J. London, 1962: The low-level jet as related to nocturnal thunderstorm over midwest U.S., J. Appl. Meteorol., 1, pp. 45-47.

Singer, Irving A. and Maynard E. Smith, 1953: Relation of gustiness to other meteorological parameters, J. Meteorol., 10, pp. 121-126.

Ward, Neil B., Kenneth E. Wilk, and William C. Herrmann, 1965: WSR-57 reflectivity measurements and hail observations, Technical Note 3-NSSL-24, pp. 1-8.

Wilk, K. E., J. T. Dooley and E. Kessler, 1965: Weather detection by ARSR-ID, ASR-4 and WSR-57 radars - a comparative study, NSSL Tech. Memo No. 1, 33 pp.

Wilson, James Warren, 1966: Movement and predictability of radar echoes, NSSL Tech. Memo No. 28, 30 pp.

APPENDIX A - Analysis of a Few T33 Aircraft Flights During Spring 1969

A.1 Aircraft Flights

On Friday, 16 May 1969, a Canadian T33 aircraft made seven individual passes through, or between, thunderstorm cells. The pilot's comments are summarized for each run and the aircraft track related to the radar echo on the CPN-18 (control radar) and the calibrated WSR-57 radar. Pilots comments are timed in hours, minutes and seconds, central standard time, with an accuracy of ± 30 sec with relation to the radar photographic times.

In interpreting the photos one must remember that the volume sampled by the radar beam averages a large area that increases with range and because of this, and the elevation angle, the precise reflectivity the aircraft passes through cannot be determined. Pilots were asked to report turbulence qualitatively using the "Turbulence Reporting Criteria Table" shown in Table 1.

Run No. 1 at 1425 to 1428 CST, at a flight level of 18,000 ft:

14.25	Data on
14.26:22	In cloud
14.26:52	Moderate to severe vertical turbulence
14.26:52	Intermittent moderate rain
14.27:06	Light turbulence (at eastern edge)
14.27:21	Smooth
14.28	Data off

Figure 43 (CPN-18 PPI) shows the track of the aircraft with the aircraft being positioned to the southwest of the cell. Figure 44 (CPN-18 PPI) shows the aircraft just after it has passed through the main cell but still in an area of rain of reflectivity, Z, of between 1.4×10^2 and $1.4 \times 10^3 mm^6 m^{-3}$ (as indicated in figure 45, WSR-57 log contour PPI). The maximum reflectivity of the echo through which penetration was made was between $1.5 \times 10^4 mm^6 m^{-3}$ and $1.7 \times 10^5 mm^6 m^{-3}$.

Run No. 2 at 1430-1436 CST, at a flight level of 18,000 ft:

14.30	Data on
14.30:53	Entering cloud
14.31	Light turbulence
14.31:15	Light turbulence
14.31:30	Light turbulence

14.32:11	Very light turbulence
14.33:02	Light turbulence
14.33:44	Light turbulence
14.33:59	Trace of ice on wings
14.34:11	Heavy turbulence, in precipitation
14.34:57	Intermittent heavy turbulence
14.36	Data off

Figures 46 and 47 (CPN-18 PPI) show the echo before and after the run. The aircraft track is shown in figure 46. As indicated by figure 48, toward the end of the run the aircraft passed through the echo with reflectivity between 1.4×10^3 and $1.5 \times 10^4 mm^6 m^{-3}$.

Run No. 3 at 1639-1643 CST, at a flight level of 10,000 ft:

16.39	Data on
16.39:51	Very light turbulence
16.40:42	Light chop
16.40:55	Moderate turbulence
16.41:06	Light precipitation
16.41:24	In clear
16.42:02	Data off

Figure 49 and 50 (CPN-18 PPI) show the echo penetrated, with aircraft track shown in figure 49. Figure 51 (WSR-57) indicates penetration through the edge of a small area reflectivity between $Z = 1.5 \times 10^4$ and 1.7×10^5.

Run No. 4 at 1643-1645 CST, at a flight level of 10,000 ft:

16.43:30	Data on
16.44:36	Very light turbulence
16.44:56	In clear
16.45:07	In clear, very light turbulence, cell decaying
16.45:18	Data off

Figures 52 and 53 (CPN-18 PPI) show the echoes between which the aircraft penetrated. The aircraft track is shown in figure 52. No WSR-57 radar log contour photo is available, but intensities derived from the CPN-18 radar indicate that the small cell north of the aircraft had a small area of reflectivity between 1.4×10^2 and $1.4 \times 10^3 mm^6 m^{-3}$, while the echo to the south of the aircraft probably had a small area whose reflectivity was between 1.4×10^3 and $1.5 \times 10^4 mm^6 m^{-3}$.

Run No. 5 at 1648-1651 CST, at a flight level of 10,000 ft:

16.48	Data on
16.49:23	Smooth, light precipitation, in cloud
16.49:34	Light precipitation, light turbulence
16.49:58	Light chop, no precipitation
16.50:11	Very light turbulence south end of cell, light precipitation
16.50:26	Almost smooth, very light precipitation
16.50:49	In clear
16.51:23	Data off

Figures 54 and 55 (CPN-18 PPI) show the cell penetrated before and after the run, with the track shown in figure 54. Figure 56 (WSR-57) indicates the track passing through a small area of reflectivity between 1.4×10^3 and $1.5 \times 10^4 mm^6 m^{-3}$.

Run No. 6 at 1653-1657 CST, at a flight level of 10,000 ft:

16.53:30	Data on
16.54:20	At south end of cell
16.55:07	Light chop only up western edge of cell
16.56:43	Data off

Figure 57 (CPN-18 PPI) and figure 58 (WSR-57) indicate the track of the aircraft down the western edge of a cell whose maximum reflectivity is about $1.4 \times 10^3 mm^6 m^{-3}$.

Run No. 7 at 1709-1712 CST, at a flight level of 10,000 ft:

17.09:15	Data on
17.09:46	Smooth, light precipitation
17.10:02	Light to moderate chop, heavier precipitation
17.10:30	Light to moderate chop, light precipitation
17.10:49	Slight jolt
17.10:58	Still in cloud
17.11:11	Light chop, still in cloud
17.11:20	Light chop, in and out of cloud
17.11:50	In clear
17.12:02	Data off

Aircraft passed approximately 5 mi northeast of $Z = 10^5 mm^6 m^{-3}$. Figures 59 and 60 (CPN-18 PPI) show the storm penetrated before and after the run with the aircraft track indicated in figure 61. Figure 61 (WSR-57) indicates the track through a reflectivity of Z between 1.5×10^4 and $1.7 \times 10^5 mm^6 m^{-3}$.

A.2 Conclusions

Interpretation of these few flights cannot be generalized, and must be considered indicative only of the conditions that may be expected if one were flying a T33 aircraft in the vicinity of similar types of thunderstorms.

In these flights moderate to severe turbulence as estimated by pilots was found within approximately 5 mi of areas with intensities above $1.5 \times 10^4 mm^6 m^{-3}$ and light turbulence occurred with maximum reflectivities below $1.5 \times 10^4 mm^6 m^{-3}$.

Table 1. Turbulence Reporting Criteria*

Intensity		Aircraft Reaction	Reaction Inside Aircraft	Reporting Term—Definition
Light	Turbulence	Turbulence that momentarily causes slight changes in aircraft attitude, altitude or heading. Report as "Light Turbulence."	Occupants may feel a slight strain against seat belts or shoulder straps. Unsecured objects remain at rest, food service may be conducted, and little or no difficulty is encountered in walking.	Occasional - Less than 1/3 of the time. Intermittent-1/3 to 2/3. Continuous - More than 2/3
	Chop	Turbulence (light bumpiness) that causes slight aircraft fluctuations at rapid intervals without appreciable change in altitude, roll or yaw. Report as "Light Chop."		Note 1. Pilots should report location(s), time, intensity, altitude, type of aircraft and, when applicable, duration of turbulence. 2. Duration may be based on time between two locations or over a single location. All locations should be readily identifiable. Examples: a. Over Omaha, 1232Z, Moderate Turbulence, Flight Level 300, B707. b. From 59 miles south of Albuquerque to 30 miles north of Phoenix, 1235Z to 1250Z, occasional Moderate Chop, Flight Level 320, DC8.
Moderate	Turbulence	Turbulence that is similar to Light Turbulence but of greater intensity. Changes in aircraft attitude, altitude or heading occur but the aircraft remains in positive control at all times. Report as "Moderate Turbulence."	Occupants feel definite strains against seat belts or shoulder straps. Unsecured objects are dislodged. Food services and walking are difficult.	
	Chop	Turbulence that is similar to Light Chop but of greater intensity. It causes rapid bumps or jolts without appreciable change in aircraft altitude, roll or yaw. Report as "Moderate Chop."		
Severe		Turbulence that causes large changes in aircraft altitude, attitude, or heading. It may cause large variations in indicated airspeed. Aircraft may be momentarily out of control. Report as "Severe Turbulence."	Occupants are forced violently and repeatedly against seat belts or shoulder straps. Unsecured objects are tossed about. Food service and walking are impossible.	
Extreme		Turbulence in which the aircraft is violently tossed about and is practically impossible to control. It may cause structural damage. Report as "Extreme Turbulence."		

*An ATCA Staff report, reprinted from Journal of ATC, courtesy of Air Traffic Control Assn., Inc.

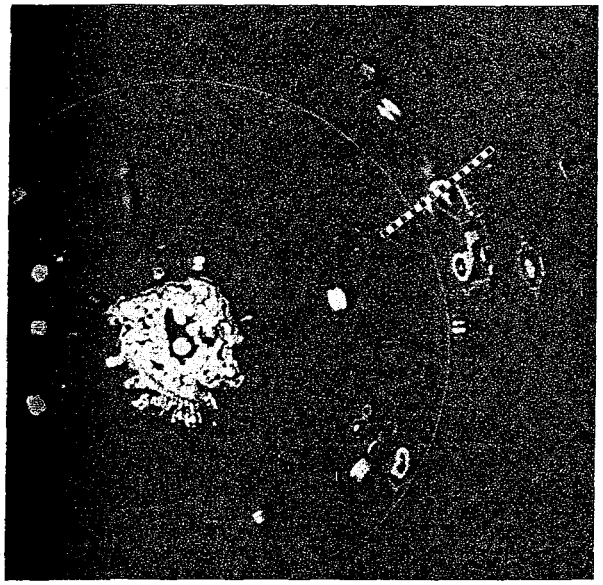

Figure 43. CPN-18 radar contoured display, 1425 CST, 16 May 1969. Start of aircraft data run No.1 at 18,000 ft. The dotted line is approximate track. The contours are not range normalized and represent only relative values of reflectivity.

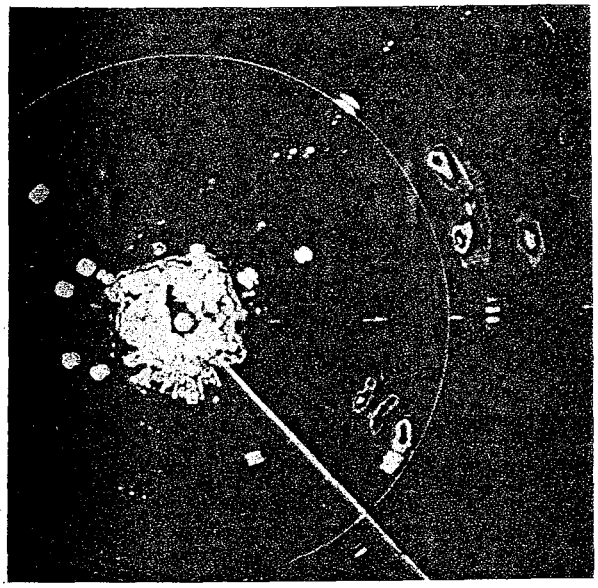

Figure 44. CPN-18 radar contoured display, 1427 CST, 16 May 1969. End of aircraft run No. 1. Range marks are 50 n mi.

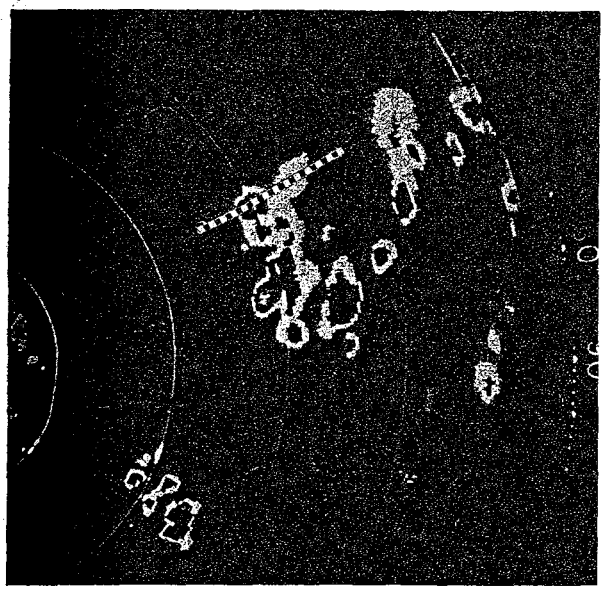

Figure 45. WSR-57 radar range normalized contoured display, 0° antenna tilt, 1427 CST, 16 May 1969. The dotted line represents the track obtained from the CPN-18 radar display. Range marks are 20 n mi.

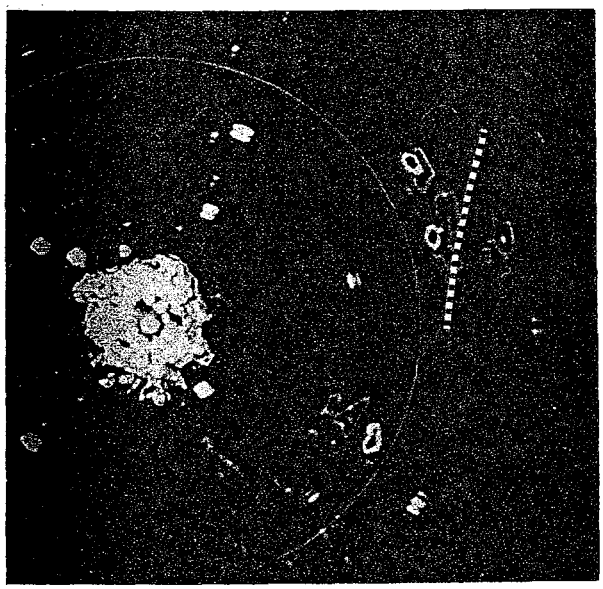

Figure 46. CPN-18 radar contoured display, 1430 CST, 16 May 1969. Start of aircraft run No. 2 at 18,000 ft.

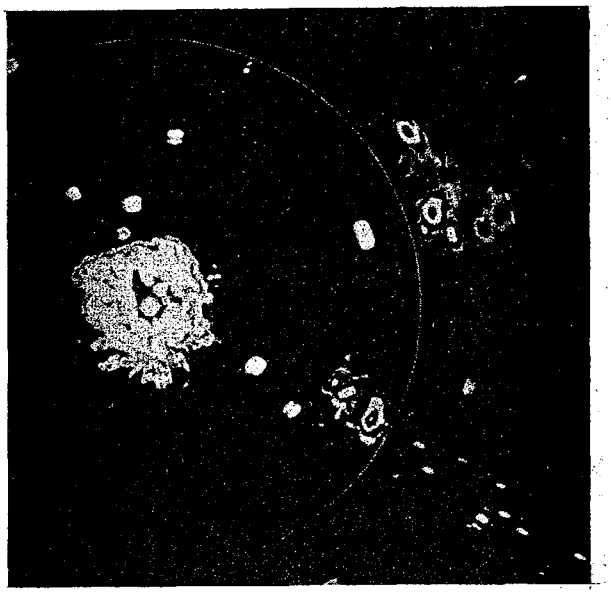

Figure 47. CPN-18 radar contoured display, 1434 CST, 16 May 1969. End of aircraft run No. 2 at 18,000 ft.

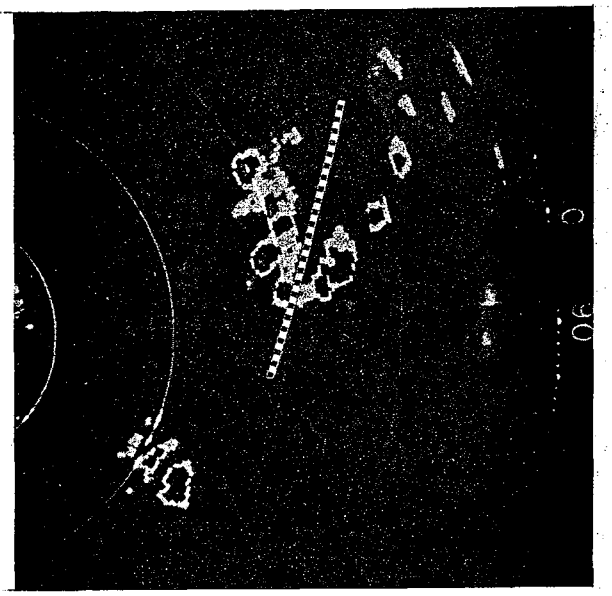

Figure 48. WSR-57 radar contoured display, 1434 CST, 16 May 1969. Start of aircraft run No. 2 at 18,000 ft.

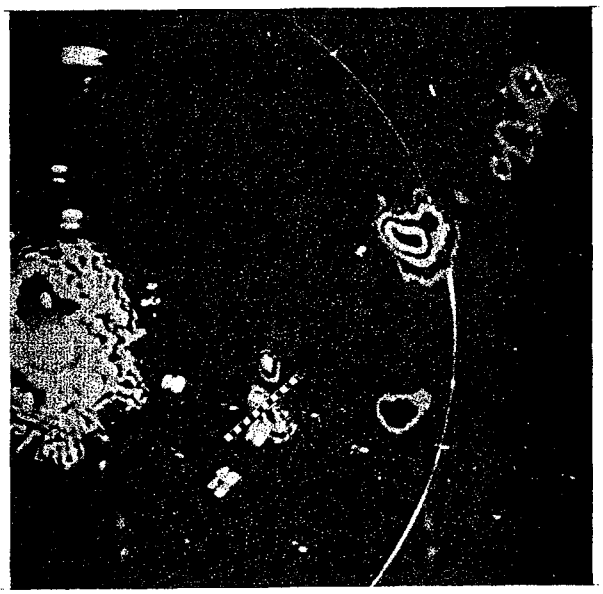

Figure 49. CPN-18 radar contoured display, 1639 CST, 16 May 1969. Start of aircraft run No. 3 at 10,000 ft.

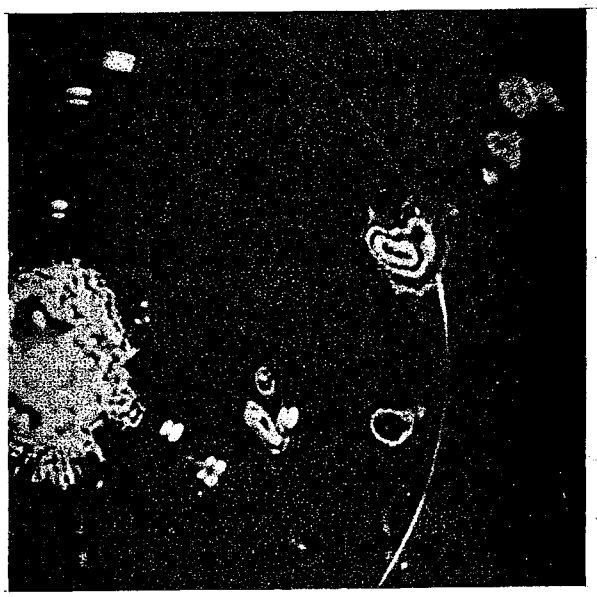

Figure 50. CPN-18 radar contoured display, 1641 CST, 16 May 1969. End of aircraft run No. 3 at 10,000 ft.

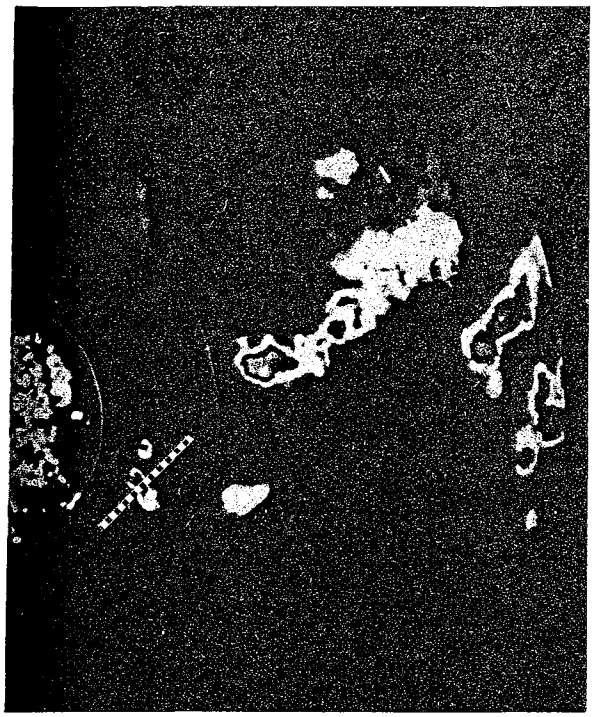

Figure 51. WSR-57 radar contoured display, 1641 CST, 16 May 1969. End of aircraft run No. 3.

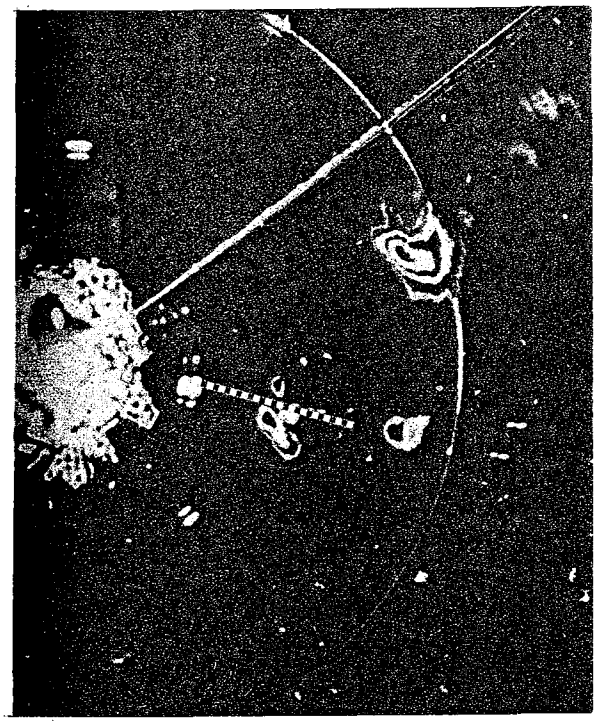

Figure 52. CPN-18 radar contoured display, 1643 CST, 16 May 1969. Start of aircraft run No. 4.

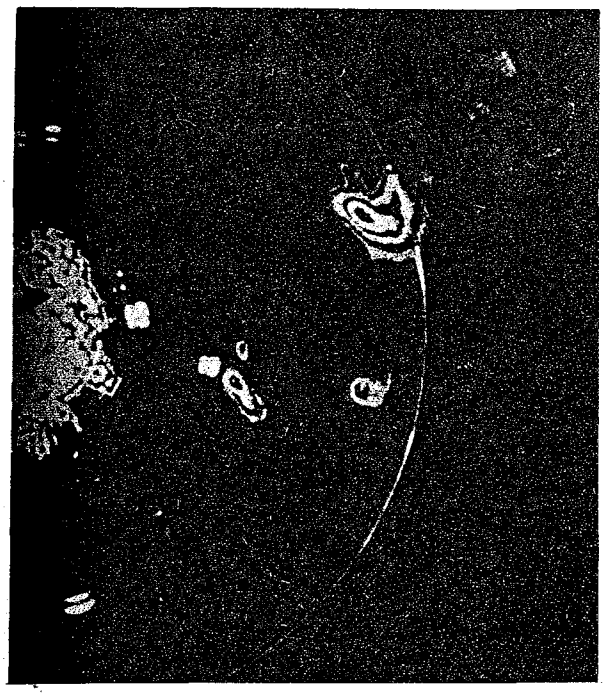

Figure 53. CPN-18 radar contoured display, 1644 CST, 16 May 1969 End of aircraft run No. 4.

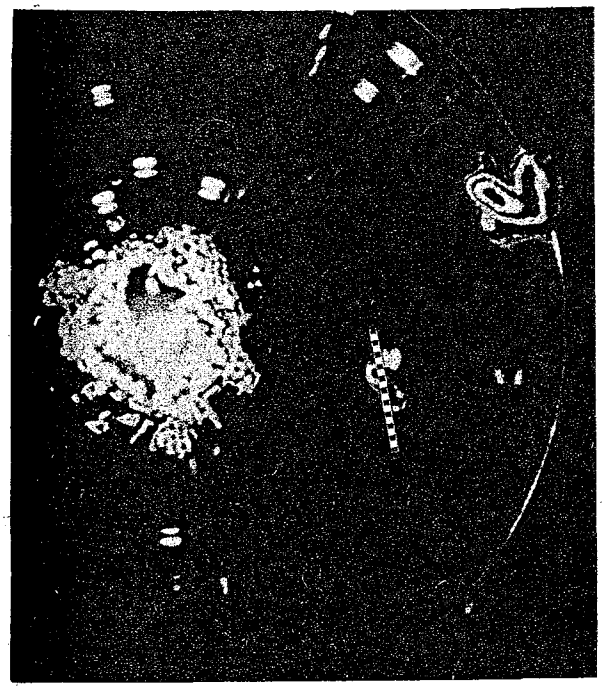

Figure 54. CPN-18 radar contoured display, 1648 CST, 16 May 1969. Start of aircraft run No. 5.

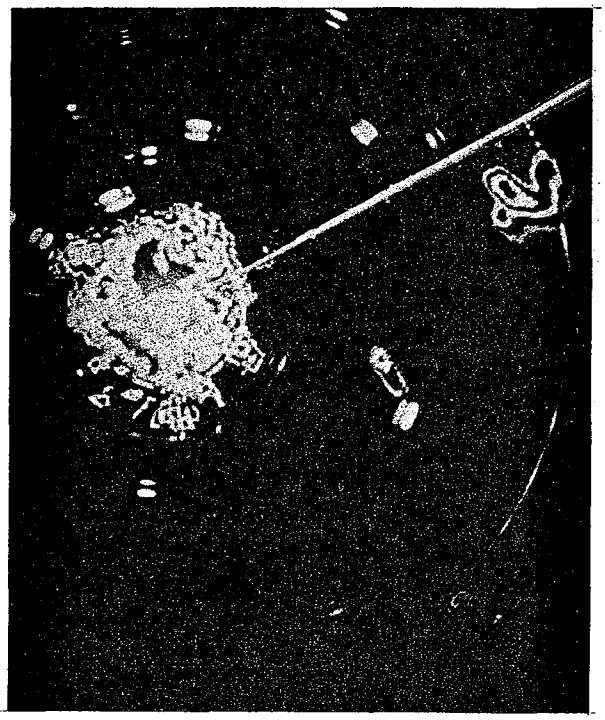

Figure 55. CPN-18 radar contoured display, 1649 CST, 16 May 1969. End of aircraft run No. 5.

Figure 56. WSR-57 radar contoured display, 1649 CST, 16 May 1969. End of aircraft run No. 5.

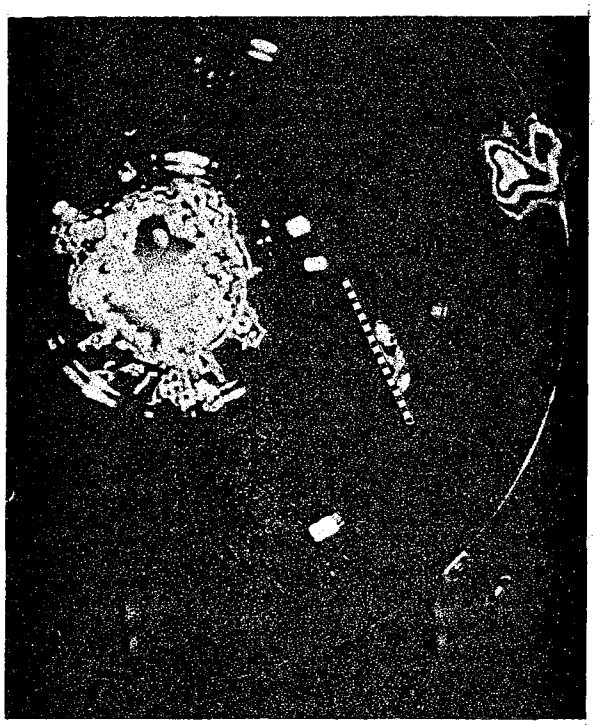

Figure 57. CPN-18 radar contoured display, 1653 CST, 16 May 1969. Start of aircraft run No. 6.

Figure 58. WSR-57 radar contoured display, 1655 CST, 16 May 1969. End of aircraft run No. 6.

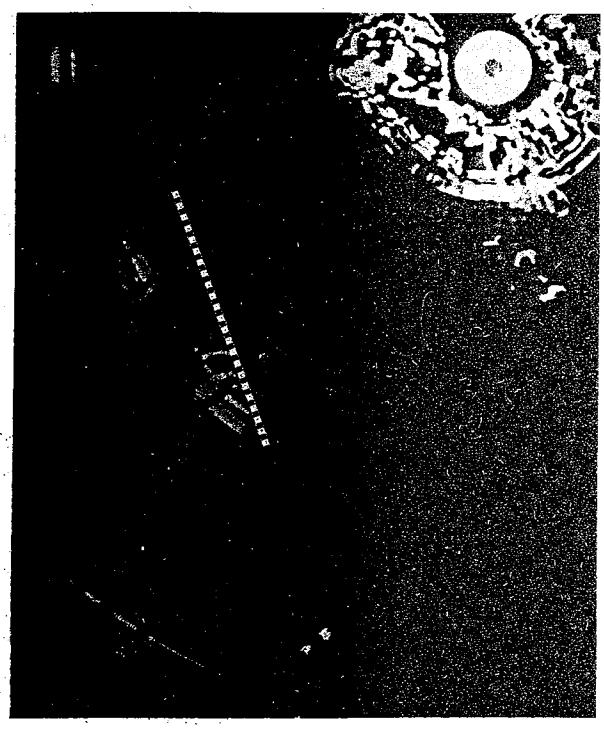

Figure 59. CPN-18 radar contoured display, 1709 CST, 16 May 1969. Start of aircraft run no. 7.

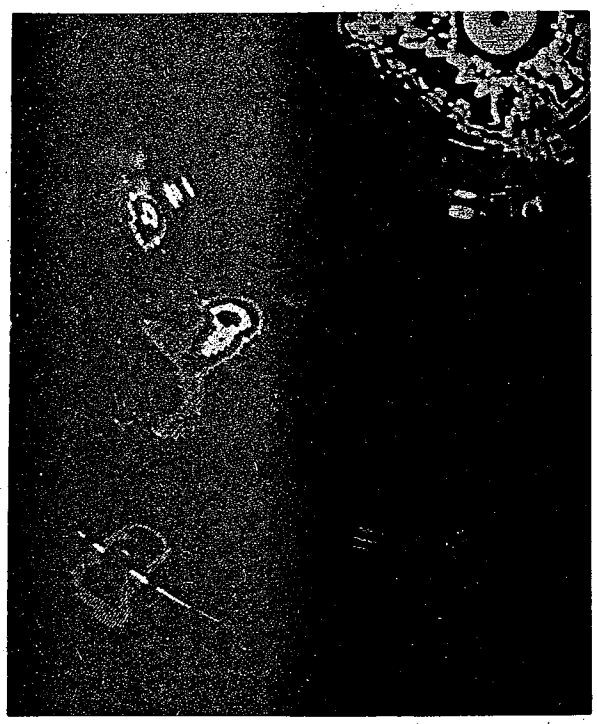

Figure 60. CPN-18 radar contoured display, 1711 CST, 16 May 1969. End of aircraft run no. 7.

Figure 61. WSR-57 radar contoured display, 1710 CST, 16 May 1969.

APPENDIX B - Objective Analyses of Surface Wind Speed during Gust Front Passage, 31 May 1969. The 3-digit values are 5-min average values of wind speed interpolated to the nearest tenth of a knot. The alpha characters (A's, B's, C's) are used to annotate the 0-10, 20-30, and 40-50 knot zones, respectively. The computer printouts are at 5-min intervals.

```
DATE 053169   TIME 2327CST   FACTOR  10.   A# 64.   B# 32.   RMAX 16.00

 0   0   0   0   0   0   0   0   0 135 130 129 131 138 146 148 143 136 130 127
 AAAAAAAAAAAAAAAAAAAAAAAAAAAAAAAAAAAAAAAAAAA
 AAAAAAAAAAAAAAAAAAAAAAAAAAAAAAAAAAAAAAAAA
 0   0   0   0   0   0   0   0 177 146 132 126 125 130 139 142 138 132 128 126
 AAAAAAAAAAAAAAAAAAAAAAAAAAAAAAAAAAAAAAAAA
 AAAAAAAAAAAAAAAAAAAAAAAAAAAAAAAAAAAAAAA
 0   0   0   0   0   0   0 233 209 168 132 118 117 121 128 135 133 130 128 126
 AAAAAAAAAAAAAAAAAAAAAAAAAAAAAAAAAAAAAAA  BBBBBBBB
 AAAAAAAAAAAAAAAAAAAAAAAAAAAAAAAAAAAAAA  BBBBBBBBB
 0   0   0   0   0   0 249 236 218 180 133 114 114 120 127 133 134 132 131 130
 AAAAAAAAAAAAAAAAAAAAAAAAAAAAAAAAAAAAA  BBBBBBBBBBBBBB
 AAAAAAAAAAAAAAAAAAAAAAAAAAAAAAAAAAAAA  BBBBBBBBBBBBBBBB
 0   0   0   0   0   0 280 249 231 213 180 135 115 117 127 137 145 144 140 138 137
 AAAAAAAAAAAAAAAAAAAAAAAAAAAAAAAAAAAAA  BBBBBBBBBBBBBBBBBBB
 AAAAAAAAAAAAAAAAAAAAAAAAAAAAAAAAAAAAA  BBBBBBBBBBBBBBBBBBBB
 0   0   0   0 332 295 245 213 193 169 136 121 127 142 155 162 156 148 144 142
 AAAAAAAAAAAAAAAAAAAAAAAAAAAAAAAAAAAAA  BBB  BBBBBBBBBBBB
 AAAAAAAAAAAAAAAAAAAAAAAAAAAAAAAAAAAAA  BBBB  BBBBBBBBBBB
 0   0   0 347 334 300 241 185 158 146 137 132 143 161 175 178 165 153 147 144
 AAAAAAAAAAAAAAAAAAAAAAAAAAAAAAAAAAAAA  BBB  BBBBBBBBB
 AAAAAAAAAAAAAAAAAAAAAAAAAAAAAAAAAAAAA  BBBB  BBBBBBBBB
 0   0 320 327 322 296 237 168 137 135 139 143 156 174 182 182 170 155 148 145
 AAAAAAAAAAAAAAAAAAAAAAAAAAAAAAAAAAAAA  BBBB  BBBBBBBBBB
 AAAAAAAAAAAAAAAAAAAAAAAAAAAAAAAAAAAAA  BBBBBBBBBBBBBBBBBBBB
 0 225 250 272 284 275 227 162 133 138 147 150 153 156 157 158 155 149 145 144
 AAAAAAAAAAAAAAAAAAAAAAAAAAAAAAAAAAAAA  BBBBBBBBBBBBBBBBBBBBBBBBBBB
 AAAAAAAAAAAAAAAAAAAAAAAAAAAAAAAAAAAAA  BBBBBBBBBBBBBBBBBBBBBBB
149 159 173 189 207 218 202 158 145 159 168 165 142 119 112 111 113 120 129 137
                                                                                AA
                                                                AAAAAAAAAAAAAAAAAAA  AAAAA
128 132 137 143 150 158 161 161 175 191 197 186 149 107  88  81  79  83  94   0
                                                        AAAAAAAAAAAAAAAAAAAAAAAAAAAAA
                                                        AAAAAAAAAAAAAAAAAAAAAAAAAAAA
123 124 125 126 129 134 143 158 175 192 200 191 159 122  94  77  68  66   0   0
                                                          AAAAAAAAAAAAAAAAAAAAAAAAAAA
                                                          AAAAAAAAAAAAAAAAAAAAAAAAAAA
124 124 123 123 125 130 141 154 167 180 189 184 161 138 117  96  79   0   0   0
                                                            AAAAAAAAAAAAAAAAAAAAAAAAA
                                                            AAAAAAAAAAAAAAAAAAAAAAAAA
124 124 124 124 126 132 143 155 165 173 179 176 160 144 132 120   0   0   0   0
                                                              AAAAAAAAAAAAAAAAAAAAAAAA
                                                              AAAAAAAAAAAAAAAAAAAAAAAA
123 124 125 126 129 138 151 160 168 175 179 176 162 148 139   0   0   0   0   0
                                                                AAAAAAAAAAAAAAAAAAAAAAA
                                                                AAAAAAAAAAAAAAAAAAAAAAA
119 122 124 127 134 149 165 174 179 183 186 184 170 154   0   0   0   0   0   0
                                                                  AAAAAAAAAAAAAAAAAAAAAA
                                                                  AAAAAAAAAAAAAAAAAAAAAA
111 117 123 129 140 158 177 188 191 192 194 192 184   0   0   0   0   0   0   0
                                                                    AAAAAAAAAAAAAAAAAAAAAAAAAAAAAA
                                                                    AAAAAAAAAAAAAAAAAAAAAAAAAAAAAA
106 113 122 133 146 164 183 194 198 198 199 198   0   0   0   0   0   0   0   0
                                                B
                                                                    AAAAAAAAAAAAAAAAAAAAAAAAAAAAAAAAAAAAAA
                                            BBBBBB  AAAAAAAAAAAAAAAAAAAAAAAAAAAAAAAAAAAAAAAAAA
104 110 122 136 152 169 185 194 199 201 202   0   0   0   0   0   0   0   0   0
                                        BBB  AAAAAAAAAAAAAAAAAAAAAAAAAAAAAAAAAAAAAAAAAAAAAAAA
                                        BBB  AAAAAAAAAAAAAAAAAAAAAAAAAAAAAAAAAAAAAAAAAAAAAAAA
102 109 120 138 158 176 188 195 199 201   0   0   0   0   0   0   0   0   0   0
```

DATE 053169 TIME 2332CST FACTOR 10. A# 64. B# 32. RMAX 16.00

```
  0    0    0    0    0    0    0    0    0  412  400  378  330  240  157  122  113  114  116  117
  AAAAAAAAAAAAAAAAAAAAAAAAAAAAAAAAAAAAAAAA   BB CC                BBBBBB
  AAAAAAAAAAAAAAAAAAAAAAAAAAAAAAAAAAAAAAAA  BBB                   BBBBBBB
  0    0    0    0    0    0    0    0  413  387  363  334  288  223  162  128  118  117  117  117
  AAAAAAAAAAAAAAAAAAAAAAAAAAAAAAAAAAAAAAAA   B  CC               BBBBBBBBBB
  AAAAAAAAAAAAAAAAAAAAAAAAAAAAAAAAAAAAAAAA  BB    CC             BBBBBBBBBBBBBB
  0    0    0    0    0    0    0  437  408  353  296  259  230  201  170  140  126  121  119  119
  AAAAAAAAAAAAAAAAAAAAAAAAAAAAAAAA  BB  CCCCCC        BBBBBBBBBBBBBBB
  AAAAAAAAAAAAAAAAAAAAAAAAAAAAAAA  BB   CCCCCCC       BBBBBBBBBBBBBBB
  0    0    0    0    0    0  445  434  403  334  247  204  190  180  167  149  134  127  124  122
  AAAAAAAAAAAAAAAAAAAAAAAAAAAAA  BB  CCCCCCCCCCC       BBBBBBBB
  AAAAAAAAAAAAAAAAAAAAAAAAAAAA  BB   CCCCCCCCCCC       BBBBBBB
  0    0    0    0    0  432  435  424  393  324  229  180  167  162  156  147  139  132  128  127
  AAAAAAAAAAAAAAAAAAAA   B  CCCCCCCCCCCCC         BBBBBBB
  AAAAAAAAAAAAAAAAAAA  BB    CCCCCCCCCCCC         BBBBBBB
  0    0    0    0  415  415  415  404  372  303  213  164  152  152  153  153  146  138  133  131
  AAAAAAAAAAAAAAAA   B  CCCCCCCCCCCCCCC            BBBBBB
  AAAAAAAAAAAAA  BBB   CCCCCCCCCCC                BBBBBB
  0    0    0  407  407  403  395  377  336  261  179  140  143  156  163  165  154  142  136  133
  AAAAAAAAAA   BB CCCCCCCCCC                    BBBBBBB
  AAAAAAAA  BBB                                BBBBBBB
  0    0  376  385  391  390  380  354  301  218  144  112  131  160  170  170  159  144  137  134
  AAAAA  BB                                  BBBBBB
  AAA  BBBB                                  BBBBBB
  0  306  324  340  355  364  361  333  271  186  124   97  114  142  148  149  147  139  135  133
  A  BBBBBB                                BBBBBBB
    BBBBBBBBBBBBBB                         BBBBBBBB
242  252  264  278  294  310  319  300  238  169  127  109  108  110  108  108  110  115  122  127
  BBBBBBBBBBBBBBBBBBBBBBBBBBBBBBBBBBBBBBBBBBBBBB                          AAAAA              AAA
  BBBBBBBBBBBBBBBBBBBBBBBBBBBBBBBBBBBBBBBBBBBBBB                        AAAAAAAAAAAAAAAAAAAAA  AAAAA
208  216  222  228  235  243  249  241  205  174  156  143  124  100   87   81   80   83   92    0
    BBBBBBBBBBBBBBBBBBBBBBBBBBBBBBBBBBBBBBBB                            AAAAAAAAAAAAAAAAAAAAAAAAAAAAAA
                BBBBBBBBBBBBBBBBBBBBBBBBBBBB                             AAAAAAAAAAAAAAAAAAAAAAAAAAAAAA
173  182  187  190  190  188  187  188  184  176  168  157  141  118   95   80   71   68    0    0
                                                                          AAAAAAAAAAAAAAAAAAAAAAAAAA
                                                                            AAAAAAAAAAAAAAAAAAAAAAAA
141  147  150  151  149  150  157  168  176  177  171  162  150  136  120  101   83    0    0    0
                                                                             AAAAAAAAAAAAAAAAAAAAA
                                                                              AAAAAAAAAAAAAAAAAAAA
127  129  130  128  127  134  150  166  176  179  175  165  154  145  136  125    0    0    0    0
                                                                            AAAAAAAAAAAAAAAAAAAAAA
                                                                            AAAAAAAAAAAAAAAAAAAAAA
119  122  123  124  126  137  156  172  181  185  182  172  160  150  144    0    0    0    0    0
                                                                              AAAAAAAAAAAAAAAAAAAAAAAAAA
                                                                            AAAAAAAAAAAAAAAAAAAAAAAAAAAA
104  114  120  124  132  148  169  183  188  190  189  182  169  157    0    0    0    0    0    0
  AA                                                                     AAAAAAAAAAAAAAAAAAAAAAAAAAAAAA
  AAAA                                                                   AAAAAAAAAAAAAAAAAAAAAAAAAAAAAA
 81   97  113  125  138  157  178  191  193  193  193  189  180    0    0    0    0    0    0    0
  AAAAAAAA                                                           AAAAAAAAAAAAAAAAAAAAAAAAAAAAAAAAAAAA
  AAAAAAAAA                                                          AAAAAAAAAAAAAAAAAAAAAAAAAAAAAAAAAAAA
 65   81  103  123  140  159  177  190  193  194  194  193    0    0    0    0    0    0    0    0
  AAAAAAAAAA                                                       AAAAAAAAAAAAAAAAAAAAAAAAAAAAAAAAAAAAAAAA
  AAAAAAAAAAA                                                    AAAAAAAAAAAAAAAAAAAAAAAAAAAAAAAAAAAAAAAAAA
 59   72   94  120  140  158  172  181  187  190  193    0    0    0    0    0    0    0    0    0
  AAAAAAAAAAAA                                             AAAAAAAAAAAAAAAAAAAAAAAAAAAAAAAAAAAAAAAAAAAAAA
  AAAAAAAAAAAAA                                          AAAAAAAAAAAAAAAAAAAAAAAAAAAAAAAAAAAAAAAAAAAAAAAA
 55   67   88  117  142  159  170  176  180  184    0    0    0    0    0    0    0    0    0    0
```

DATE 053169 TIME 2337CST FACTOR 10. A# 64. B# 32. RMAX 16.00

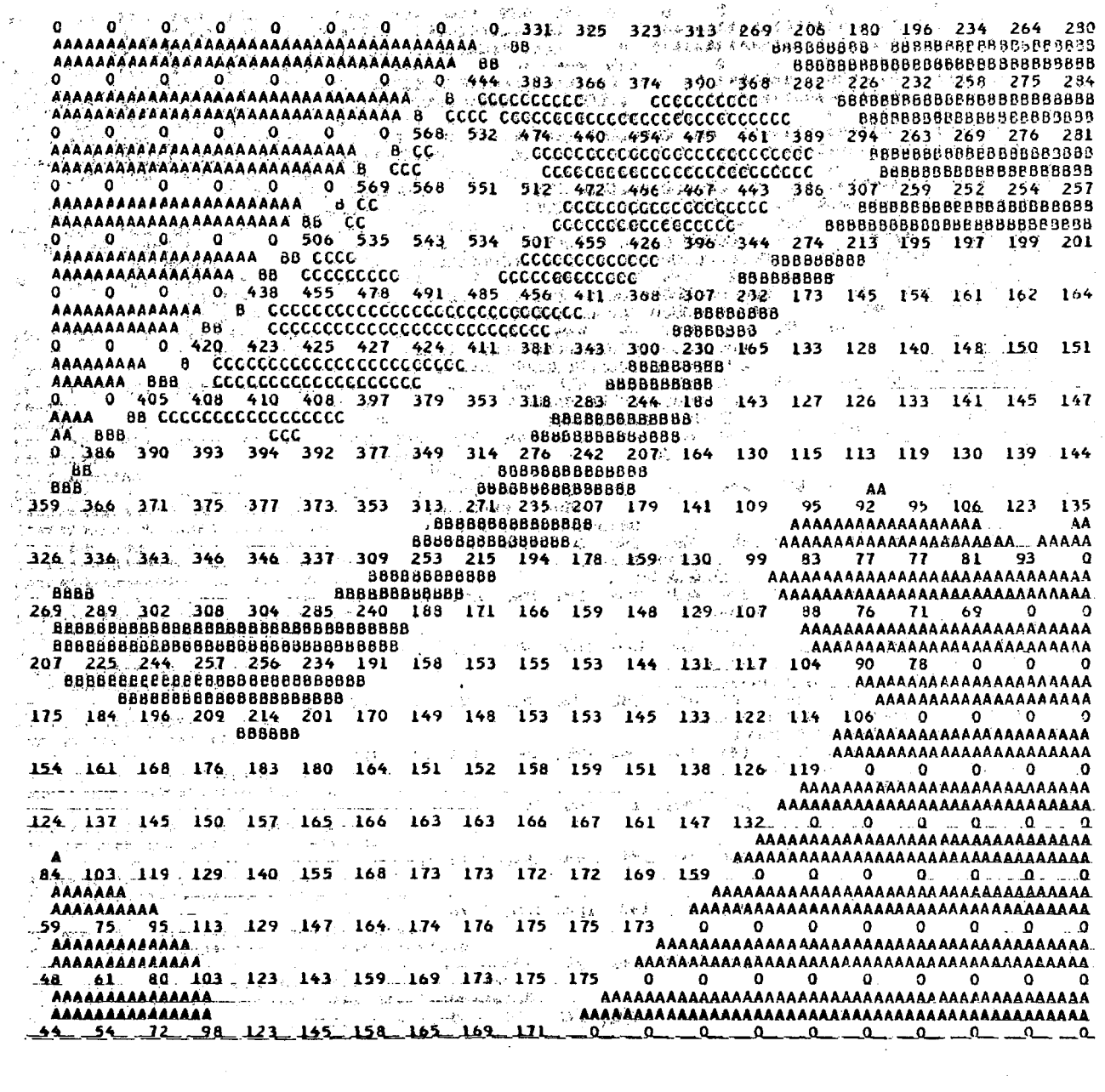

DATE 053169 TIME 2342CST FACTOR 10. A# 64. B# 32. RMAX 16.00

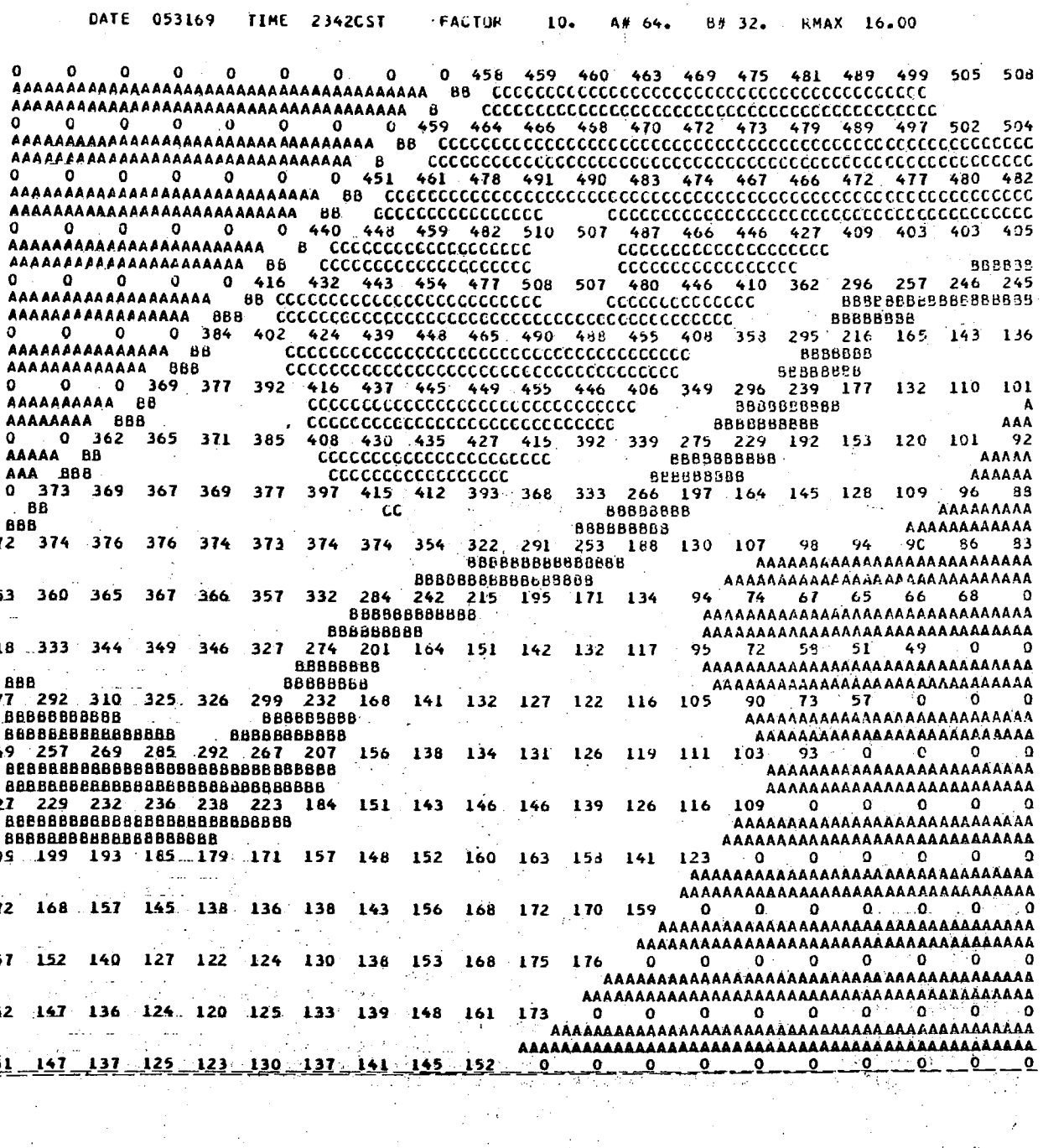

DATE 053169 TIME 2347CST FACTOR 10. A# 64. B# 32. RMAX 16.00

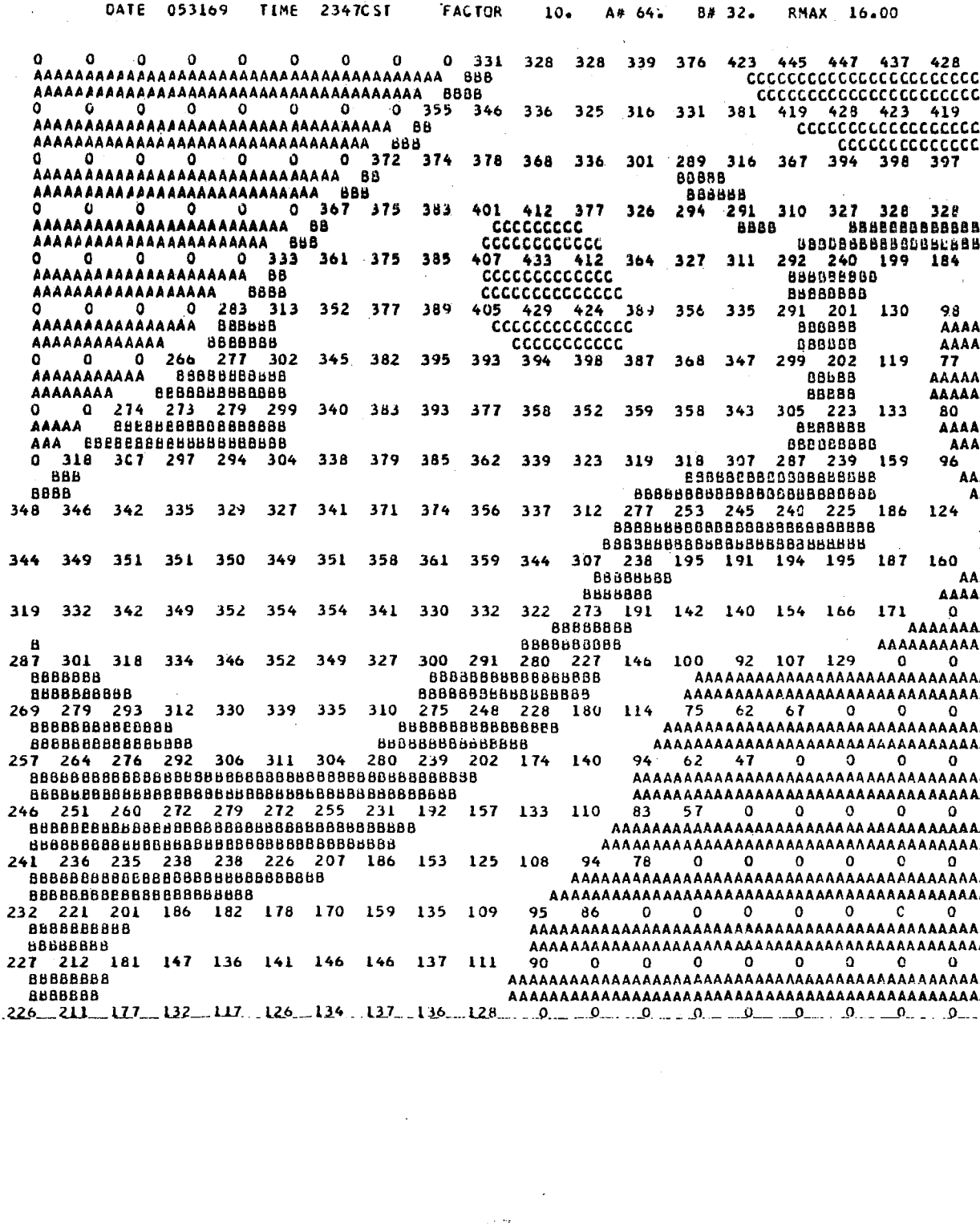

No. 26 Probing Air Motion by Doppler Analysis of Radar Clear Air Returns. Roger M. Lhermitte. May 1966. (PB-170636)

No. 27 Statistical Properties of Radar Echo Patterns and the Radar Echo Process. Larry Armijo. May 1966. The Role of the Kutta-Joukowski Force in Cloud Systems with Circulation. J. L. Goldman. May 1966. (PB-170756)

No. 28 Movement and Predictablity of Radar Echoes. James Warren Wilson. November 1966. (PB-173972)

No. 29 Notes on Thunderstorm Motions, Heights, and Circulations. T. W. Harrold, W. T. Roach, and Kenneth E. Wilk. November 1966. (AD-644899)

No. 30 Turbulence in Clear Air Near Thunderstorms. Anne Burns, Terence W. Harrold, Jack Burnham, and Clifford S. Spavins. December 1966. (PB-173992)

No. 31 Study of a Left-Moving Thunderstorm of 23 April 1964. George R. Hammond. April 1967. (PB-174681)

No. 32 Thunderstorm Circulations and Turbulence from Aircraft and Radar Data. James C. Fankhauser and J. T. Lee. April 1967. (PB-174860)

No. 33 On the Continuity of Water Substance. Edwin Kessler. April 1967. (PB-175840)

No. 34 Note on the Probing Balloon Motion by Doppler Radar. Roger M. Lhermitte. July 1967. (PB-175930)

No. 35 A Theory for the Determination of Wind and Precipitation Velocities with Doppler Radars. Larry Armijo. August 1967. (PB-176376)

No. 36 A Preliminary Evaluation of the F-100 Rough Rider Turbulence Measurement System. U. O. Lappe. October 1967. (PB-177037)

No. 37 Preliminary Quantitative Analysis of Airborne Weather Radar. Lester P. Merritt. December 1967. (PB-177188)

No. 38 On the Source of Thunderstorm Rotation. Stanley L. Barnes. March 1968. (PB-178990)

No. 39 Thunderstorm - Environment Interactions Revealed by Chaff Trajectories in the Mid-Troposphere. James C. Fankhauser. June 1968. (PB-179659)

No. 40 Objective Detection and Correction of Errors in Radiosonde Data. Rex L. Inman. June 1968. (PB-180284)

No. 41 Structure and Movement of the Severe Thunderstorms of 3 April 1964 as Revealed from Radar and Surface Mesonetwork Data Analysis. Jess Charba and Yoshikazu Sasaki. October 1968. (PB-183310)

No. 42 A Rainfall Rate Sensor. Brian E. Morgan. November 1968. (PB-183979)

No. 43 Detection and Presentation of Severe Thunderstorms by Airborne and Ground-Based Radars: A Comparative Study. Kenneth E. Wilk, John K. Carter, and J. T. Dooley. February 1969. (PB-183572)

No. 44 A Study of a Severe Local Storm of 16 April 1967. George Thomas Haglund. May 1969. (PB-184-970)

No. 45 On the Relationship Between Horizontal Moisture Convergence and Convective Cloud Formation. Horace R. Hudson. March 1970.

NATIONAL SEVERE STORMS LABORATORY

The NSSL Technical Memoranda, beginning with No. 28, continue the sequence established by the U. S. Weather Bureau National Severe Storms Project, Kansas City, Missouri. Numbers 1-22 were designated NSSP Reports. Numbers 23-27 were NSSL Reports, and 24-27 appeared as subseries of Weather Bureau Technical Notes. These reports are available from the Clearinghouse for Federal Scientific and Technical Information, 5285 Port Royal Road, Springfield, Virginia 22151, for $3.00, and a microfiche version for $0.65. CFTSI numbers are given below in parentheses.

No. 1 National Severe Storms Project Objectives and Basic Design. Staff, NSSP. March 1961. (PB-168207)

No. 2 The Development of Aircraft Investigations of Squall Lines from 1956-1960. B. B. Goddard. (PB-168208)

No. 3 Instability Lines and Their Environments as Shown by Aircraft Soundings and Quasi-Horizontal Traverses. D. T. Williams. February 1962. (PB-168209)

No. 4 On the Mechanics of the Tornado. J. R. Fulks. February 1962. (PB-168210)

No. 5 A Summary of Field Operations and Data Collection by the National Severe Storms Project in Spring 1961. J. T. Lee, March 1962. (PB-165095)

No. 6 Index to the NSSP Surface Network. T. Fujita. April 1962. (PB-168212)

No. 7 The Vertical Structure of Three Dry Lines as Revealed by Aircraft Traverses. E. L. McGuire. April 1962. (PB-168213)

No. 8 Radar Observations of a Tornado Thunderstorm in Vertical Section. Ralph J. Donaldson, Jr. April 1962. (PB-174859)

No. 9 Dynamics of Severe Convective Storms. Chester W. Newton. July 1962. (PB-163319)

No. 10 Some Measured Characteristics of Severe Storms Turbulence. Roy Steiner and Richard H. Rhyne. July 1962. (N62-16401)

No. 11 A Study of the Kinematic Properties of Certain Small-Scale Systems. D. T. Williams. October 1962. (PB-168216)

No. 12 Analysis of the Severe Weather Factor in Automatic Control of Air Route Traffic. W. Boynton Beckwith. December 1962. (PB-168217)

No. 13 500-Kc./Sec. Sferics Studies in Severe Storms. Douglas A. Kohl and John E. Miller. April 1963. (PB-168218)

No. 14 Field Operations of the National Severe Storms Project in Spring 1962. L. D. Sanders. May 1963. (PB-168219)

No. 15 Penetrations of Thunderstorms by an Aircraft Flying at Supersonic Speeds. G. P. Roys. Radar Photographs and Gust Loads in Three Storms of 1961 Rough Rider. Paul W. J. Schumacher. May 1963. (PB-168220)

No. 16 Analysis of Selected Aircraft Data from NSSP Operations, 1962. T. Fujita. May 1963. (PB-168221)

No. 17 Analysis of Methods for Small-Scale Surface Network Data. D. T. Williams. August 1963. (PB-168222)

No. 18 The Thunderstorm Wake of May 4, 1961. D. T. Williams. August 1963. (PB-168223)

No. 19 Measurements by Aircraft of Condensed Water in Great Plains Thunderstorms. George P. Roys and Edwin Kessler. July 1966. (PB-173048)

No. 20 Field Operations of the National Severe Storms Project in Spring 1963. J. T. Lee, L. D. Sanders and D. T. Williams. January 1964. (PB-168224)

No. 21 On the Motion and Predictability of Convective Systems as Related to the Upper Winds in a Case of Small Turning of Wind with Height. James C. Fankhauser. January 1964. (PB-168225)

No. 22 Movement and Development Patterns of Convective Storms and Forecasting the Probability of Storm Passage at a Given Location. Chester W. Newton and James C. Fankhauser. January 1964. (PB-168226)

No. 23 Purposes and Programs of the National Severe Storms Laboratory, Norman, Oklahoma. Edwin Kessler. December 1964. (PB-166675)

No. 24 Papers on Weather Radar, Atmospheric Turbulence, Sferics, and Data Processing. August 1965. (AD-621586)

No. 25 A Comparison of Kinematically Computed Precipitation with Observed Convective Rainfall. James C. Fankhauser. September 1965. (PB-168445).